CRANFIELD UNIVERSITY

FLORIAN KOKOSHI

ALTERNATIVE GAS TURBINE ARCHITECTURES FOR MIDDLE-OF-MARKET ENGINES

SCHOOL OF AEROSPACE, TRANSPORT AND MANUFACTURING
Thermal Power

MSc
Academic Year: 2017–2018

Supervisor: Prof V. Pachidis
Co-Supervisors: Dr C. Mourouzidis, Mr A. Pellegrini
August 2018

CRANFIELD UNIVERSITY

SCHOOL OF AEROSPACE, TRANSPORT AND MANUFACTURING
Thermal Power

MSc

Academic Year: 2017–2018

FLORIAN KOKOSHI

Alternative Gas Turbine Architectures for Middle-of-Market Engines

Supervisor: Prof V. Pachidis
Co-Supervisors: Dr C. Mourouzidis, Mr A. Pellegrini
August 2018

This thesis is submitted in partial fulfilment of the requirements for the degree of MSc.

Dedicated to my Grandfather

Abstract

This thesis focuses on the research of alternative turbofan architectures for the Middle-of-Market aircraft category. The alterations to the conventional direct drive architecture include the adoption of a power gearbox, the substitution of the full-axial high-pressure compressor with an axi-centrifugal configuration and the installation of a variable area fan nozzle. The thesis aims to provide a turbofan architecture optimised for mission fuel burn in a typical Middle-of-Market aircraft mission profile.

The methodology followed in the realisation of this project starts with a cycle design optimisation through the application of genetic algorithms, which results in a Pareto front of optimum individuals in terms of cruise SFC and specific thrust. It follows a weight and size estimation phase for all the individuals of the Pareto front. Eventually, the installed performance of the investigated turbofans is assessed through the mission fuel burn analysis. The mission profile adopted in this study has a range of 3000nm, and it is performed by a 180 seat aircraft type. The project workflow involves the utilisation of the EPIDOSYS platform, specifically developed for the assessment of civil turbofans.

The results demonstrate that the adoption of a power gearbox enables a reduction of about 2.5% in mission fuel burn relative to the conventional direct drive architecture. Additionally, above a determined fan diameter, the geared architecture results in lighter turbofans relative to the direct drive. Moreover, the alteration from a full-axial high-pressure compressor to an axi-centrifugal allows an ulterior 1.2% reduction in mission fuel burn with the additional advantage of a lighter and

more compact architecture. Eventually, the adoption of the variable area fan nozzle component demonstrated a small improvement in mission fuel burn of 0.2% in the geared turbofans.

Keywords

Alternative Architectures; Axi-centrifugal; Geared Turbofans; Middle-of-Market; Mission Fuel Burn; Optimisation; Variable Area Fan Nozzle

Contents

Abstract iv

Contents vi

List of Figures ix

List of Tables xiv

Nomenclature xv

Acknowledgements xix

1 Introduction 1
- 1.1 Background . . . 1
  - 1.1.1 Alternative gas turbine architectures . . . 3
  - 1.1.2 The Middle-of-Market segment . . . 3
- 1.2 Aim and objectives . . . 4
- 1.3 Thesis structure . . . 5

2 Literature Review 6
- 2.1 Turbofan engine cycle fundamentals . . . 6
  - 2.1.1 Thermal Efficiency . . . 6
  - 2.1.2 Propulsive efficiency . . . 8
  - 2.1.3 Overall Efficiency . . . 9
  - 2.1.4 Specific fuel consumption . . . 10
- 2.2 Engine preliminary design . . . 12
  - 2.2.1 Mission Analysis . . . 12
  - 2.2.2 Single point design . . . 13
  - 2.2.3 Multipoint design . . . 13
- 2.3 Specific thrust and bypass ratio . . . 14
- 2.4 Geared Turbofans . . . 18
  - 2.4.1 Comparison with Direct Drive Turbofans . . . 19
  - 2.4.2 LPT considerations . . . 20
  - 2.4.3 Power gearbox . . . 21
- 2.5 Axial and centrifugal compressors . . . 24
  - 2.5.1 Axial compressors . . . 24
  - 2.5.2 Centrifugal compressors . . . 26

2.5.3 Axi-centrifugal compressors 28
2.6 Variable Area Fan Nozzle 29
2.7 State-of-the-art turbofans 31

3 Methodology **34**
3.1 Overview 34
3.2 MoM engines cycle design optimisation 37
3.2.1 MoM enignes simulation 39
3.2.2 Engine models 39
3.2.3 Thermodynamic cycle design 43
3.2.4 Turbomachinery efficiencies estimation 44
3.2.5 Estimation of turbine cooling fractions 46
3.3 MoM engines weight and size estimation 47
3.3.1 Nacelle weight estimation 50
3.4 MoM engines mission fuel burn calculation 51

4 Results and discussion **57**
4.1 Cycle design optimisation results 57
4.1.1 Axi-centrifugal HPC geared turbofan cases 58
4.1.2 Axi-centrifugal HPC direct drive turbofan cases 63
4.1.3 VAFN effect on running lines 67
4.1.4 Axial HPC geared turbofan case 69
4.1.5 Axial HPC direct drive turbofan case 72
4.1.6 Cycle designs comparison 75
4.1.6.1 Comparison between VAFN and FIXED configurations 76
4.1.6.2 Comparison between axi-centrifugal and axial HPC configurations 77
4.1.6.3 Comparison between geared and direct drive configurations 80
4.1.6.4 Overview of comparisons 82
4.2 Engine weight and size estimation results 84
4.2.1 Axi-centrifugal HPC geared engines 84
4.2.2 Axi-centrifugal HPC direct drive engines 86
4.2.3 Axial HPC geared engines 88
4.2.4 Axial HPC direct drive engines 89
4.2.5 Weight and size comparisons 90
4.2.5.1 Geared and direct drive models 90
4.2.5.2 Axi-centrifugal and axial models 92
4.2.5.3 Overall comparison 94
4.2.6 Engine annulus designs comparison 95
4.3 Mission fuel burn results 97

5 Conclusions and future work **101**
5.1 Significant outcomes 101
5.2 Future work possibilities 103

References **106**

A NASA FLOPS input data **115**

List of Figures

1.1 Variation of aircraft fuel burn, emissions and noise with the increase in fan diameter. [3] 2
1.2 The Middle-of-Market sweet spot in the current civil aircraft market.[5] 4

2.1 Velocities and pressures in a level flight turbofan. 9
2.2 Turbofan trends in terms of Cruise SFC, Bypass Ratio and OPR from 1970 to 2010.[12] 11
2.3 Turbine Entry Temperature (TET) values evolution from 1940 to 2010. [13] 12
2.4 Design and performance considerations for aero engines.[14] . . 13
2.5 Variation in direct drive engine size with increasing BPR. [7] 16
2.6 Smith diagram used to evaluate turbine stage efficiency. [17] . . . 17
2.7 SFC variation as a function of bypass ratio for a conventional turbofan. [7] 17
2.8 Architectural differences between a geared and a direct drive turbofan at the same bypass ratio. [7] 18
2.9 Comparison between a Direct Drive Turbofan (below) and a Geared Turbofan (above). [19] 19
2.10 Comparison between a direct drive and a geared turbofan in terms of noise, TSFC and fuel burn as a function of specific thrust.[18] . 20
2.11 Cross-sectional representation of a power gearbox. [21] 22
2.12 The power gearbox of the Pratt&Whitney PurePower family engines.[25] 23
2.13 A typical multistage axial compressor [28] 25
2.14 Variation of the properties of a fluid moving through the stages of a multistage compressor. [29] 26
2.15 A sectional view of a centrifugal compressor and the thermodynamic and aerodynamic properties of the fluid. [29] 27
2.16 Fan map for a very low specific thrust engine with 3 operation points: Take-off (To), Cruise (CR), Climb (CL). [8] 30
2.17 Left: Prototype of a VAFN with flaps mounted on inclined fixture elements [39]. Right: Pratt&Whitney PW1000G with VAFN [40] . . 30
2.18 Longitudinal section of a PW1000G. [42] 32
2.19 Sectional[44] and longitudinal[45] view of a TFE731 32

3.1 Frontal view of an Airbus A321 taken as the reference aircraft model for this project. In red and black are indicated the fan dimensions analised during the optimisation process. [47] 35
3.2 The EPIDOSYS platform from which the modules utilised in this project are derived. [11] 36
3.3 Schematic representation of CYCLOPS. [11] 37
3.4 Schematic representation of the baseline turbofan model utilised in this study with the architectural options in red. 41
3.5 Pressure distribution along the span of a fan blade. [11] 42
3.6 Principal engine modules and their submodules included in the ATLAS code. [48] 48
3.7 Schematic representation of the main dimensions of a turbofan nacelle. [33] 50
3.8 Correlation between the fan diameter and the VAFN component weight. [11] 51
3.9 Airbus A-321 frontal view with part of the main aircraft geometry values indicated. [47] 52
3.10 Typical A-320 aircraft type mission profile. [56] 53
3.11 The FLOPS modules and their relationships. [57] 54
3.12 Workflow utilised in the project for the mission fuel burn analysis. . 56

4.1 Variation of SFC and cycle determining temperatures as a function of specific thrust for the axi-centrifugal HPC geared cases. The SFC values are normalised with the SFC of the AXC_GEAR_FIX with the smallest fan diameter. The temperature values are normalised with the T40 limit. 59
4.2 Variation of BPR, fan diameter and core size as a function of specific thrust for the axi-centrifugal HPC geared cases. The baseline is represented by the AXC_GEAR_FIX with the smallest fan diameter. 60
4.3 Variation of OPR at EOR, ToC and CRZ as a function of the specfic thrust for the axi-centrifugal HPC geared cases. The OPR values are normalised with the OPR at TOC of the AXC_GEAR_FIX with the smallest fan diameter. 62
4.4 Variation of efficiencies as a function of specific thrust for the axi-centrifugal HPC geared cases. The efficiency values are normalised with the transfer efficiency of the AXC_GEAR_FIX with the smallest fan diameter. 63
4.5 Variation of SFC and cycle determining temperatures as a function of specific thrust for the axi-centrifugal HPC direct drive cases. The SFC values are normalised with the SFC of the AXC_DD_FIX with the smallest fan diameter. The temperature values are normalised with the T40 limit. 64

4.6 Variation of BPR, fan diameter and core size as a function of specific thrust for the axi-centrifugal HPC direct drive cases. The baseline is represented by the AXC_DD_FIX with the smallest fan diameter. 65
4.7 Variation of OPR at EOR, ToC and CRZ as a function of the specfic thrust for the axi-centrifugal HPC direct drive cases. The OPR values are normalised with the OPR at TOC of the AXC_DD_FIX with the smallest fan diameter. 66
4.8 Variation of efficiencies as a function of specific thrust for the axi-centrifugal HPC direct drive cases. The efficiency values are normalised with the transfer efficiency of the AXC_DD_FIX with the smallest fan diameter. 66
4.9 Fan tip map of an axi-centrifgual HPC direct drive turbofan. 68
4.10 Fan tip map of an axi-centrifgual HPC geared turbofan. 68
4.11 Variation of SFC and cycle determining temperatures as a function of specific thrust for the axial HPC geared case. The SFC values are normalised with the SFC of the AX_GEAR_FIX with the smallest fan diameter. The temperature values are normalised with the T40 limit. 69
4.12 Variation of BPR, fan diameter and core size as a function of specific thrust for the axial HPC geared case. The baseline is represented by the AX_GEAR_FIX with the smallest fan diameter. 70
4.13 Variation of OPR at EOR, ToC and CRZ as a function of the specfic thrust for the axial HPC geared case. The OPR values are normalised with the OPR at TOC of the AX_GEAR_FIX with the smallest fan diameter. 71
4.14 Variation of efficiencies as a function of specific thrust for the axial HPC geared case. The efficiency values are normalised with the transfer efficiency of the AX_GEAR_FIX with the smallest fan diameter. 71
4.15 Variation of SFC and cycle determining temperatures as a function of specific thrust for the axial HPC direct drive case. The SFC values are normalised with the SFC of the AX_DD_FIX with the smallest fan diameter. The temperature values are normalised with the T40 limit. 72
4.16 Variation of BPR, fan diameter and core size as a function of specific thrust for the axial HPC direct drive case. The baseline is represented by the AX_DD_FIX with the smallest fan diameter. . . 73
4.17 Variation of OPR at EOR, ToC and CRZ as a function of the specfic thrust for the axial HPC direct drive case. The OPR values are normalised with the OPR at TOC of the AX_DD_FIX with the smallest fan diameter. 74
4.18 Variation of efficiencies as a function of specific thrust for the axial HPC direct drive case. The efficiency values are normalised with the transfer efficiency of the AX_DD_FIX with the smallest fan diameter. 74

4.19 Comparison of the variation of SFC as a function of the specific thrust for all the models studied. 76
4.20 Variation of OPR at CRZ as a function of the specific thrust for the axi-centrfugal and axial HPC geared and direct drive models. . . . 78
4.21 Variation of HPC polytropic efficiency as a function of specific thrust for axi-centrifugal and axial architectures. 79
4.22 LPT (above) and fan (below) polytropic efficiency variations as a function of the fan diameter for the axi-centrifugal HPC geared and direct drive engines. 82
4.23 Weight and length variation as a function of the fan diameter for the axi-centrifugal geared FIXED models. The model with the smallest fan diameter is taken as a baseline. 85
4.24 Weight and length variation as a function of the fan diameter for the axi-centrifugal geared VAFN models. The model with the smallest fan diameter is taken as a baseline. 85
4.25 Variation of weight and length (above) and configuration (below) as a function of the fan diameter for the axi-centrifugal direct drive VAFN case. The model with the smallest fan diameter is taken as a baseline. 86
4.26 Variation of weight and length (above) and configuration (below) as a function of the fan diameter for the axi-centrifugal direct drive FIXED case. The model with the smallest fan diameter is taken as a baseline. 87
4.27 Weight and length variation as a function of the fan diameter for the axial geared FIXED models. The model with the smallest fan diameter is taken as a baseline. 88
4.28 Variation of weight and length (above) and configuration (below) as a function of the fan diameter for the axial direct drive FIXED engines. The model with the smallest fan diameter is taken as the baseline. 89
4.29 Variation of weight and length as a function of fan diameter for the axi-centrifugal geared and direct drive models FIXED. The baseline is represented by the AXC_DD_FIX model with the smallest fan diameter. 91
4.30 Variation of weight and length as a function of fan diameter for the axial geared and direct drive models FIXED. The baseline is represented by the AX_DD_FIX model with the smallest fan diameter. 91
4.31 Variation of weight and length as a function of fan diameter for the axial and axi-centrifugal geared FIXED models. The baseline is represented by the AXC_GEAR_FIX model with the smallest fan diameter. 93
4.32 Variation of weight and length as a function of fan diameter for the axi-centrifugal and axial direct drive FIXED models. The baseline is represented by the AX_DD_FIX model with the smallest fan diameter. 93
4.33 Engine weight variation as a function of the fan diameter for all the models considered in this study. 95

4.34 Annulus design of the architectures under investigation. 96
4.35 Mission fuel burn variation as a function of fan diameter for all the models investigated. 97

List of Tables

2.1 Performance and design data of a TFE731-60 [46]. 33

3.1 Thrust requirements in the main operating points. 35
3.2 Set of decision variables, constraints and objectives for the cycle optimisation system. 38
3.3 Engine deck layout adopted for the mission fuel burn analysis in NASA FLOPS. 54

4.1 Decision variable ranges applied in the cycle design optimisation. . 57
4.2 Percentual differences between the optimum SFC values among all the architectures studied. 83
4.3 Percentual differences at the minimum MFB value among all the architectures investigated. 99

A.1 NASA FLOPS input data regarding the aircraft geometry. [47] . . . 115

Nomenclature

Abbreviations

ACARE	Advisory Council for Aerospace Research in Europe
AX	Axial
AXC	Axi-centrifugal
BPR	Bypass Ratio
CFD	Computational Fluid Dynamics
CRZ	Cruise
DD	Direct Drive
DP	Design Point
EOR	End of Runway
FAR	Fuel-to-Air Ratio
FHV	Fuel Heating Value
FPR	Fan Pressure Ratio
GR	Gear Ratio
HPC	High-Pressure Compressor
IPC	Intermediate-Pressure Compressor
LPT	Low-Pressure Turbine
MFB	Mission Fuel Burn
MoM	Middle-of-Market
NMA	New Midsize Airplane
NSGA	Non-dominated Sorting Genetic Algorithm

NGV	Nozzle Guide Vanes
NS	Stage Number
OPR	Overall Pressure Ratio
PCN	Corrected Rotational Speed
PGB	Power GearBox
SATM	School of Aerospace, Technology and Manufacturing
SFC	Specific Fuel Consumption
SFN	Specific Thrust
SL	Stage Length
TOC	Top of Climb
TET	Turbine Entry Temperature
UHBPR	Ultra High Bypass Ratio
VAFN	Variable Area Fan Nozzle
VLST	Very Low Specific Thrust
WAR	Water-to-Air Ratio

Latin Symbols

A	Area
A_j	Nozzle Area
B	Biot Number
CO_2	Carbon Dioxide
C_p	Specific Heat Capacity at constant pressure
C_v	Specific Heat Capacity at constant volume
D	Diameter
F or FN	Thrust
H	Total Enthalpy
h/t	Hub-to-tip Ratio
k	Surface density

L	Length
M	Mach Number
N	Rotational Speed
NOx	Nitrogen Oxides
P	Total Pressure
p	Static Pressure
Q	Non-dimensional mass flow
Q_{net}	Net Heat Exchange
Q_R	Fuel Heating Value
R	Universal Gas Constant
r	Radius
St	Stanton Number
T	Total Temperature
t	Thickness
T40	Combustor Outlet Temperature
T30	HPC Outlet Temperature
U	Blade Speed
V_a	Axial Velocity
V_j	Jet Velocity
V_0	Flight Speed
W or $\dot{m}$	Air Mass Flow
W_C	Coolant mass flow
W_f	Fuel Flow
WT	Weight

Greek Symbols

α	Speed of Sound
γ	Heat Capacities Ratio

Δ	Variation
ε_0	Convective Cooling Effectiveness
ε_F	Film Cooling Effectiveness
η_{cool}	Cooling Efficiency
η_{core}	Core Efficiency
η_{is}	Isentropic Efficiency
η_O	Overall Efficiency
η_p	Propulsive Efficiency
η_{poly}	Polytropic Efficiency
η_S	Stage Efficiency
η_{th}	Thermal Efficiency
η_{tr}	Transmission Efficiency
θ	Outer Annulus Line Angle
λ	Constant
π	Pressure Ratio
ρ	Density
σ	Stress
σ_y	Yield Stress
τ	Temperature Ratio
ϕ	Flow Coefficient
ψ	Loading Coefficient
Ω	Angular Velocity

Acknowledgements

I would like to thank my supervisor Prof Vassilios Pachidis for giving me the possibility of working on this project within the Cranfield University UTC and following me through this process.

My special thanks to Dr Christos Mourouzidis for his availability, his guidance and help in the realisation of this project. His expertise has given a significant contribution to my work. An acknowledgement goes to Mr Alvise Pellegrini and Mr Salvatore Ippedico for the help they provided in software-related matter.

I would like to thank Mr Steve Brown for the guidance through all the phases of the realisation of this project with his extensive industrial experience.

My immense gratitude goes to my father and mother for giving me the all the love and support that I needed in my life. A special thank to my sister and her family for being near to me in every moment. A special mention goes to my beloved niece, Giulia.

A particular acknowledgement goes to my long-standing friends with whom I have shared part of my best experiences and memories.

A special thank to my housemates for having shared with me the Cranfield everyday life, making it enjoyable and memorable. Many thanks to all those people I met here in Cranfield that shared with me the best moments during this year and provided me with memories that I will remember my whole life.

Chapter 1

Introduction

1.1 Background

Aviation is a big economic sector in Europe, and it is capable of generating 220 billions Euro and offering 4.5 million jobs. Worldwide, there is an average potential for a $4-5\%$ growth in air traffic, with high rates mostly in the Middle East and Asia[1].

The European Commission has studied the development of this sector and has devised flightpaths to be followed in order to reach determined targets in the near future: VISION 2020 [2] and VISION 2050 [1]. Given the fact that the first milestone is considerably near, the attention of researchers nowadays is focused mainly in the second target.

The whole discussion and targets can be found in Reference [1], here it is presented a summary of the primary goals regarding the aeronautic propulsion field:

- Reduction [1] of 75% in CO_2 emissions per passenger kilometre.
- Reduction of 90% in NOx emissions per passenger per kilometre.
- Reduction of 65% in perceived noise emission.

[1] Relative to a typical new aircraft in 2000

In the last decades, there has been a rising concern regarding the environmental impact of transportation and aviation has been affected. This justifies the fact that some of the most critical targets set by the European Community for the near future are related to this topic.

Among these main targets, the primary aim of aircraft manufacturer regards the economic aspect of flying. Generally, the priority is given to the efficiency and the cost effectiveness of the mission. Since the engine represents one of the protagonists in the cost definition process, the aims of the aircraft manufacturers meet with the engine manufacturers research in improving the efficiency of their engine continuously and reduce the fuel consumption. This aim reconnects back with the targets imposed by the European Community since more efficient engines produce fewer emissions and noise. As it can be seen in Figure 1.1 , the

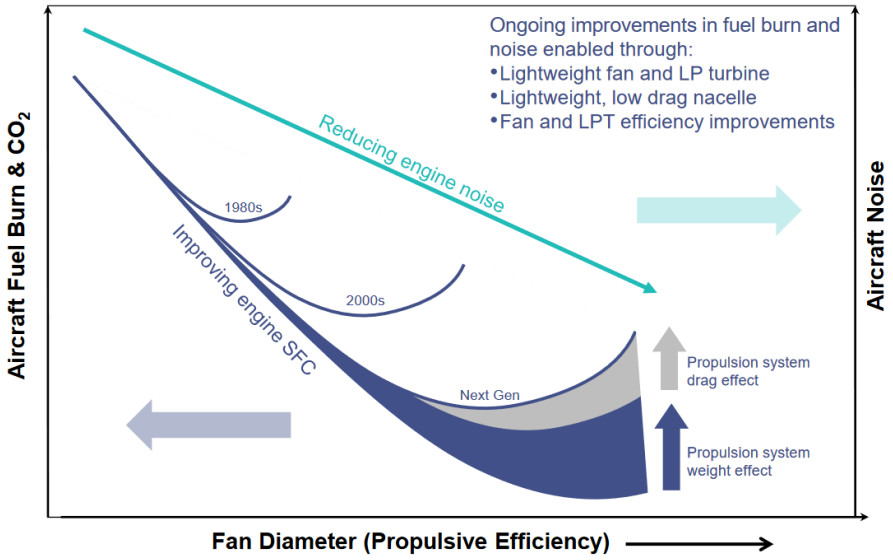

Figure 1.1: Variation of aircraft fuel burn, emissions and noise with the increase in fan diameter. [3]

trend along the years has been to increase the fan diameter in order to improve the engine's specific fuel consumption and reduce emissions in terms of CO_2 and noise. Along with the increase in fan diameter, additional benefits can be obtained from the utilisation of lightweight materials in the heaviest components of the engines, such as the fan or the low-pressure turbine (LPT).

1.1.1 Alternative gas turbine architectures

In this thesis the effect of the fan diameter increase in turbofan's performance is studied. Additionally, architectural modifications are introduced to the conventional direct drive turbofan in order to assess their impact on performance. The alternative components studied in this project are listed below.

- Fan power gearbox (PGB): it decouples the fan from the rest of the turbomachinery on the low-pressure spool; therefore it allows to each component to rotate at its desired rotational speed.
- Axi-centrifugal high-pressure compressor (HPC): the combination of an axial and a centrifgual section allows a reduced number of stages in the HPC with potential benefits in terms of efficiency, weight and length of the whole engine.
- Variable area fan nozzle (VAFN): the adoption of this component allows safer operability of the fan during the take-off condition in terms of surge and flutter.

In this study a conventional direct drive turbofan with a fully axial HPC is taken as a reference to indicate the most diffused turbofan architecture nowadays. Additionally, 5 architectures are obtained from the combination of the abovementioned components; therefore this project assesses and compares the performance of 6 different turbofan archtitectures for the Middle-of-Market engines.

1.1.2 The Middle-of-Market segment

Due to the rapid increase in air transport requirements during the last years, the sky is getting very crowded very quickly. Airliners want to cover longer distances and connect more cities directly, without any transfer. Popular routes such as New York to Los Angeles or Beijing to Shanghai require aircrafts bigger than the typical

Airbus A-320 or the Boeing B737 but smaller than the long-range Airbus A-350 or Boeing 777. This category of aircraft is called the ”Middle-of- Market” (MoM). In Figure 1.2 it can be seen that these aircraft can potentially fly from 3000 to 6500 nautical miles and carry from 180 to 350 passengers in single or twin-aisle configurations. [4]

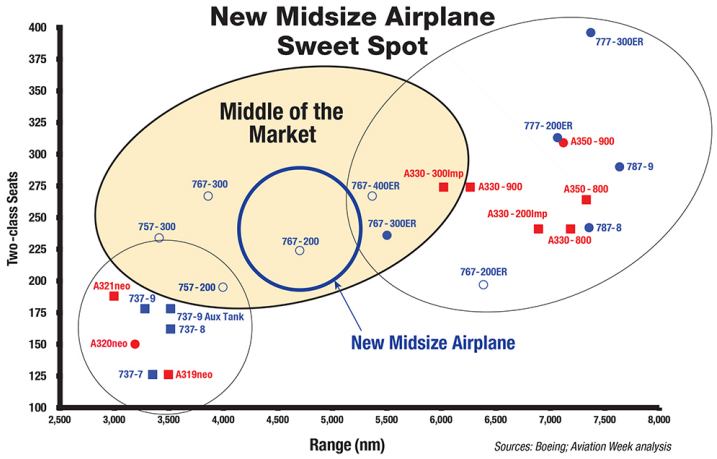

Figure 1.2: The Middle-of-Market sweet spot in the current civil aircraft market.[5]

The Airbus A-321 is the dominant aircraft of the MoM sector nowadays, while the B757 represented Boeing, but it is not in production anymore. Having studied the potentialities of this market, Boeing is planning to build a New Midsize Airplane (NMA or Boeing B797) that could enter into service around 2025 [5].

1.2 Aim and objectives

The project aims to perform a design space exploration for near future Middle-of-Market turbofans and deliver fuel burn optimum engine designs for a specific aircraft application. Moreover, the primary objectives are:

- perform a cycle design optimisation for all the 6 abovementioned MoM turbofan architectures;

- estimate engine sizes and weights for all the configurations,
- perform total mission fuel burn estimations for a typical Middle-of-Market aircraft type of mission;
- quantify and evaluate the potential benefits of alternative turbofan architectures.

1.3 Thesis structure

This thesis is divided into five chapters organised in this order:

- Chapter 1 gives a general introduction to the project topic and sets the background for the development of the project description.
- Chapter 2 gives a resume of the whole literature study that has been conducted by the author to deeply understand the central aspect of the project. In this chapter, it is possible to find a basic introduction to the aircraft propulsion thermodynamic principles, a description of the engine preliminary design phases, an explanation of the main aspects of geared turbofans and a generic commentary on the architectural components studied in this project.
- Chapter 3 explains the methodology followed in the realisation of this project. It offers a description of the cycle design optimisation process, the engine weight and size estimation and the mission fuel burn studies.
- Chapter 4 presents the results obtained in the project and commentary on them. All the study cases are explained and widely compared.
- Chapter 5 represents the conclusion of the thesis, and there are some ideas for future work starting from this project as a base.

Chapter 2

Literature Review

2.1 Turbofan engine cycle fundamentals

Aircraft have evolved from the first rudimentary internal combustion engines to high-efficiency turbofans. During this evolution, the challenges that engineers had to solve changed radically. In the first decades of flights, the critical challenges were weight, performance and reliability. In the modern times, the same challenges are still present, but there are new ones related to economics and environmental issues.

The objective of this section is to give an elementary understanding of the key thermodynamic concepts that represent the foundations of turbofan engines.

2.1.1 Thermal Efficiency

This particular efficiency generally tells how much of the energy contained in the fuel that we burn in an engine is effectively converted into shaft power, in the case of a power generation gas turbine, or into kinetic energy of the gas that moves through the machine, in an aero engine case.

A generic definition of thermal efficiency is given by Reference [6]:

$$\eta_{th} = \frac{Useful\ Work}{Heat\ Input} \tag{2.1}$$

Reference [7] provides a thermal efficiency definition that is suitable for a simple turbojet:

$$\eta_{th} = \frac{\frac{1}{2}W_9V_9^2 - \frac{1}{2}W_0V_0^2}{W_fFHV} \tag{2.2}$$

In this formula, the terms indicated with the subscript "9" are referred to the nozzle exit, while V_0 is the flight speed and W_0 is the air mass flow entering into the engine.

In the case of a turbofan engine the thermal efficiency can be split into two terms:

- core efficiency
- transfer efficiency.

Reference [7] gives the definitions of both the abovementioned terms.

Core efficiency is given by the ratio between the amount of energy still present in the gas at the exit of the turbofan core and the total energy available in the fuel:

$$\eta_{core} = \frac{W_{core}(dH_{is} - V_0^2/2)}{W_fFHV} \tag{2.3}$$

In this expression, the dH term indicates an isentropic expansion of the gas from the condition at the core exit to ambient conditions.

Transfer efficiency indicates how well the energy is transferred from the stream passing through the core to the one in the bypass:

$$\eta_{tr} = \frac{Bypass\ \ Jet\ \ Kinetic\ \ Power}{Core\ \ Power - Core\ \ Jet\ \ Kinetic\ \ Power} = \frac{\eta_{th}}{\eta_{core}} \tag{2.4}$$

According to Giannakakis in Reference [8], the transfer efficiency is determined by the LPT and fan isentropic efficiencies, as well as BPR and pressure

losses in the bypass and core ducts. Guha has demonstrated, in Reference [9], that the transfer efficiency is slightly dependent on the specific thrust as well. Given that the highest influence in the transfer efficiency is given by the isentropic efficiencies of the fan and LPT, in this project, to simplify the analysis, it will be considered:

$$\eta_{tr} \simeq \eta_{is\ fan} * \eta_{is\ LPT} \tag{2.5}$$

2.1.2 Propulsive efficiency

During its flight, an aircraft is subjected to several forces, but in the specific condition of a level flight with a velocity V_0 the main forces are two: thrust and drag. According to Reference [10], the net thrust provided by an engine is the combination of two terms: momentum thrust and pressure thrust.

$$F = \dot{m}(V_j - V_0) + A_j(p_j - p_a) \tag{2.6}$$

To maintain a constant velocity level flight of the aircraft, the thrust must be equal to the drag, but in the opposite direction. In the condition of a fully expanded nozzle, the gas pressure at the exit of the engine (p_j) is equal to the ambient pressure (p_a), therefore the thrust expression can be simplified to:

$$F = \dot{m}(V_j - V_0) \tag{2.7}$$

It is possible to observe from this equation that there are two principal components in the simple definition of thrust: the air mass flow ($\dot{m}$) and the velocity difference ($V_j - V_0$). Consequently, there are two ways to obtain the required thrust:

- small mass flow and high jet velocity,
- high mass flow and small jet velocity.

It is essential to recognise which one of the two ways is more efficient. According to Saravanamuttoo [10] the propulsive efficiency η_p is given by the ratio between the thrust power ($F * V_0$) and the sum of the thrust power and the kinetic energy [1] lost in the jet without being used.

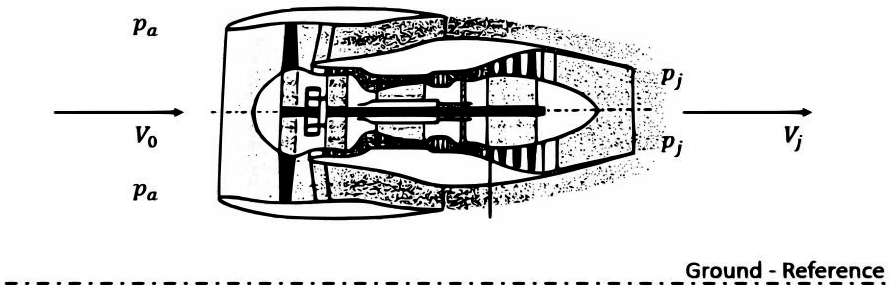

Figure 2.1: Velocities and pressures in a level flight turbofan.

For turbofan engines an expression of the propulsive efficiency is provided by Reference [11]:

$$\eta_p = \frac{Specific\ Thrust * V_0}{\frac{1}{2}(Specific\ Thrust + V_0)^2 * \left(\frac{\left(\frac{1}{\eta_{tr}^2} + BPR\right)(1+BPR)}{(\frac{1}{\eta_{tr}} + BPR)^2} \right) - \frac{1}{2}V_0^2} \tag{2.8}$$

In a turbofan, the separation of the inlet mass flow and the subsequent mixing of the hot and the cold jets generates jet velocities nearer to the flight speed, thus improved propulsive efficiency and fuel consumption.

2.1.3 Overall Efficiency

Considering the engine generically as a system in which fuel is introduced and burnt in order to produce thrust, the overall efficiency of it can be simply defined as the ratio between the thrust power produced (useful work) and the energy obtained from the combustion of the fuel. References [7] and [10] provide with a

[1] This kinetic energy is relative to the earth.

mathematical expression of this efficiency as:

$$\eta_O = \frac{FV_0}{W_f FHV} \tag{2.9}$$

Looking at the previous equations of the propulsive efficiency and the thermal efficiency, an alternative expression of overall efficiency can be derived:

$$\eta_O = \eta_{th} * \eta_{prop} = \eta_{core} * \eta_{tr} * \eta_{prop} \tag{2.10}$$

Considering the definitions of each one of the efficiencies that form the overall, it is clear the dependency of the overall efficiency from the aircraft speed.

2.1.4 Specific fuel consumption

The concept of overall efficiency for aircraft engines can be ambiguous, therefore, instead, it is preferable to consider the specific fuel consumption (SFC). This term is defined, in Reference [10], as the ratio between the fuel flow and the thrust obtained :

$$SFC = \frac{W_f}{F} \tag{2.11}$$

By introducing this expression in the equation (2.9) and by rearranging, it is possible to obtain a new definition of SFC as:

$$SFC = \frac{V_0}{\eta_{core}\eta_{tr}\eta_{prop}FHV} \tag{2.12}$$

This equation enlightens a dependency of SFC from overall efficiency, therefore the specific fuel consumption is intrinsically linked to the flight velocity as well.
Over the years, due to the continuous research in the gas turbines field, specific fuel consumption values have been improving along with an increase in overall

pressure ratio and bypass ratio, consequently with a decrease in specific thrust, as it is reported in Reference [12] and represented in Figure 2.2

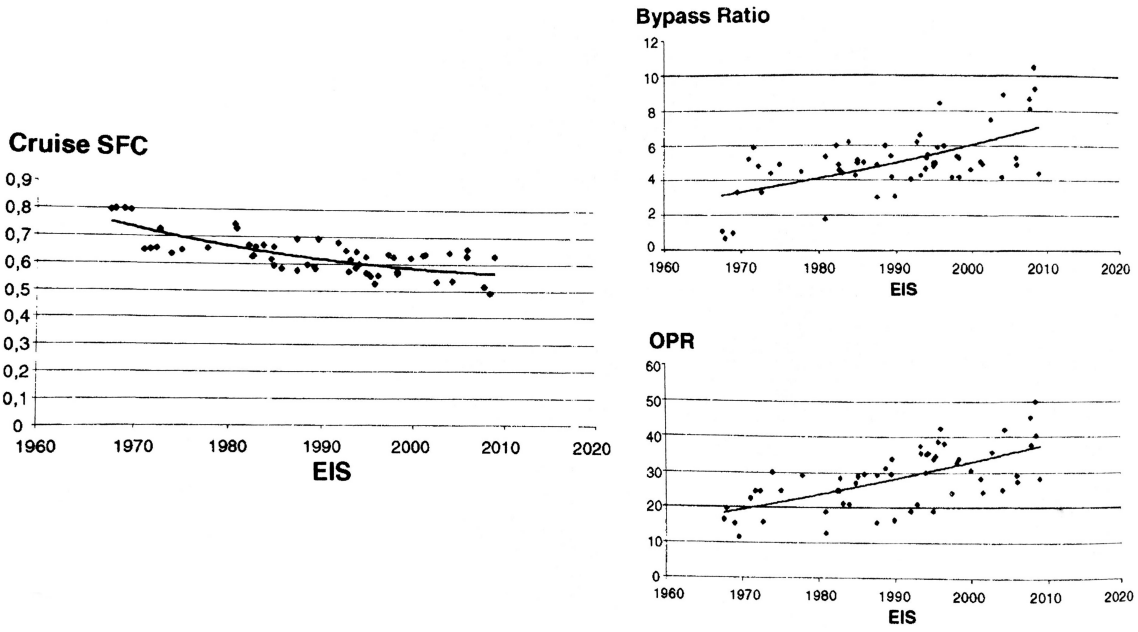

Figure 2.2: Turbofan trends in terms of Cruise SFC, Bypass Ratio and OPR from 1970 to 2010.[12]

An additional parameter that has permitted to reach lower SFC values is the TET. During the years, due to improved techniques in turbine cooling, TET values have been increasing and this has led to an improvement in overall efficiencies and specific fuel consumptions. In the chart represented in Figure 2.3, it is enlighted the trend to increase the TET along with the improvements in turbine blade materials and cooling techniques.

During the last years, modern engines have reached OPR and TET values near to the optimum along with an improvement in compressor and turbine efficiencies. This means that the remaining margin to improve is narrow. There is a possibility of increasing the core efficiency by using heat exchangers, but it is complicated and impractical to implement. Given the impracticability of using heat exchangers, the most practical method to reduce SFC remains improving the propulsive efficiency.

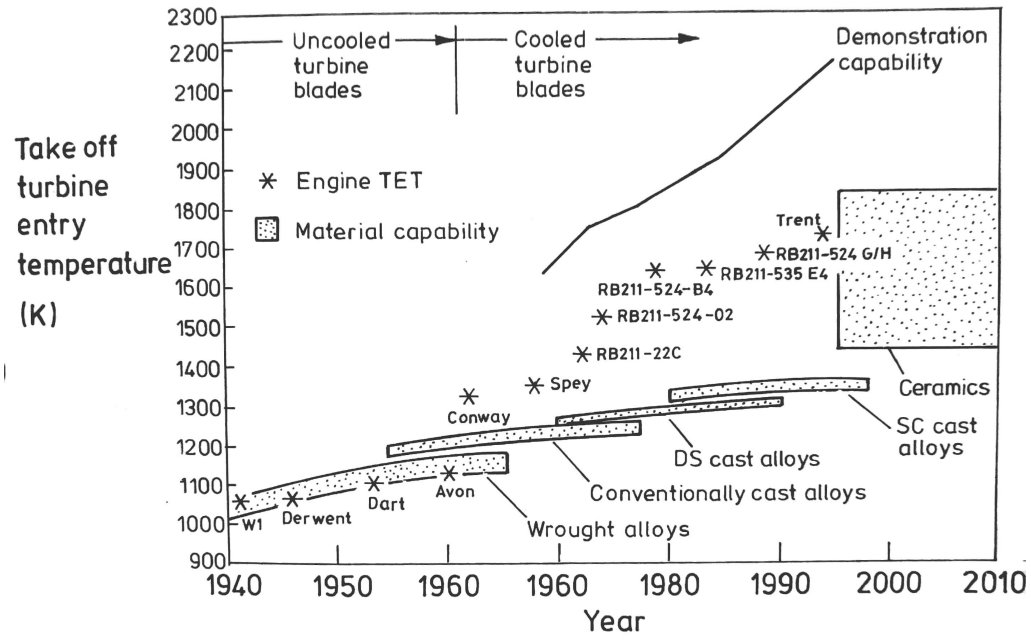

Figure 2.3: Turbine Entry Temperature (TET) values evolution from 1940 to 2010. [13]

2.2 Engine preliminary design

In the realisation process of a turbofan engine, the outcomes of the preliminary design phase define its 3 main characteristics: thermodynamic cycle, annulus design and bearing arrangement.

2.2.1 Mission Analysis

Given the fact that the engine manufacturer receives an input from an aircraft manufacturer before starting a new project, each new gas turbine design is led by the requirements of the market, that, in turn, are originated by the aircraft application. Clearly, the cycle of an engine is determined by the mission followed by the aircraft on which it is installed.

From Figure 2.4 it is possible to understand which parameter, among SFC and specific thrust, is more important for different categories of aircraft and engine utilisation.

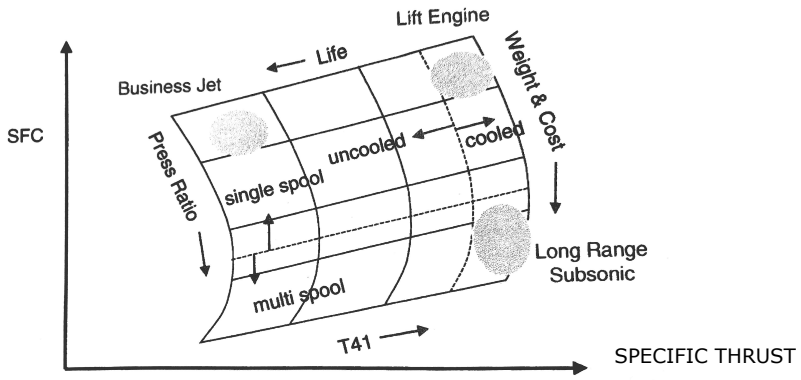

Figure 2.4: Design and performance considerations for aero engines.[14]

The competitiveness of an engigne is related to the values of thermal and propulsive efficiencies that, combined, result in the SFC. Apparently, considering the relation (2.11) between SFC and fuel burn, having as an objective lower SFC means going after lower mission fuel burn. On the other hand, weight is significant as well, and it also plays a crucial role in the definition of the mission fuel burn. Consequently, depending on the typology of utilisation that the engine is designed for, the designers focus the attention on one or another performance parameter.

2.2.2 Single point design

Gas turbines used for power generation perform in a very narrow range of operating conditions, therefore the cycle for these applications is optimised for the simple design point. However, all gas turbines are subjected to variations in pressures, temperatures and spool speeds, thus it means that the off-design behaviour is always important to be considered since the preliminary design phase.

2.2.3 Multipoint design

Gas turbines utilised as aero engines have to face various operating conditions depending on the primary sequences of an aircraft's mission: *taxi, take-off, climb, descent, land and roll to gate*[7]. Among these sequences, there are 3 that set

cycle limits and requirements and, consequently, are used to intially design the engine:

- Take-off: requires the highest TET and spool speeds.
- Top of climb: represents the mission phase with the highest demand for compressors and the maximum OPR value is reached.
- Cruise: in this phase temperatures and spool speeds are relatively lower, however, because this represents the design point for the engine, significant importance is given to efficiency; therefore to SFC.

Typically, the design of a civil aircraft engine is considered to be a ”three-point design”. As mentioned above, the design point is the cruise, and the annulus of the engine is optimised for this condition. Moreover, the fan is sized to cope with the air mass flow requirements at the top of climb condition. The hot day take-off condition is taken as a reference to size the mechanical and the cooling system because there are present the maximum temperatures and spool speeds.

2.3 Specific thrust and bypass ratio

With the term specific thrust (SFN) we refer to the value of thrust per unit of mass flow entering into the engine [15].

$$SFN = \frac{FN}{W_0} \tag{2.13}$$

It gives a first idea about the size, volume and frontal area of the engine. Usually for civil subsonic turbofans, the trend is to go to lower specific thrust values in order to improve the SFC of the engine. For military applications, instead, the objective is to get the maximum specific thrust in order to minimise the frontal area of the engine and make it suitable for supersonic flights reducing its drag .

As it has been mentioned previously in equation (2.10), the overall efficiency of a gas turbine is composed of three factors: core efficiency, transfer efficiency and propulsive efficiency. Reference [11] explains that the core efficiency depends on the TET, the turbomachinery isentropic efficiency and the OPR, while the transfer efficiency is a function of the efficiencies of the components connected to the LP spool. Considering that the improvement of these two efficiency terms has been the centre of the attention for many years so far, nowadays there's the necessity to look at the propulsive efficiency as the primary parameter to affect the overall efficiency of the modern turbofans.

Considering equation 2.8, it appears that the propulsive efficiency is a function of the specific thrust (SFN) and it increases as the specific thrust decreases; therefore, in order to improve the propulsive efficiency, it is necessary to move towards engine designs with increased fan diameters.

A term that is strictly related to the specific thrust is the bypass ratio, defined in [16] as:

$$BPR = \frac{W_{bypass}}{W_{core}} \tag{2.14}$$

It is the ratio between the mass flow that goes through the bypass duct and the mass flow that enters in the core of the engine.

In Reference [7] is presented a study that aims to enlight the benefits and the effects caused by the increase in bypass ratio in two significant cases: conventional direct drive and geared turbofans. From this study emerges that increasing the BPR from 6 to 10 in a conventional direct drive turbofan changes considerably the architecture of the engine. It can be clearly seen in Figure 2.5 that with the increase in BPR there is also an improvement in SFC and an increase in the thrust as well. The increase in BPR is linked to the decrease in specific thrust so it can be seen as the fan diameter increases by 30% going from 6 to 10 in BPR. The overall architecture of the engine changes as well because the number of LPT stages goes from 5 to 9 as the BPR increases and the disk shapes of the

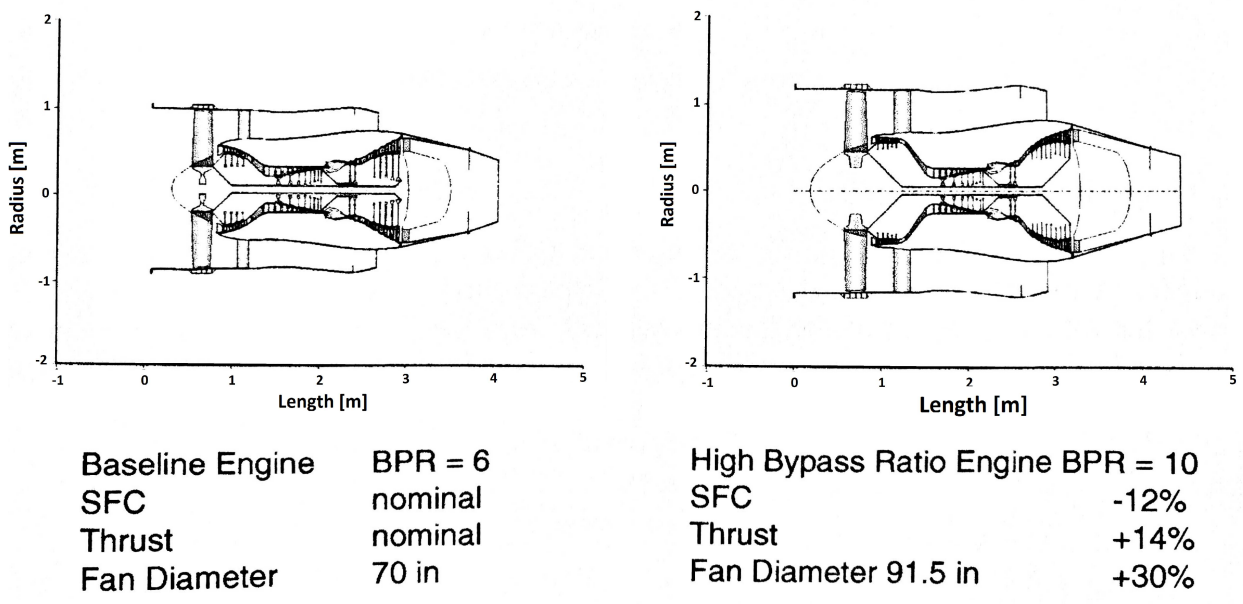

Figure 2.5: Variation in direct drive engine size with increasing BPR. [7]

IPC and LPT stages changes.

It can be deduced from Figure 2.5 that, in order to keep a high polytropic efficiency, the number of LPT stages has to be increased as the fan diameter increases. In fact, the aerodynamic loading of the LPT augments with bypass ratio because of the reduction in fan tip speed consequent of the increase of the fan diameter. In order to maintain the position in the ideal efficiency line that cuts the Smith chart (Figure 2.6), to a specific flow coefficient should correspond a determined stage loading. As the LPT aerodynamic loading increases with fan diameter, it is necessary to increase the number of LPT stages; otherwise the polytropic efficiency of the LPT falls.

In Figure 2.7 it is enlighted that if the number of LPT stages is increased accurately with the increase in BPR, then the SFC gain goes near to the values predicted by assuming a constant LPT polytropic efficiency [7].

The utilisation of a gearbox decouples the fan rotational speed from the booster and LPT rotational speeds, therefore it allows reducing the aerodynamic loading and, due to this, fewer stages of LPT are sufficient for achieving acceptable effi-

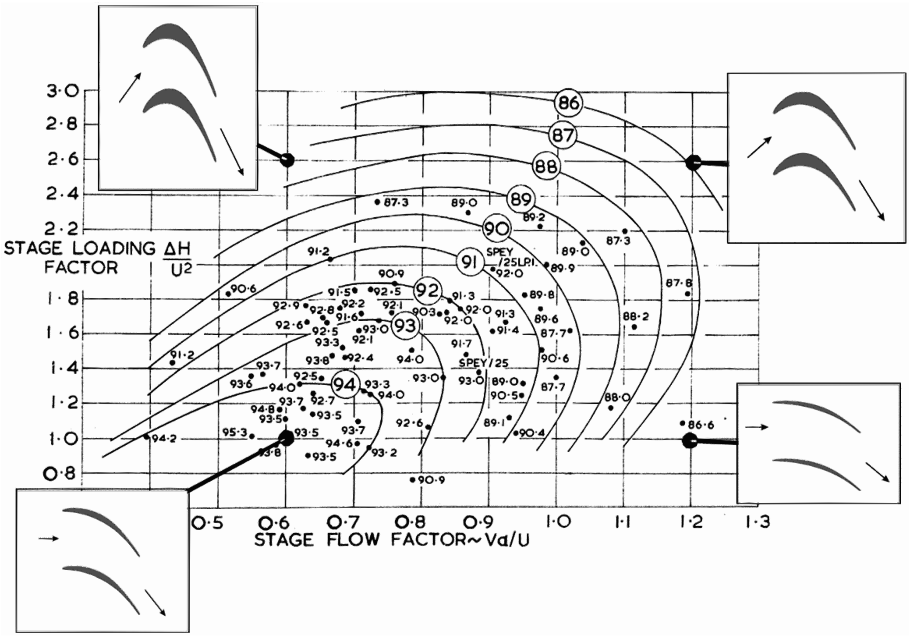

Figure 2.6: Smith diagram used to evaluate turbine stage efficiency. [17]

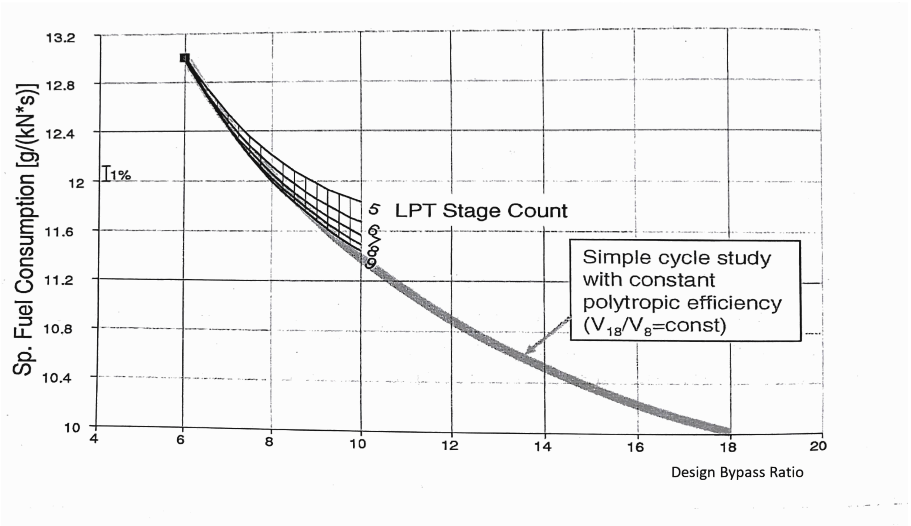

Figure 2.7: SFC variation as a function of bypass ratio for a conventional turbofan. [7]

ciencies. Moreover, with the adoption of a gearbox, there is no necessity to move outwards the flow annulus, therefore the cross-sectional area of a geared turbofan differs significantly from a conventional direct drive one, as it can be seen in Figure 2.8.

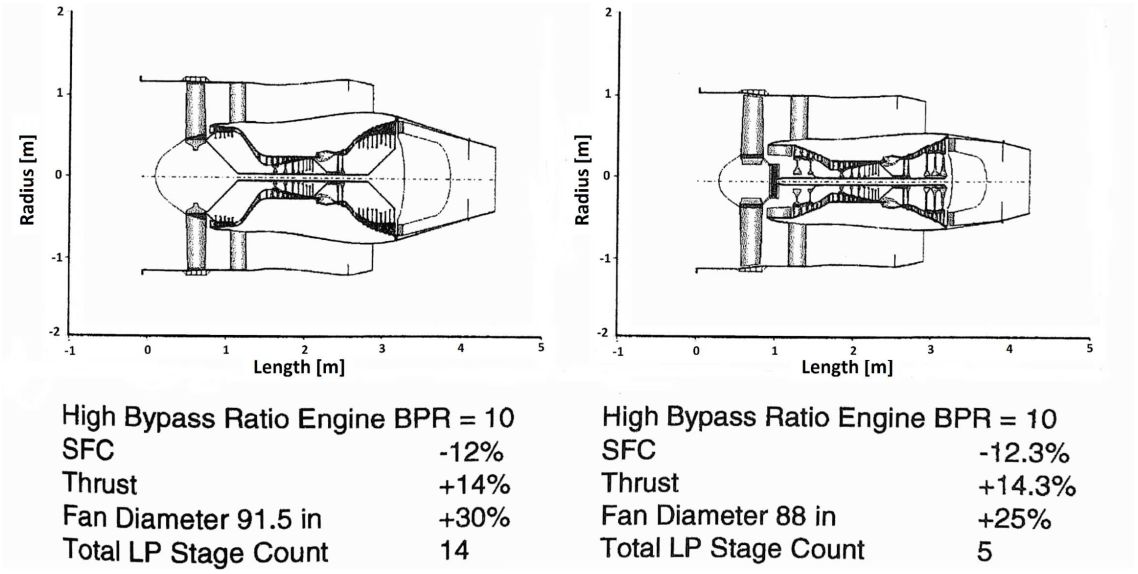

High Bypass Ratio Engine BPR = 10	
SFC	-12%
Thrust	+14%
Fan Diameter 91.5 in	+30%
Total LP Stage Count	14

High Bypass Ratio Engine BPR = 10	
SFC	-12.3%
Thrust	+14.3%
Fan Diameter 88 in	+25%
Total LP Stage Count	5

Figure 2.8: Architectural differences between a geared and a direct drive turbofan at the same bypass ratio. [7]

2.4 Geared Turbofans

In searching for lower fuel consumption, weight and cost, as well as noise and emissions reduction, the jet engine manufacturers have reached the limits of the boundaries in the conventional turbofan designs. Nowadays, the requirements keep becoming more and more optimistic; thus the manufacturers are pushed to introduce a step change in the turbofan engines architectures. An up-and-coming concept that has been investigated for three decades is the introduction of a gearbox between the fan, acting as the slow spinning side, and the low-pressure compressor (LPC) and the low-pressure turbine (LPT), acting as the fast spinning side. This brings to a decoupling of the fan rotational speed from the rest of the low-pressure spool turbomachinery and allows an additional degree of freedom to optimise the turbomachinery independently. The fan rotational speed and pressure ratio are reduced, whereas the LPC and LPT rotational speeds are increased, bringing these elements to higher efficiencies and lower number of airfoils. [18]

Wilfert, in Reference [18], considers the utilisation of a gearbox very interest-

ing because it allows reducing the specific thrust in turbofans, since the fan is enabled to increase in size, given its ability to rotate at a lower rotational speed relative to a direct drive case, thus avoiding transonic losses at the tip. The reduction in specific thrust improves consequently the propulsive efficiency of the turbofan and reduces its specific fuel consumption. The technological level required for the realisation of a geared turbofan is very high, but engine manufacturers are looking at it with more and more interest. Some of them have managed to realise models that are already flying nowadays, such as the Pratt and Whitney PW1000 family.

2.4.1 Comparison with Direct Drive Turbofans

Applying the concept of very low specific thrust to a direct drive engine creates some limitations due to the weight, length and cost increase of the LPC and LPT.

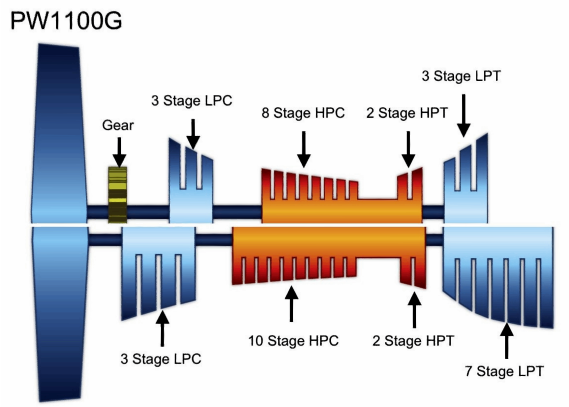

Figure 2.9: Comparison between a Direct Drive Turbofan (below) and a Geared Turbofan (above). [19]

In a direct drive architecture, the size increase in the fan and the consequent reduction in spool speed of the low-pressure shaft brings additional stages in the LPT turbine, as it is noticeable from Figure 2.9. This is because both the LPC and the LPT have to provide the work required by a bigger fan with lower rotational speed; therefore a higher number of airfoils and stages is required. The issue

presents the opportunity to use a gearbox between the fan and the LPC and LPT in order to decouple their rotational speeds and not limit the high-speed side, thus reducing length, weight and cost of the engine. The advantage of reducing the number of LPT stages is impaired by the additional weight of the gearbox. Overall, the reduction in LPT weight overcomes the addition of the gearbox, causing a clear advantage in terms of length and weight in the geared architecture relative to the direct drive [18].

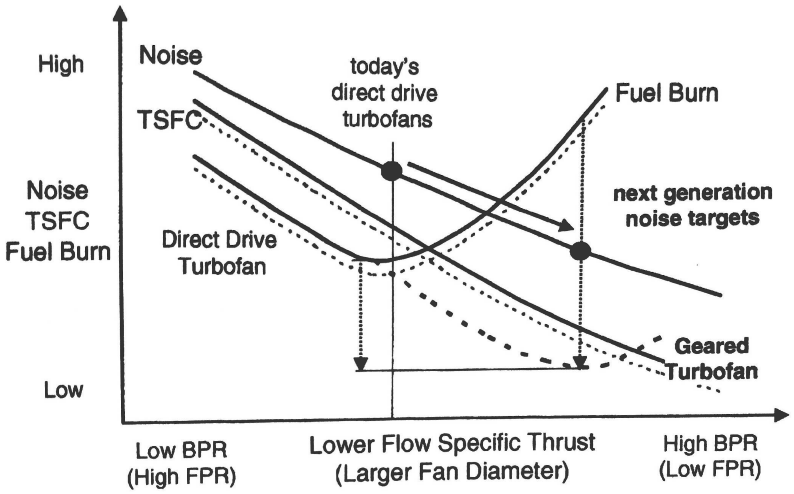

Figure 2.10: Comparison between a direct drive and a geared turbofan in terms of noise, TSFC and fuel burn as a function of specific thrust.[18]

In Figure 2.10 it is enlighted the fact that a geared turbofan presents the minimum fuel burn at a lower specific thrust, corresponding to a higher fan diameter, so it allows us to go beyond today's values and achieve advantages in terms of specific fuel consumption and noise emissions.

2.4.2 LPT considerations

The adoption of a gearbox allows to reach the optimal rotational speed in the LPT; therefore causing a reduction in the stage count to roughly half relative to a conventional direct drive configuration [18]. Given the higher rotational speed of the LPT rotor, the disks are subjected to higher centrifugal loads leading to an

increase in weight. Nevertheless, because of the lower number of stages and airfoils, the overall LPT weight of the geared configuration is lower than the equivalent in a direct drive configuration. Reference [18] enlights that, at an optimum bypass ratio for both the cases, the weight of the LPT in a geared configuration can be reduced down to 70% of the direct drive configuration.

The high rotational speed allows the LPT to be able to achieve higher specific work output per stage compared to a conventional configuration. A direct consequence of this is that the aerodynamic loading $\Delta H/u^2$ can be kept into values that are lower compared to the direct drive case. This enables the LPT turbine within a geared configuration to reach a higher efficiency relative to the direct drive.

The rotor high rotational speed presents a considerable challenge from the mechanical point of view in the design of a geared turbofan LPT. In fact, the centrifugal load to which the LPT disk is subjected is proportional to AN^2 (with N as rotational speed and A as annulus area); thus it is directly affected by the increase in rotational speed. [18]

2.4.3 Power gearbox

The power gearbox, within a turbofan, is a component that can undoubtedly enable significant advantages compared to direct drive architectures, but it is a complex mechanical system that requires a meticulous design.

The position of the power gearbox in the turbofan architecture is between the IPC and the Fan. According to Reference[20], the major components in a power gearbox are:

- fixed star gear support
- sun gear coupling diaphragm
- sun gear

- planetary gears
- ring gear
- lubrication system

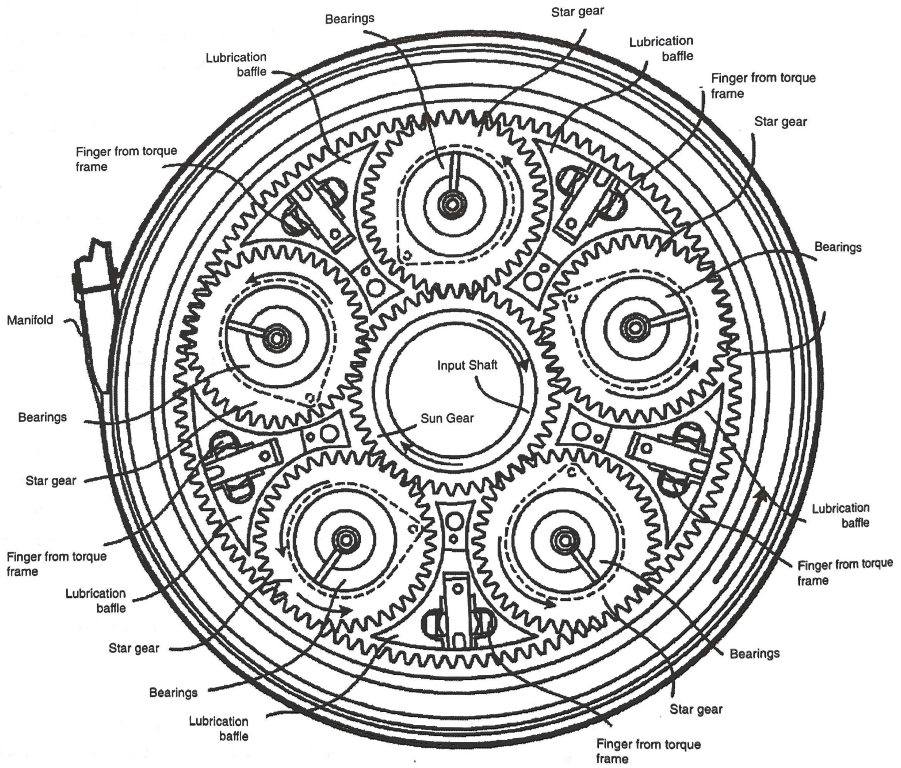

Figure 2.11: Cross-sectional representation of a power gearbox. [21]

Observing Figure 2.11, at the centre the sun gear rotates with a fixed position, while the planetary gears rotate all around it and are connected to it through the planet carrier. The ring gear, the largest of the concentric rings, encompasses the planetary and the sun gears [22][23].

The number of revolutions of each gear relative to the other is known as the gear ratio [22]. As an example, a gear ratio of 3:1 means that the planetary gears can achieve 3 revolutions for each complete revolution of the sun gear. According to References [22][23] the gear ratio is dependent on the ratio between the number of teeth on the input gear and the number on the driven gear. By varying the

number of teeth and the torque applied to the power gearbox, it is possible to obtain the maximum efficiency from it.

The type of gearboxes used for the geared turbofans applications has an architecture with an epicyclic gear. This choice is made because this set configuration guarantees optimum performance in a relatively compact size [11]. These gearboxes are typically single stage non-differential epicyclic gearboxes [11], which means that all the gears are free to move, except one that is fixed. In Reference [24], 3 principal arrangements for epicyclic gears are indicated: star, planetary, solar.

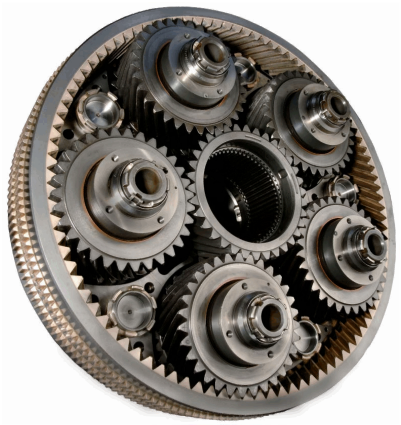

Figure 2.12: The power gearbox of the Pratt&Whitney PurePower family engines.[25]

Reference [23] explains the advantages and disadvantages of epcyclic gear systems. The main advantages are:

- the load can be shared between several gears,
- the arrangement is compact and efficient in terms of space and weight,
- the concentric rotation of input and driven gears reduces the bending moment caused by the radial forces;

however, on the other hand, there are disadvantages:

- the design is complex,

- in the case of a non-inline assembly, it requires additional gears.

One of the most advanced power gearbox systems is installed on the Pratt & Whitney engines of the family PurePower. As it can be seen in Figure 2.12, it is an epicyclic gearbox setup with 5 planet gears.

2.5 Axial and centrifugal compressors

A turbofan can be considered as a combination of various components to deliver a required thrust for a specified mission delivered by a specific aircraft. This generic definition gives equal importance to all the components within the system, but an engine can be seen as an organism that has vital organs. In the mechanical case of a gas turbine the vital organs are represented by turbomachinery: compressors and turbines.

Peviously, there have been enlightened differences in the LPT system between geared and direct drive turbofans and this is one of the main comparisons that are an object of this project. Moreover, a second significant comparison regards the high-pressure compression system (HPC). In fact, one of the objectives of this project is to assess two different architectures of HPC: axial and axi-centrifugal.

This section aims to give a general explanation of the principal aspects of axial and centrifugal compressors, enlighting the differences and the similarities between the two systems.

2.5.1 Axial compressors

Being one of the most critical components in a gas turbine, the axial compressor has been studied for many years, and it is continuously at the centre of the focus of many studies that have brought this component to improve considerably

through the years. Consequently, there are thousands of finely written books and papers about the topic. Among these, References [26] and [27] are widely recognised as the most significant books concerning axial compressors.

The compression in an axial turbomachinery is composed of two parts: firstly the fluid is accelerated and then it is diffused; therefore the result is a pressure increase. The acceleration is accomplished by the rotor, while the diffusion is obtained by the stator. The increase in velocity is converted into an increase in pressure thanks to the diffusion process [26].

An axial compressor is usually a multistage machine and the pressure increase obtained by the fluid through each stage is limited, therefore, in order to obtain the high pressure ratios that are present in the modern turbofans, several stages are necessary [27], as it can be seen in Figure 2.13.

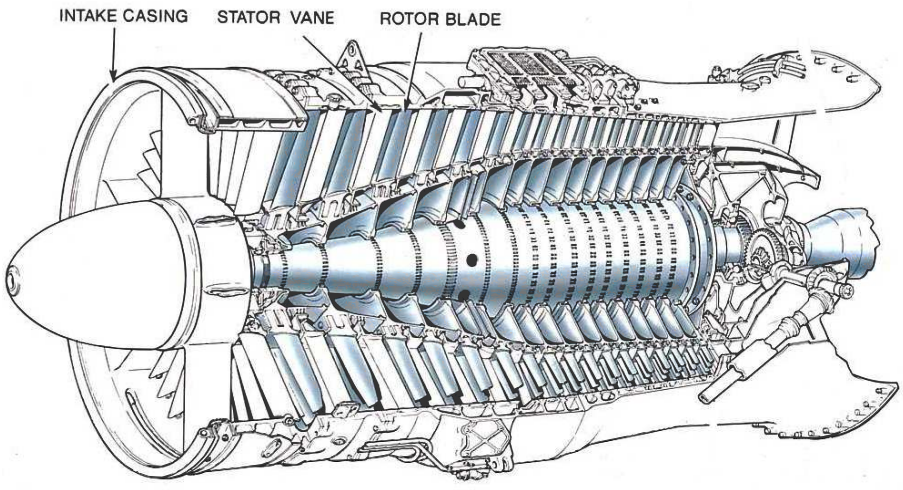

Figure 2.13: A typical multistage axial compressor [28]

In Figure 2.14 it is depicted how the properties of the fluid change through an axial compressor. It can be seen that the total pressure and temperature are continually increasing through the stages, because the rotors are doing work onto the fluid, increasing its energy. The static pressure increases as well, and this represents the principal objective of an axial compressor. It has been explained that the principle of working of an axial compressor is to accelerate and decelerate

the fluid in order to increase its pressure. That is explicitly confirmed by the velocity trend that increases through the rotor blades and decreases through the stator blades.

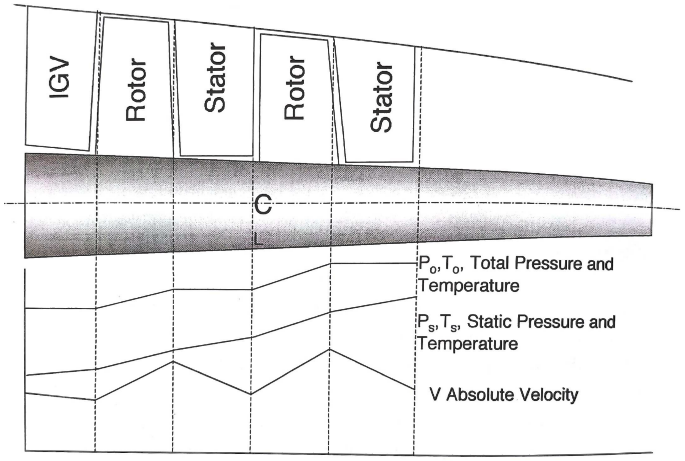

Figure 2.14: Variation of the properties of a fluid moving through the stages of a multistage compressor. [29]

2.5.2 Centrifugal compressors

A centrifugal compressor increases the pressure of a fluid firstly by accelerating it through a rotating impeller, then by converting the kinetic energy into pressure [30]. In Figure 2.15 it is represented a schematic of a centrifugal compressor. The fluid enters in the centre and is radially accelerated by the rotation of the impeller. The deceleration happens in the diffuser by changing the direction of the fluid. The fluid is then ejected through a discharge nozzle [30].

Centrifugal compressors find various applications in industrial engineering, but they are also used in gas turbines with a range of pressure ratios that goes from 3:1 to 7:1 [29].

Typically, centrifugal compressors are designed in such a way that the pressure rise is divided half in the impeller and half in the diffuser [29].

The function of the impeller is to introduce energy into the fluid, and it is constituted by 2 parts: an inducer, that collects the flow entering into the compres-

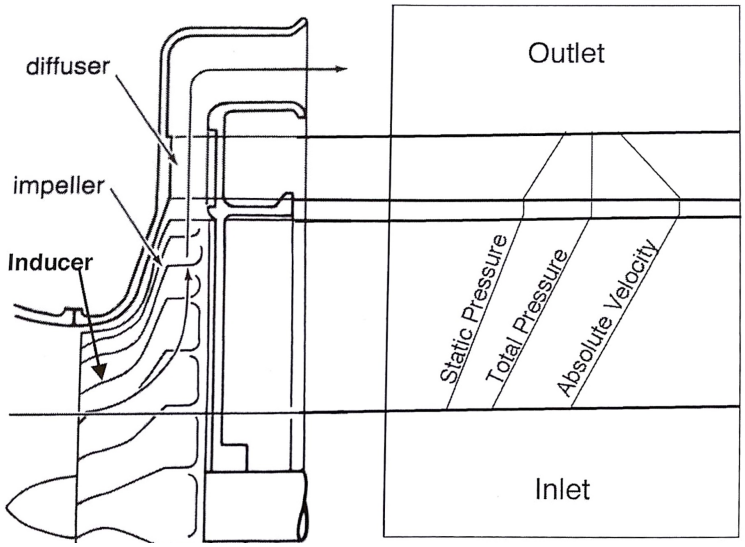

Figure 2.15: A sectional view of a centrifugal compressor and the thermodynamic and aerodynamic properties of the fluid. [29]

sor and the radial blades that provide the energy to the fluid by centrifugal force [29][30].

The function of the diffuser is to convert the kinetic energy into pressure rise. This is the essential part of a centrifugal compressor, but usually also the most complicated to design. The design of the diffuser consists of vanes passages that diverge, therefore the velocity of the flow is reduced and converted into pressure[29].

In comparison with an axial compressor, the centrifugal is shorter but has a larger diameter; moreover the flow is turned from the axial direction by 90^o. While the centrifugal is able to provide a pressure ratio higher than 4:1 in a single stage, the axial compressor have a pressure ratio around 1.4:1 [31]. So, at equal pressure ratio, more stages of axial, so more weight, are required, while a single stage centrifugal can be used.

A peculiar characteristic of centrifugal compressors is that they can recover from a surge condition relatively easily, while for an axial compressor this condition is catastrophic [31].

In terms of efficiency, Reference [29] indicates the axial compressor as more

efficient relative to the centrifugal. The same does Reference [31], but he claims that the efficiency of centrifugal compressors can potentially be higher in the future if the same effort is invested in research as it is done for axial compressors.

2.5.3 Axi-centrifugal compressors

Generally, axial compressors are used in conventional turbofans. It is well known and widely demonstrated, in References [6], [10],[13] , that one way to improve the overall efficiency of a gas turbine is to increase the OPR. By using axial compressors, this means increasing the number of stages, consequently the length, weight and size of the engine. This can bring a weight penalty that reflects in higher fuel burn despite the improved efficiency of the engine itself. A solution to reduce the weight penalty induced by higher OPR is to move from a ”full-axial” architecture to an ”axi-centrifugal” one in the HPC. This configuration is realised by the combination of one or more axial stages with a centrifugal stage[32].

The centrifugal compressor allows pursuing higher OPR without increasing the number of stages furthermore; therefore realising shorter and more efficient engines. On the other side, the diameter of the engine may increase because of the important radial dimension of the centrifugal compressor. Typically, in designing axi-centrifugal compressors, engine manufacturers tend to increase more the aerodynamic loading on the centrifugal side rather than the axial, pursuing the benefits from the stability and performance robustness of the radial compressor [32]. High loadings on the centrifugal compressor also mean high weight of the disc and diameter of the compressor, so it is important to understand the limiting point above which the weight penalty of the centrifugal compressor becomes relevant and detrimental for the efficiency improvement. This represents one of the objectives of this project, that is understanding the weight and size improvements and limitations that are introduced by the utilisation of a centrifugal compressor and realise how they affect the efficiency and the fuel burn of the engine.

2.6 Variable Area Fan Nozzle

It has been demonstrated previously that one of the methods for having more efficient turbofans is to decrease the specific thrust, this is done by increasing the fan diameter and leads to an increase in bypass ratio and a decrease in fan pressure ratio (FPR). This can lead to difficulties in the operability of the fan. In fact, several References ([33], [34], [35], [36], [37]) agree in indicating a FPR of 1.45 as the minimum below which there may potentially be the problems of surge and flutter of the fan.

The critical point for the surge and flutter of the fan is represented by the take-off condition. In fact, at low Mach numbers the ram compression at the engine's intake is reduced and this, combined with low values of FPR, brings a pressure ratio at the bypass nozzle that is lower than the critical one, causing the bypass nozzle to unchoke. An unchoked nozzle has a reduced flow capacity; therefore the operating line of the fan moves towards the surge line in the fan map [11][38]. This phenomenon can be graphically seen in Figure 2.16, that represents the fan map for a very low specific thrust engine. It is clear that at take-off conditions the operation point moves above the surge line of the fan, therefore the engine cannot be safely operated.

Generally, the solution to this problem may be found in the implementation of a variable area fan nozzle (VAFN). This solution allows to control and augment the flow capacity of the fan nozzle at take-off by increasing its area, leading the operating point back to the stable zone of the fan map [8][11][38]. Figure 2.17 shows a tested and a prototype application of the VAFN concept for very low specific thrust turbofans. Despite its clear advantage in terms of fan operability, the VAFN system adds weight, drag and complexity to the engine. It has actuators and weight that have to be scaled based on the dimensions of the engine itself. Consequently, there is the necessity to assess the real advantages and compro-

mises of this component and this represents one of the objectives of this project.

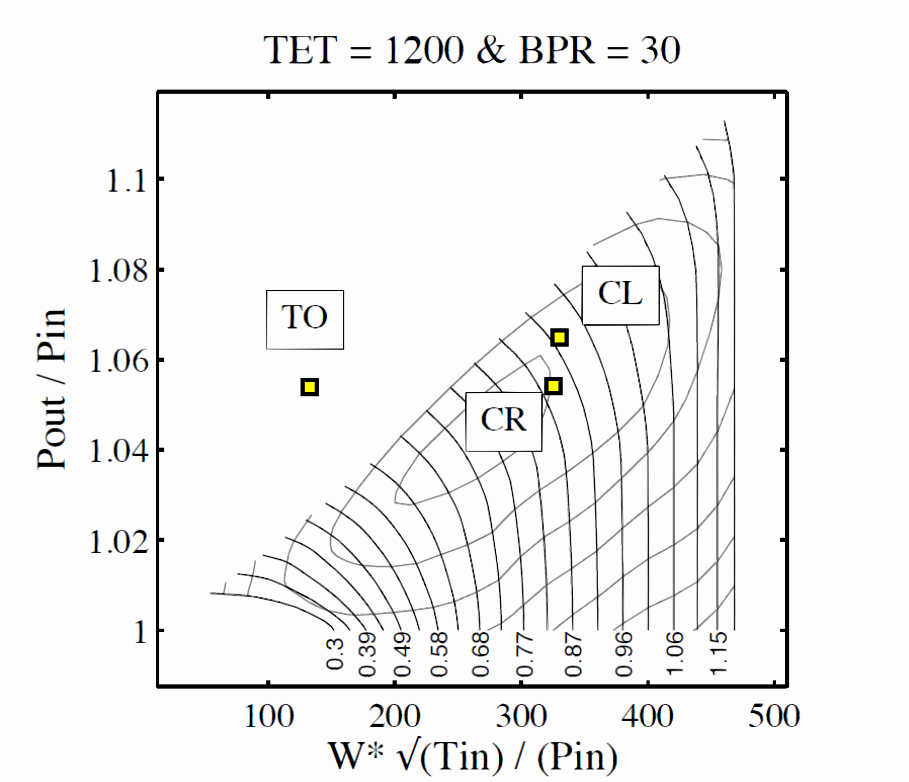

Figure 2.16: Fan map for a very low specific thrust engine with 3 operation points: Take-off (To), Cruise (CR), Climb (CL). [8]

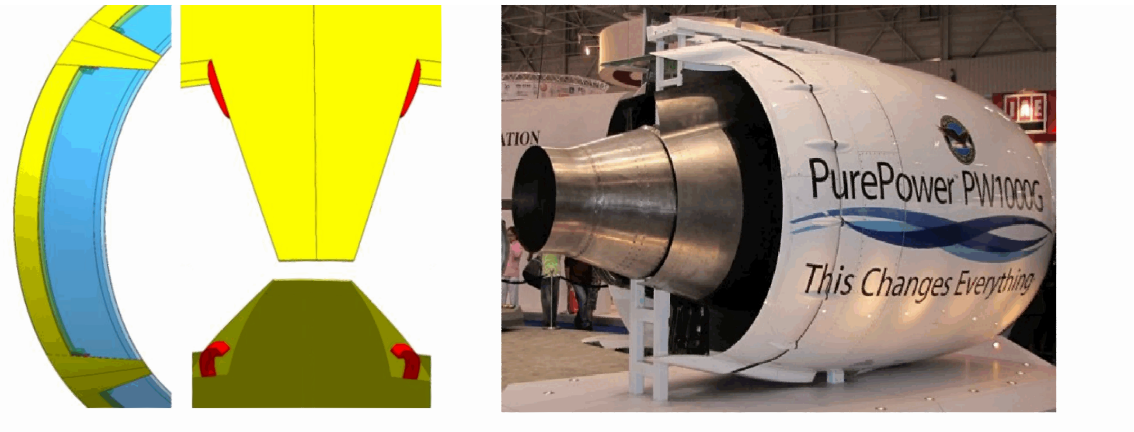

Figure 2.17: Left: Prototype of a VAFN with flaps mounted on inclined fixture elements [39]. Right: Pratt&Whitney PW1000G with VAFN [40]

2.7 State-of-the-art turbofans

The turbofan architectures that are defined ”alternative” in this project in some cases have already been developed, but they are not as much diffused as the direct drive fully axial HPC one, that represents the most utilised turbofan configuration for civil aircraft nowadays. Therefore, it is significant to provide some examples of the effective applications of the alternative architectures considered in this project.

Regarding the geared turbofans, NASA started looking at the development of this architecture alredy in 1977 with the QCSEE project [20]. The aim of this project was to provide two geared turbofan architectures for civil applications designed for being installed over or under the wing.

Over the years, different tests were conducted in order to assess the feasability of this architecture, but few cases resulted in an effective application of it in civil aircraft turbofans. An example of geared turbofans utilised nowadays is represented by the Pratt&Whitney PurePower family of engines, which first flight can be dated back to 2016 [41]. In Figure 2.18 it is represented a longitudinal view of a component of this family, in which is clearly visible the position of the PGB between the IPC and the fan. Moreover, the presence of the PGB allows a configuration of the LPT with only 3 stages. It can be seen from Figure 2.17 that the one of the components of the PurePower family of engines has been designed with a VAFN configuration as well. Nevertheless, the manufacturer did not consider profitable to proceed with its development; therefore it remains just a prototipe at the moment.

A peculiar example of a geared turbofan equipped with an axi-centrifugal compressor is the Honeywell TFE731. It is a two-spool turbofan specifically designed for business jets, but it has also some military declinations. As it can be seen in Figure 2.19, the low-pressure compressor is full axial and presents 4 stages,

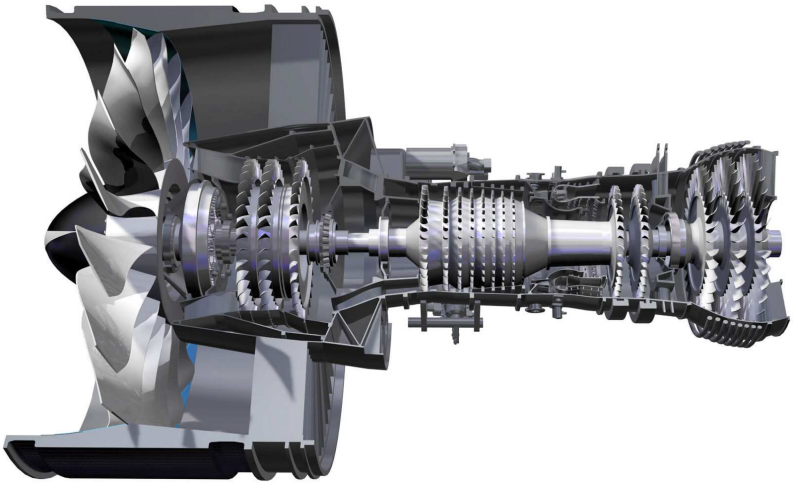

Figure 2.18: Longitudinal section of a PW1000G. [42]

while the high-pressure side is represented by a single stage centrifugal compressor. The HPT is a single stage while the LPT can have 3 or 4 stages, depending on the engine version [43]. Another peculiar characteristic of this engine is represented by its combustor. In fact, considering the flow exiting radially from the centrifugal HPC, in order to reduce the length and the losses introduced by a duct that brings the direction back to axial, a reverse flow combustor is adopted. In this way, the flow is brought back to the axial direction while the combustion process happens.

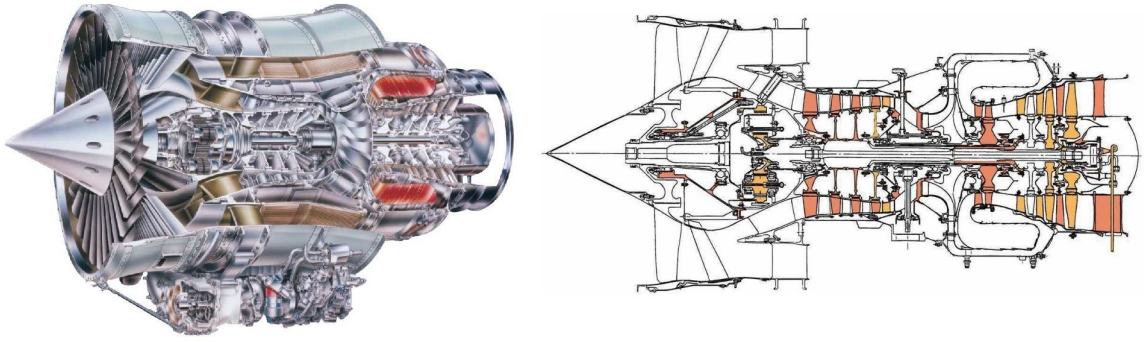

Figure 2.19: Sectional[44] and longitudinal[45] view of a TFE731 .

Considering the area of application of this engine, it is essential to minimise the mission fuel burn and the maintenance cost. This explains the choice made by Honeywell to use a centrifugal HPC and a gearbox because it reduces the

weight, the manufacturing and the maintenance cost of the engine, due to the reduced number of components, as it is claimed by Reference [46]. In Table 2.1 are summarised some of the performance and design data of a TFE731-60.

Performance

	Net Thrust	TSFC
Thermodynamic, Sea Level, Static, ISA	5500 lb	0.405
Takeoff, Sea Level, Static (Available to 87° F)	5000 lb	0.405
Max Cruise, 40,000 ft, Mach 0.8 (ISA)	1120 lb	0.679

Design Data

Pressure Ratio:	Fan: 1.70	Cycle 22
Basic Engine Weight:	988 lb	
Bypass Ratio:	3.9	
Bleed Air Flow:	10% Core Flow (max)	
Airflow:	187 lbs/sec	
Service Ceiling:	51,000 ft	
Airstart:	35,000 ft	
Starting:	Electric	
Accessory Power Extraction:	45 hp(max)	

Table 2.1: Performance and design data of a TFE731-60 [46].

Chapter 3

Methodology

In this chapter it is described the workflow followed in the realisation of this project. The chapter starts with a description of the investigated design space, it follows a explanation of the procedures utilised for the design space exploration and optimisation. Afterwards, it is described the procedure that brings to the weight and size estimation and mission fuel burn calculation.

3.1 Overview

As it has been declared previously, the design space investigated by this project regards the Middle-of-Market turbofan category. The airframe investigated is an Airbus A321 type, Figure 3.1, and the mission targeted has a range of 3000 nm.

The engine design process satisfies the thrust requirements, shown in Table 3.1, in 3 critical points of the mission: take off, top of climb and cruise. The altitudes, Mach numbers and EOR thrust value for a typical A-321 aircraft have been found in Reference [47]. From this last value, the CRZ thrust has been derived using T_{EOR}/T_{CRZ} in Reference [11]. Eventually, the ToC thrust requirement has been derived from the ratio T_{ToC}/T_{CRZ} in Reference [8].

The realisation of this project has involved the utilisation of the EPYDOSIS

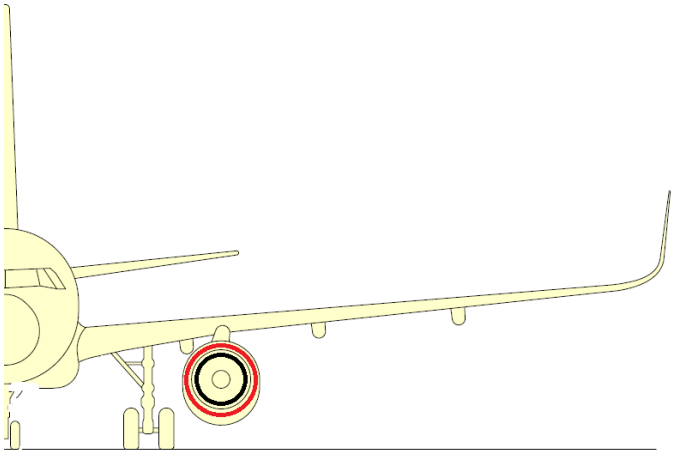

Figure 3.1: Frontal view of an Airbus A321 taken as the reference aircraft model for this project. In red and black are indicated the fan dimensions analised during the optimisation process. [47]

	CRZ	ToC	EOR
Altitude [m]	10668	10668	0
DT amb [K]	0	10	15
Mach	0.82	0.82	0.25
Thrust [N]	20500	26000	105000

Table 3.1: Thrust requirements in the main operating points.

(Engine Preliminary Design Optimisation) platform, that is schematically described in Figure 3.2, designed by the Cranfield University UTC for aero civil engines studies [11]. The general platform presents a wide range of capabilities, reduced in this project to the case study interest.

The workflow begins with the definition of the initial inputs, mostly regarding the requirements of the baseline aircraft. In particular, in this phase are specified the range, the flight envelope, the mission and the thrust requirements of the specified aircraft type.

The following step regards the engine simulations from two points of view: the thermodynamic and the mechanical. In the simulations work the first step is the cycle design and optimisation, that gives a Pareto front of optimum individuals in terms of minimum cruise SFC and maximum specific thrust simultaneously, that

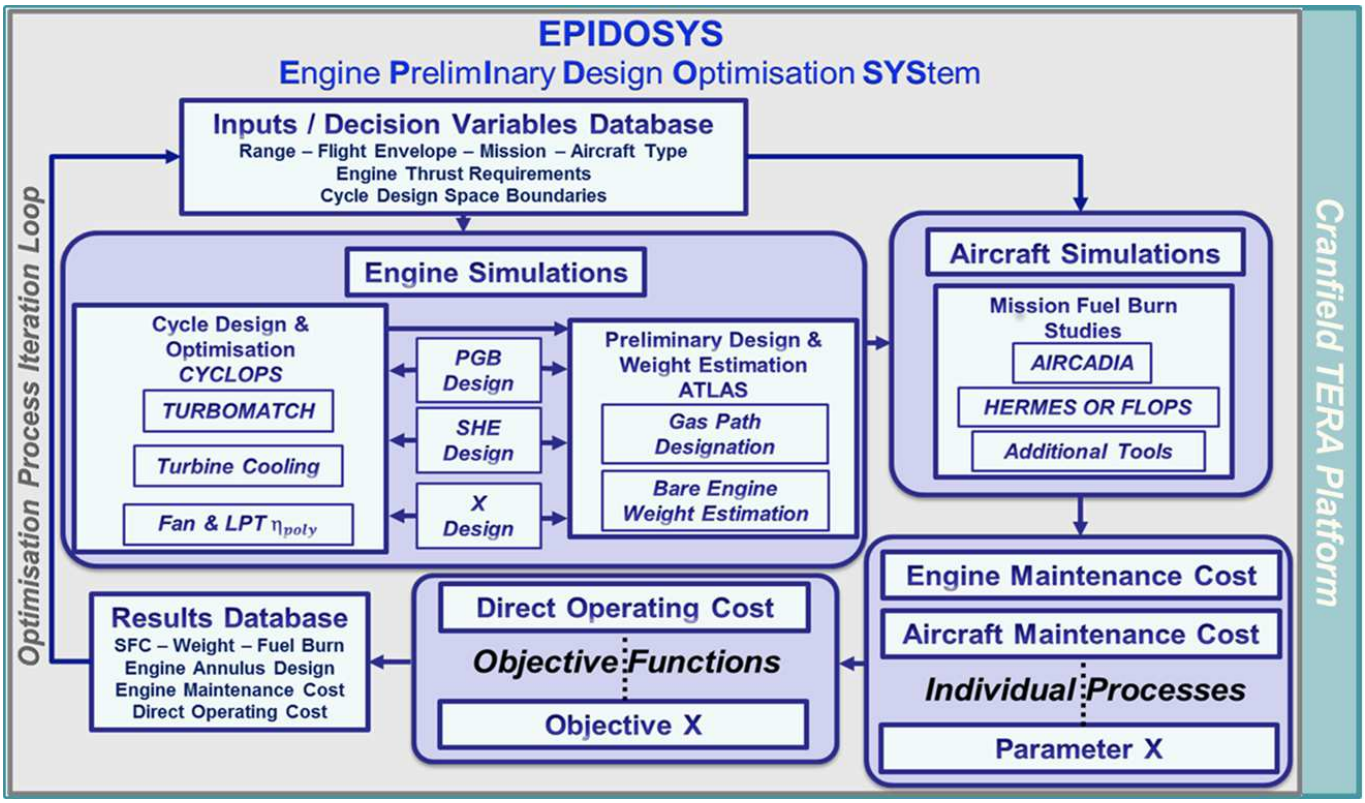

Figure 3.2: The EPIDOSYS platform from which the modules utilised in this project are derived. [11]

respect the thrust requirements previously defined. Consequently, the thermodynamic cycles are converted into plausible engines through the utilisation of the Cranfield University in-house software ATLAS, a modular code that has the capabilities to estimate the weight and size of the main components of a turbofan [48].

Once the engine simulation phase is concluded, there are available a set of thermodynamic and mechanical data the determine the operation and the size of the engine in the uninstalled condition. Therefore, in order to asses the engine for fuel burn, there is the necessity to install it virtually on a proper aircraft and make it perform a typical mission. This is done by the utilisation of the NASA FLOPS software, that is able to calculate the installed performance of an enigne including weight, drag, installation constrains and interference between the nacelle and the wing [49].

The end of this process leads to a set of output data regarding SFC, weight, mission fuel burn and annulus design of the optimal engines for the given mission requirements.

3.2 MoM engines cycle design optimisation

It can be seen from Figure 3.2 that the start of the workflow of this project is represented by the cycle design optimisation. This is operated through the EPY-DOSIS module called CYCLOPS, described in Figure 3.3. CYCLOPS is based on a PYTHON coded Non-Dominated Sorting Genetic Algorithm II (NSGA II), explained in details in Reference [50].

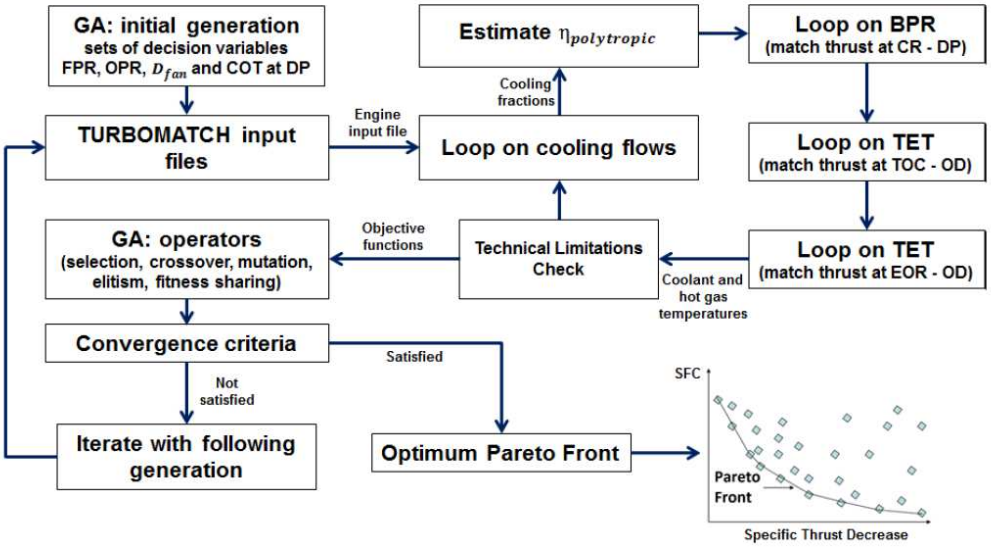

Figure 3.3: Schematic representation of CYCLOPS. [11]

Being a genetic algorithm, CYCLOPS backbone is represented by 3 categories of parameters: decision variables, constraints and objective functions. The range decision variables and the constraints values need to be defined as an input, while the objective functions require just a definition of ”maximum” or ”minimum” to allow the optimiser to choose the right individuals. The set of decision variables, constraints and objective functions utilised for this project can be seen

in Table 3.2.

Decision Variables	Constraints	Objective Functions
Fan Diameter	W max ToC	SFC
OPR	W min ToC	Specific Thrust
Fan tip PR	Cooling fractions	
TET	T30	
(VAFN)	TET	
	T41	

Table 3.2: Set of decision variables, constraints and objectives for the cycle optimisation system.

The range of fan diameters has been defined considering the ground clearances of a typical MoM aircraft, while OPR, fan tip PR and TET are decided on considerations about the modern technological level of engine manufacturers. The VAFN is a decision variable only in the models that are equipped with this component. The decision variables values are referred to the design point condition, except the VAFN that is used only during the take off for the safe operability of the fan.

The constraints are specified considering modern technological limitations of engine manufacturers, since this project is looking at engines that can potentially be introduced in the market in the near future.

Since the primary aim of this thesis is to provide an engine model optimised for mission fuel burn, the SFC needs to be minimised during the optimisation process; therefore the minimum SFC individuals for each value of specific thrust are considered.

Each combination of the decision variables gives an engine model that is then introduced in TURBOMATCH, a Cranfield University in-house software capable of simulating engine performance in design and off-design conditions [51]. If the model can be simulated in the 3 points of interest (CRZ, ToC and MTO), then the results in terms of SFC and specific thrust are stored. If the model can't be simulated in the 3 points, it is discarded.

3.2.1 MoM enignes simulation

The software used to simulate all the engine cycles is TURBOMATCH, a Cranfield University prorietary code, written in FORTRAN in 1974 [51], capable of assessing engine performance in design point, off-design and transient. The off design calculation, as well as the transient, is based on the balance in mass and energy among all the engine components carried out iteratively. The component behaviors in design point and off design are described by the experimentally derived maps included in the software library [51].

The engine architecture is built through bricks. Each brick represents a single component in the engine and it simulates the behavior of it. The combination and the simulation of each component gives the final performance of the enigne in terms of gross and net thrusts, specific fuel consumptions, specific thrust and fuel flow. Each brick has an inlet and an outlet station to position it into the engine architecture. Moreover, it is described by the brick data that contain the properties of the component represented. Depending on the brick characteristics, it can require additional engine vector data and deliver engine vector results [51].

The modularity given by the bricks allows TURBOMATCH to carry out performance evaluations for various engine architectures. This represents the main motivation for the use of TURBOMATCH for a project in which different engine architectures are involved.

3.2.2 Engine models

Since the project involves the introduction of alternative engine architectures, it is useful to compare these with conventional ones in order to understand what are the advantages. Therefore, in this project, 6 different engine models will be considered:

- Axi-centrifugal HPC Geared Turbofan with Variable Area Fan Nozzle (**AXC**_

GEAR_VAFN),

- Axi-centrifugal HPC Geared Turbofan with Fixed Area Fan Nozzle (**AXC_GEAR_FIX**),
- Axi-centrifugal HPC Direct Drive Turbofan with Variable Area Fan Nozzle (**AXC_DD_VAFN**),
- Axi-centrifugal HPC Direct Drive Turbofan with Fixed Area Fan Nozzle (**AXC_DD_FIX**),
- Axial HPC Geared Turbofan with Fixed Area Fan Nozzle (**AX_GEAR_FIX**),
- Axial HPC Direct Drive with Fixed Area Fan Nozzle (**AX_DD_FIX**).

The models reflect the combination of the different alternative architectures that this project aims to assess: axi-centrifugal HPC, PGB and VAFN. This number of cases has been chosen in order to understand and explain what changes in performance and size are introduced by each one of the alternative architectures.

In order to assess the advantages, relative to a conventional case, introduced by the utilisation of an axi-centrifugal HPC, two of the models are replicated with fully axial HPCs.

Moreover, for the axi-centrifugal cases, the models are realised with and without a VAFN, to understand if this solution is able to give some real advantages.

Eventually, the models are equally divided between geared and direct drive to assess the effects introduced by the adoption of a PGB in different architectures.

Figure 3.4 presents a schematic representation of the baseline turbofan model utilised in this project with the indication of the architectural alternatives studied in this project.

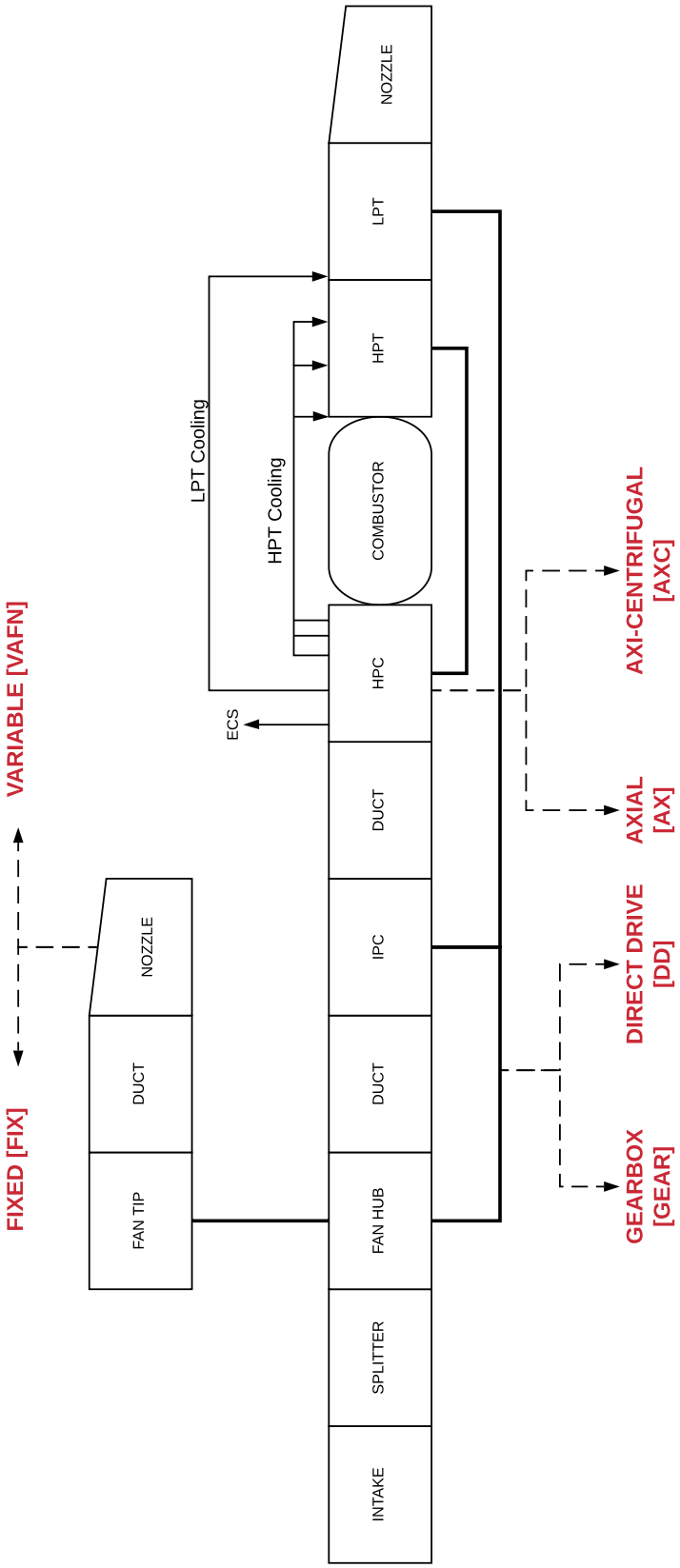

Figure 3.4: Schematic representation of the baseline turbofan model utilised in this study with the architectural options in red.

A common characteristic of all the models is the inlet. The division between the air mass flow that enters into the core and the part that enters into the bypass is realised through a splitter positioned immediately behind the intake. This splitter divides the mass flow entering the engine according to the bypass ratio value that is given to the model. Downstream there is the fan. It represents the primary protagonist of the performance of a turbofan, and it is important to simulate it as close as possible to the reality, in order to capture with high confidence the behaviour of the engine itself. As it can be seen from Figure 3.5, a fan blade doesn't present the same pressure ratio along its span, but has a higher one at the tip and lower at the hub. TURBOMATCH is a 0-D code, therefore it is not able to catch this difference in pressure ratio along the blade. In order to estimate as much realistically as possible the fan performance, it is divided into two bricks, a hub and a tip, which are treated by the code as two different compressors, with two different maps.

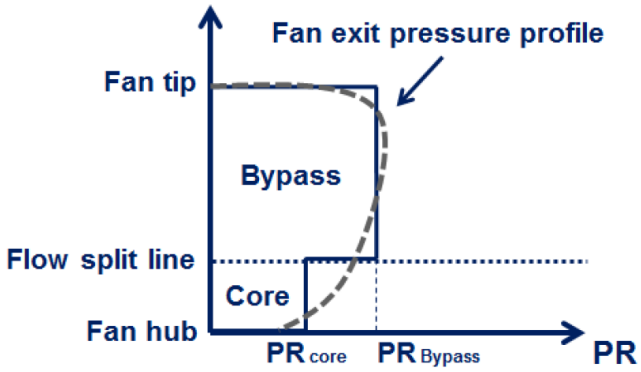

Figure 3.5: Pressure distribution along the span of a fan blade. [11]

Another significant aspect of the engine models realisation is the design of the secondary air system. As it has been stated in precedence, turbine cooling is one of the most important aspects that has led to the efficiency improvement of gas turbines along the years. It is equally essential to simulate them in the adequate manner and to choose the right position within the engine model. In this case, the positions of the cooling bleeds are different between the axial and

the axi-centrifugal models. In the full axial models, the HPC is divided into 4 parts and in each one of the separations there are bleeds exporting cool air to the turbines. The turbine stage in which the cooling air is transferred depends on the pressure and the temperature that are present at the position in which the bleed is in the compressor. Undoubtedly, the pressure of the station in which the bleed is positioned should be higher than the one in which the cooling air is delivered and the temperature should be low enough to guarantee the right heat exchange without requiring high amounts of mass flow from the compressor.

In the axi-centrifugal model, since the number of axial stages is reduced thanks to the introduction of the centrifugal stage, the position of the bleeds can't follow the same scheme as the full-axial configuration. In fact, in this case, the separation between the axial and the centrifugal compressor becomes a useful position for the low-pressure bleeds and the rest of them are located behind the centrifugal HPC. Here there are the bleeds for the HPT rotor and NGV cooling.

The geared models present an appropriate bleed for the cooling and the sealing of the power gearbox that is located before the HPC position.

In the VAFN models, the exit area of the bypass nozzles becomes a variable that changes during the EOR phase to simulate its opening.

3.2.3 Thermodynamic cycle design

Starting from the specified mission requirements, there's the need to design the thermodynamic cycle that allows to respect them. As it has been stated previously, this project follows a three-point design process. Among these conditions, the cruise (CRZ) is chosen as the design point, while the other two are treated like off-design cases.

To design an engine specific targets and limitations are required. The targets are set by the aircraft manufacturer that needs a determined engine to perform a specified mission. On the other side, the limitations can be determined by dif-

ferent aspects. From the structural point of view, the ground clearances of the aircraft on which the engine is designed to be installed can set the limits in terms of fan diameter and overall size of the engine. From a cycle point of view, there are constraints on the operating temperatures set by the turbine cooling techniques and material limitations. Eventually, there are constraints on the efficiency values of the components within the engine given by the technological level of the manufacturer.

The thermodynamic cycle design follows the process created by Mourouzidis and explained in details in Reference [11]. This process involves the building of an engine performance model and its simulation through TURBOMATCH matching the thrust requirements at design point and in the two off-designs. The outcome of this process is a set of output parameters for different fan diameters that creates the design space of interest.

It is important to specify that in this project it is considered constant the ratio of pressure ratios in the core compressors, since it is out of scope an optimisation based on the core compressors work split.

The polytropic efficiency of the HPT is considered constant as well among all the engine architectures investigated. This is due to the fact that the HPT turbine is the only component that remains invariant among all the models; therefore its characteristics don't deviate considerably. Eventually, a polytropic efficiency suitable for the considered technological level has been adopted and kept constant.

For the models equipped with an axi-centrifugal HPC, the polytropic efficiency estimation of the centrifugal section is based on the results carried out from ATLAS.

3.2.4 Turbomachinery efficiencies estimation

The performance of a gas turbine is highly dependent on turbomachinery efficiencies. Therefore, it is essential, in order to achieve as much realistic results as

possible, to correctly estimate the efficiencies.

In turbomachinery, there is a primary distinction between mechanical and thermodynamical efficiencies. This project focuses on the thermodynamic aspect of the efficiencies; therefore the mechanical ones are considered constant and strictly related to the technological level of the manufacturer. In the thermodynamic side, there are two principal elements: isentropic efficiencies and polytropic efficiencies.

The isentropic efficiency evaluates how near to the ideal work is the one that the turbomachine is doing [26].

The polytropic efficiency can be considered as the value of the isentropic efficiency of a single stage with a pressure ratio that is infinitesimally higher than unity [26].

The fan tip polytropic efficiency estimation is based on the process developed by Mourouzidis in Reference [11]. This process considers the fan tip polytropic efficiency as a function of:

$$\eta_{fan\,tip\,poly} = f(a, b, \gamma, M_{rel\,fan\,tip}, FPR, \psi_{fan\,tip}) \tag{3.1}$$

where a and b are constants. The parameters from which $\eta_{fan\,tip\,poly}$ depends are known for each combination of decision variables during the cycle design optimisation process.

The axial compressor polytropic efficiency estimation process utilises a Cranfield University UTC in-house PYTHON code based on the information and equations found in References [10] and [26]. The process starts with multiple inputs regarding flow properties at the inlet as well as geometrical characteristics of the compressor. Afterwards, the number of compressor stages is calculated and it follows a stage by stage design process that defines the de Haller numbers, Mach numbers distribution and the space-to-chord ratios. Eventually, rotor and stator

blades are designed and their efficiency is estimated taking into consideration profile, secondary and annulus losses. Once the efficiencies of the blades are calculated, the polytropic efficiency of the whole compressor can be estimated.

The LPT polytropic efficiency estimation is again based on the method developed and explained in details by Mourouzidis in Reference [11]. This process estimates the LPT polytropic efficiency based on the Smith diagram, in Figure 2.6, therefore the stage flow factor $\phi = V_a/U$ and the stage loading factor $\psi = \Delta H/U^2$ are necessary. For the geared models the stage loading factor is considered constant through the whole turbine and equal to $\psi_{LPT\ stage\ mean}$; therefore the flow factor is the only one that needs to be calculated in order to estimate the polytropic efficiency of the LPT. For the direct drive models the stage loading factor is not considered constant anymore but need to be calculated as well as the stage flow factor. In the direct drive cases is the enthalpy drop per stage $\Delta H_{LPT\ stage}$ that is assumed constant during the process.

3.2.5 Estimation of turbine cooling fractions

As the thermodynamic cycles change during the design space exploration, so do the temperatures; therefore there is the necessity to account for the variability in turbine cooling requirements. In this project the turbine cooling fractions are calculated exploiting the method explained in details in Reference [52].

Mourouzidis [11] simplifies the equations indicated in Reference [52] by introducing thechnology terms (from C_1 to C_5):

$$Convective\ Cooling \quad \frac{W_{cool}}{W_{core}} = C_1 \frac{\varepsilon_0}{1-\varepsilon_0} \tag{3.2}$$

$$Film\ and\ Convective\ Cooling \quad \frac{W_{cool}}{W_{core}} = C_2 \frac{(C_3\varepsilon_0 - C_4)}{C_5(1-\varepsilon_0)} \tag{3.3}$$

The term ε_0 that appears in these equations represents the cooling effectiveness,

while W_{core} represents the the mass flow just upstream the bleed valve.
The technologic factors include terms like the space to chord ratio, c_p ratios, swirl angles and Stanton numbers. This values are considered constant and assumed based on the technological level of the engine manufacturer.

3.3 MoM engines weight and size estimation

This process is operated through the utilisation of ATLAS, which is a Cranfield University in-house software, created in FORTRAN, that allows estimating weight and size of different engine architectures. The whole process starts with a flow path design and successively it moves to the design of the single engine's components. The detailed explanation of this software, made by Lolis, can be found in Reference [48], whereas in this section just an overview will be given.

A peculiar characteristic of ATLAS is its modularity. In fact, the engine is divided into its fundamental components, each one of them is a module within the ATLAS code. This allows the code to be polyhedric, thus being able to assess different configurations and being suitable for future modifications just by adding new modules. As it can be seen in Figure 3.6, the main components of the engine form the principal modules. Each principal module has then submodules containing singular characteristics of the represented component.

Generally, the fan represents the heaviest module in a turbofan, and it is composed by the disk, the blades, the nose cone, the casing and the connecting hardware. The turbine and the compressor modules are similar between them, and they differ from the fan module in the absence of the nose cone characteristic. The combustor module comprises characteristics regarding the cooling passages, the pre-diffuser, the dump diffuser and the dome. ATLAS has the capability of estimating weight and size of the three principal combustor configurations: annular, tubular and tubo-annular. Moreover, ATLAS has the capability

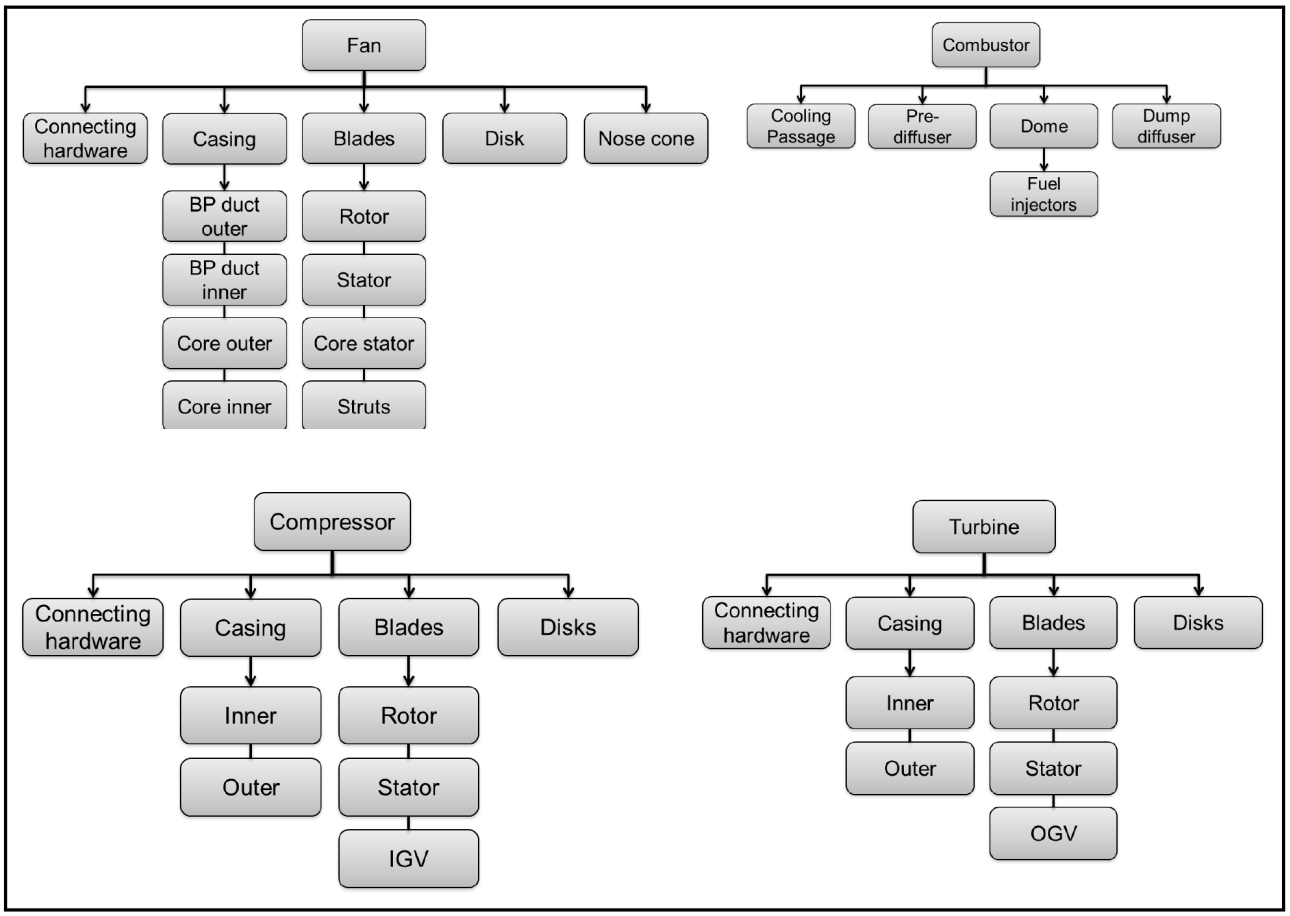

Figure 3.6: Principal engine modules and their submodules included in the ATLAS code. [48]

to evaluate also the ducts present within the engine, the frames and the shafts. The auxiliary systems weight is determined based on the simplistic assumption that it can be considered as an additional 10% on the overall engine weight, as it is demonstrated in References [53] and [54]. For each component a material is indicated, and ATLAS has a library with all the properties of all the most representative aeronautical materials.

In order to start a preliminary weight and size estimation for a specific engine model with ATLAS, it is necessary to provide two input files:

- performance input,
- geometry input.

Each component is positioned within the engine configuration through two station numbers: inlet and outlet. In the performance input for each one of the principal engine modules it has to be indicated, in the inlet and outlet positions, the values of mass flow, total pressure, total temperature, FAR (fuel-to-air ratio) and WAR (water-to-air ratio). These values can be easily derived from the TURBOMATCH output file and are necessary for ATLAS in order to define component pressure ratios, efficiencies, temperature ratios and other performance-related parameters.

The geometry input file contains the geometrical and mechanical specifications of each one of the components within the engine. Depending on the component considered, the specifications that need to be indicated may vary.

Based on the input data, by using work compatibility and mass flow continuity equations, ATLAS defines initially a gas path and then it starts designing the engine annulus. The turbomachinery design process is iterative and finishes when the technological limitations and targets are met by the critical parameters.

The ducts are estimated assuming them as two concentric cones. Their length are defined thanks to the duct angle and the length to inlet height ratio given as input. The thickness is derived by assuming it as a pressure vessel [11]:

$$t_{duct} = \frac{p\,D}{2\sigma_{yield}} \tag{3.4}$$

The component casing thickness is designed to be safe even in case of a blade failure and it changes between different components as the blade kinetic energy changes.

The shafts are simply considered as concentric and with increasing length going from the outer to the inner. The main assumption is that the shafts have constant thickness and the maximum stress at which they are subjected is calculated through:

$$\sigma_{max} = \left(\frac{16\,P_{transmitted}\,D_{out}}{\omega\,\pi(D_{out}^4 - D_{in}^4)} \right) \tag{3.5}$$

The rotating discs are designed by determining firstly the minimum volume, then the minimum weight shape to satisfy the limitations in tems of stress to which the disk is subjected. This approach follows the guidelines dictated by the NASA WATE method [55]. The same method is also applied in estimating the weight of the frames, which are the support struts and lugs within the engine. The approach considers 4 frame configurations and, for each one of them, the weight is determined following a specific function that relates the square of the radius with the weight of the component.

3.3.1 Nacelle weight estimation

The nacelle represents a significant influence in the engine installed performance; therefore it is important to evaluate its size and weight. In this project, it has been followed the method developed by Jackson in Reference [33] that estimates the weight of the nacelle based on its principal dimensions, indicated in Figure 3.7.

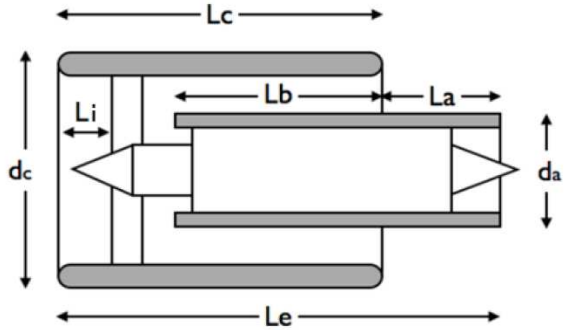

Figure 3.7: Schematic representation of the main dimensions of a turbofan nacelle. [33]

$$WT_{nac} = \pi k_{nac}(2L_c d_c + L_b d_a + 2L_a d_a) \tag{3.6}$$

The value of the surface based nacelle density (k_{nac}) is taken from state-of-the-art MoM turbofans. The length and diameter values involved in this fomula are referred to 3 components: the nacelle (L_c and d_c), the bypass (L_b) and the core

cowl (L_a and d_a). The calculation of these parameters is based on a simplified approach that correlates them to the fan inlet tip diameter, as explained in Reference [11].

Due to the fact that in this project there are some models equipped with a variable area fan nozzle, it is necessary to account also for its weight. In this case the weight is estimated assuming a translating cowl configuration for the VAFN. Based on the empirical correlation developed by Mourouzidis in Reference [11], it is possible to determine the weight of this component simply by adopting a quadratic dependence of the VAFN weight from the fan tip diameter, as it can be observed in Figure 3.8.

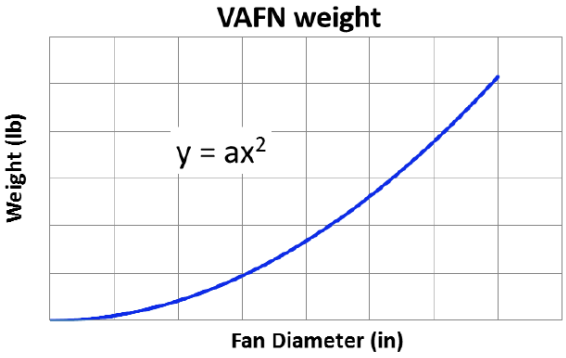

Figure 3.8: Correlation between the fan diameter and the VAFN component weight. [11]

In this way, by knowing the fan tip diameter value and the proportionality coefficient (a), it is possible to account for the weight of the VAFN component.

3.4 MoM engines mission fuel burn calculation

The conclusion of the project's cycle is represented by the mission fuel burn calculation, where the engines are evaluated in their installed performance. The fuel burn its a direct indication of how well an engine behaves when it is actually operated in the mission it has been designed for. The installed performance in fact

includes weight, size and drag considerations that are not included in the thermodynamic cycle simulations. Moreover, the fuel burn gives a direct indication of the operating cost of an engine.

Since this project considers 6 different engine architectures, the same number of mission fuel burn studies are made for the whole range of individuals indicated as optimums by the optimiser. All the engines are mounted on an aircraft similar to an Airbus A-321, represented in Figure 3.9, performing a 3000nm mission, that is similar to the A-320 mission schematically resumed in Figure 3.10.

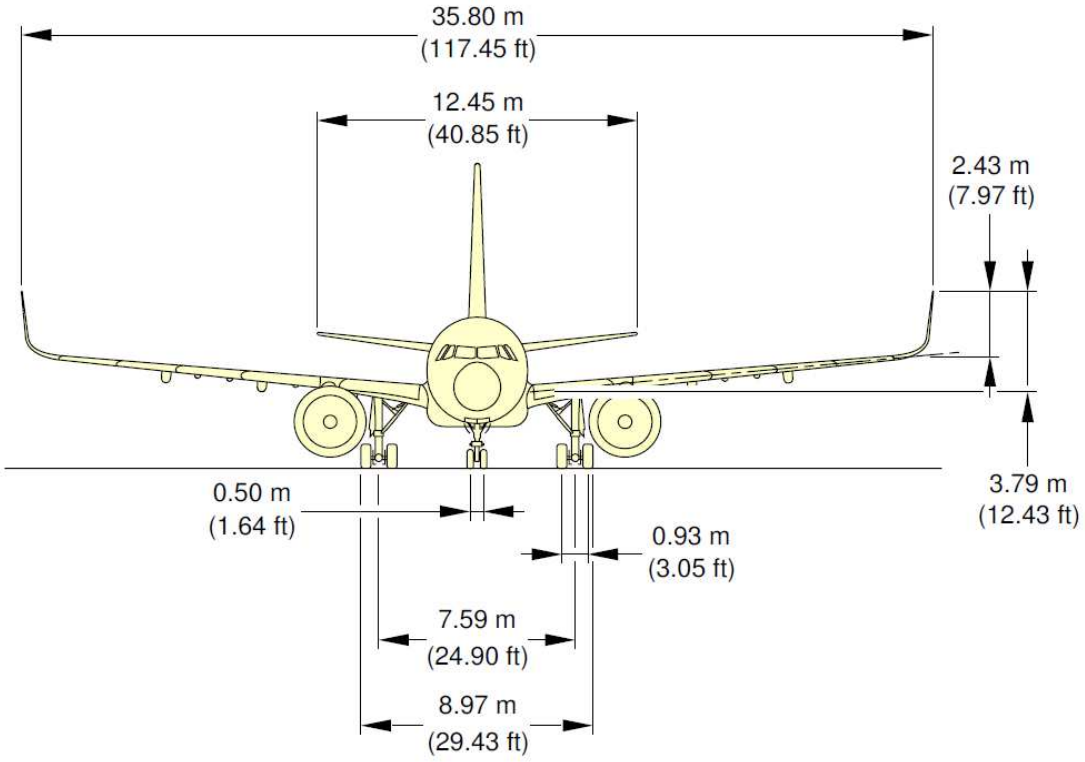

Figure 3.9: Airbus A-321 frontal view with part of the main aircraft geometry values indicated. [47]

The mission profile followed in this study resembles a typical civil aircraft mission. It also considers a fuel reserve for diversion cases.

In the NASA FLOPS Manual [49] it is possible to find all the detailed information about the processes implemented within the software and the equations exploited. In this section, the objective is to give an overall glance over this software and its capabilities. FLOPS is a unique software that includes engine cycle

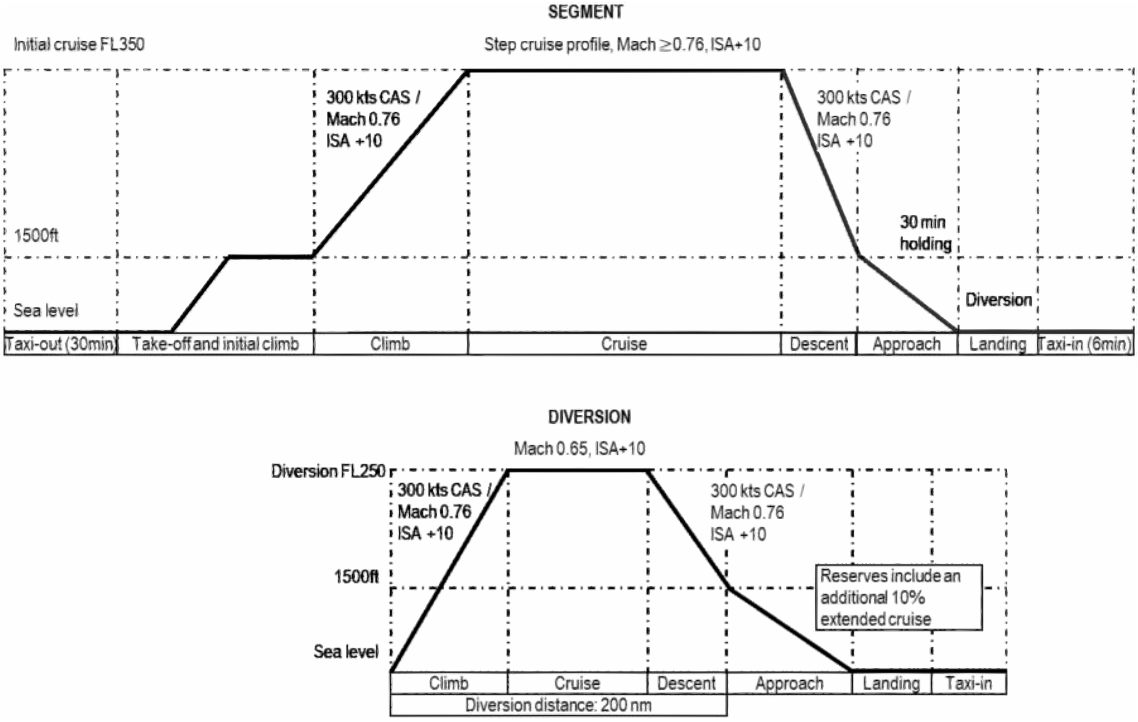

Figure 3.10: Typical A-320 aircraft type mission profile. [56]

analysis, propulsion data, weight estimation, noise estimation and cost analysis [57]. It has been developed by NASA with the aim to assess the impact of the introduction of novel technologies at a preliminary design level. The software is composed of a central module that can call 8 other modules. The relationships between these models are schematised in Figure 3.11.

Each one of the modules is able to estimate a specific aspect of the aircraft performance during its typical mission. The capabilities are various: engine cycle analysis, weight estimation, aerodynamics, propulsion data analysis and noise estimation. All these aspects are estimated during all the phases of the mission and this allows the software to compute mission fuel burn and cost analysis. The cost doesn't refer only to the mission but also to the building of the whole aircraft that performs it [57].

In order to evaluate the engine performance, the software requires an engine deck intended as a combination of fuel flow and net thrust values at different flight conditions and throttle settings. Despite NASA FLOPS has the capability

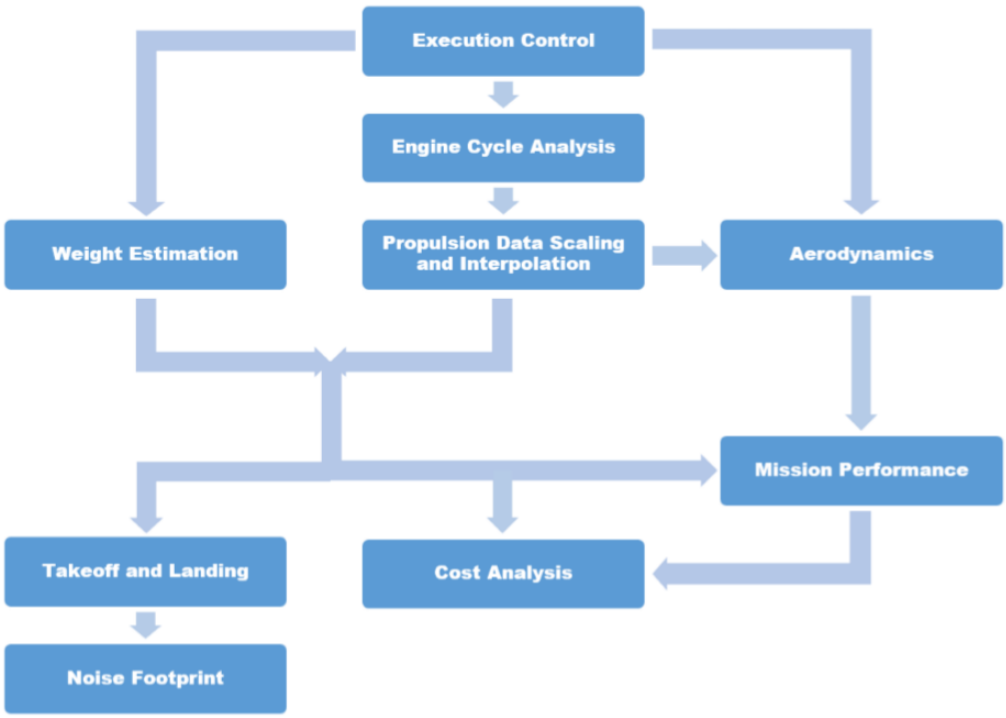

Figure 3.11: The FLOPS modules and their relationships. [57]

of creating automatically an engine deck, in this project it has been decided to calculate it and insert it as an input. The engine deck layout adopted in this analysis is shown in Table 3.3.

Altitude	Mach Number	min LP PCN	max LP PCN	Points
10668	0.85	0.8	max T30	5
9144 6096 3048	0.85 - 0.6 - 0.4	0.8	max T30	5
914	0	0.8	max static Thrust	5
0	0 0.25	0.8	max static Thrust max EOR Thrust	5

Table 3.3: Engine deck layout adopted for the mission fuel burn analysis in NASA FLOPS.

The engine deck is created by the combination of different altitudes, Mach number and throttle settings, that in this case is represented by the low-pressure

spool non-dimensional rotational speed (LP PCN). For each altitude and Mach number, 5 different points are created from the minimum LP PCN value to the maximum. The range of LP PCN considered goes from a common minimum of 0.8 to a maximum that is calculated differently depending on the altitude. From cruise to 3048 m of altitude the max LP PCN is the one that allows the engine to reach the maximum T30 value. At low altitudes, the upper limit of the LP PCN values is the one that allows the engine to obtain the maximum net thrust at static or EOR conditions, depending on the Mach number considered.

Once the engine deck is given as an input, the propulsion data scaling and interpolation module uses linear and non-linear interpolation to scale the provided data to the requested thrust.

The mission performance module uses the data derived from the other modules (weights, propulsion data and aerodynamics) to assess the performance. This module can calculate optimum conditions for: climb profiles, cruise altitude or Mach number and lift-drag ratio for descent [49].

The program control module, through the use of the secondary modules, can analyse design point simulations as well as optimise a certain configuration for specified design variables, that in the case of the aircraft are represented by wing and fuselage geometry, while in the engine are the FPR, OPR, TET and BPR [49].

In this project, it has been used an automatic deck generator and FLOPS launcher developed within the Cranfield UTC. Its operations are explained in the scheme represented in Figure 3.12. Basically, the mission fuel burn analysis is conducted for all the range of engines that compose the Pareto front in the optimisation process, after having estimated their weight and length through ATLAS. In order to generate the engine deck, it is necessary to provide engine cycle data, which are derived from the outputs of CYCLOPS. For each one of the engines, the deck is generated. Since the FLOPS software requires input data in terms of

aircraft geometry, represented in Figure, and mission (indicated in Appendix A), engine weight, size and deck, three different input are collected and introduced into the input file. The origin of the inputs depends on their characteristics; it may be ATLAS for the engine weight and size or simply the public domain for the aircraft and mission data. Eventually, FLOPS creates an output file in which various performance results are collected. Among these results there are also the indications about the mission fuel burn, that is the interest of this analysis. The mission fuel burn results are then collected and post-processed.

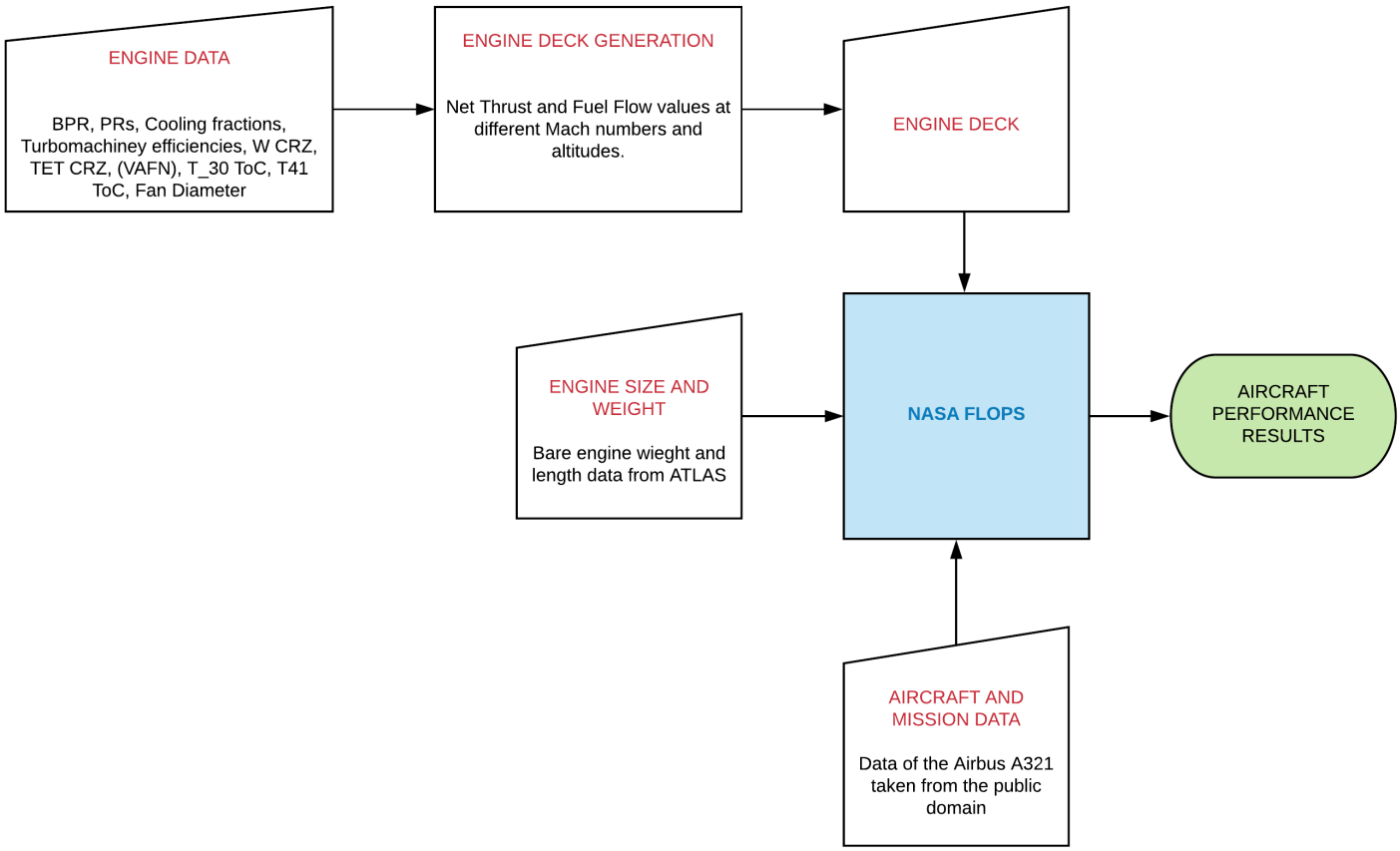

Figure 3.12: Workflow utilised in the project for the mission fuel burn analysis.

Chapter 4

Results and discussion

In this chapter, the results of the project are exposed and commented, following the workflow previously discussed in the Methodology chapter. The whole chapter can be divided into 3 main sections. The first one presents the results of the design space exploration and cycle design optimisation. The second section contains the results of the engine weight and size estimation. Eventually, the third section presents the results of the mission fuel burn analysis.

4.1 Cycle design optimisation results

In order to allow the optimiser to cover all the design space with individuals, it is necessary to define the decision variables ranges, as it has been mentioned in the Methodology. For the design space of interest, the selected ranges are listed in Table 4.1.

Decision Variable	**Range**
Fan diameter [m]	1.95-2.35
OPR	40-65
TET at CRZ [K]	1500-1650
FPR tip	1.2-1.6

Table 4.1: Decision variable ranges applied in the cycle design optimisation.

The fan diameter range has been determined considering the ground clearances of an Airbus A-321 and its available space under the wing. To this it has been added the assumption of optimised engine integration and nacelles that would allow in the future bigger fan diameters than the actual ones. Moreover, the possibility of new MoM aircraft introduction, reported in Reference [5], in the near future has pushed the upper boundary to higher values suitable for new airframes.

The upper limitation in the OPR range can be calculated based on the maximum T30 at the EOR condition determined in the constraints set. The lower value has been selected in order to keep a wide range and not to neglect any potential optimum solution.

The ranges in TET and FPR have been selected to be wide enough to create a high number of combinations without affecting negatively the computational time.

4.1.1 Axi-centrifugal HPC geared turbofan cases

The first set of results regards the axi-centrifugal geared turbofans. This model has been analysed in two versions with and without the VAFN component. Since the results were very similar in trends and absolute values, the author has established to represent both the cases into the same charts, with darker (VAFN) and lighter colours (FIXED). In all the charts, the discrepancies between the two models will be enlightened and explained. It is important to clarify that the x-axis in each one of the charts presents a decreasing specific thrust in the positive direction.

In Figure 4.1 there are plotted the SFC and main temperature values variations with the decrease of specific thrust. In this case, the normalisation of all the cycle parameters is done by taking the axi-centrifugal HPC FIXED turbofan with the smallest fan diameter as a baseline. It can be seen that, as the specific thrust reduces, therefore as the fan diameter increases (as it represented in Figure 4.2),

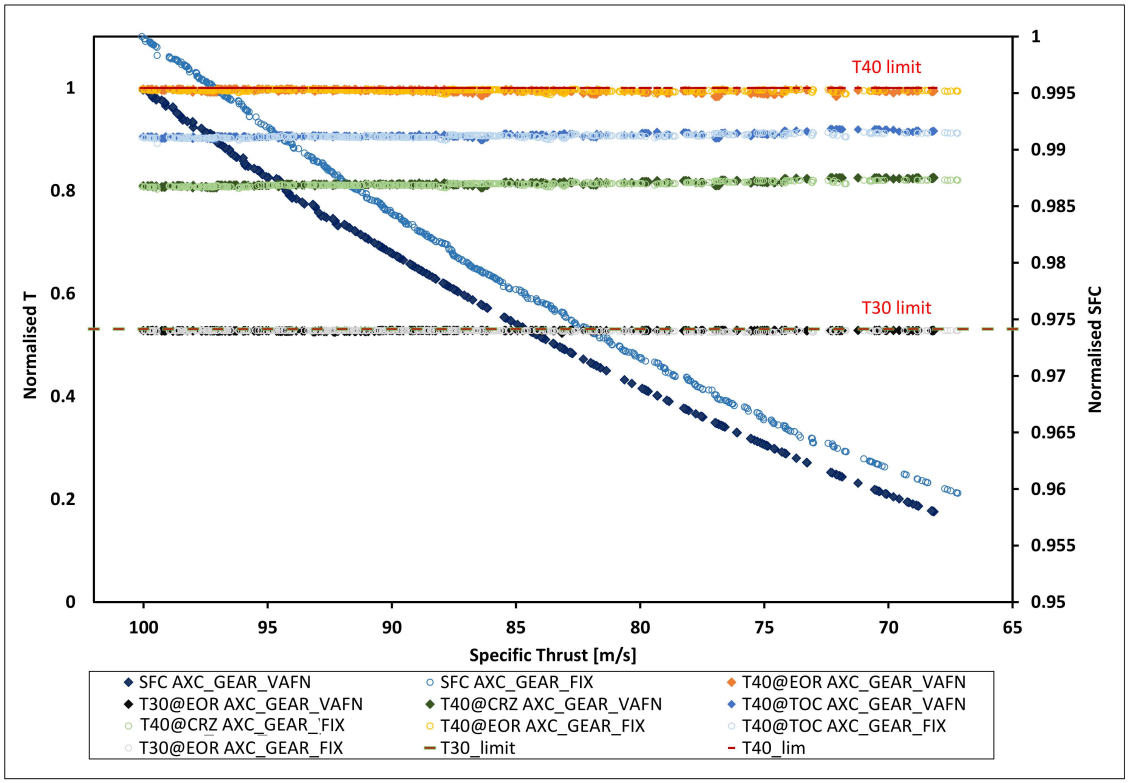

Figure 4.1: Variation of SFC and cycle determining temperatures as a function of specific thrust for the axi-centrifugal HPC geared cases. The SFC values are normalised with the SFC of the AXC_GEAR_FIX with the smallest fan diameter. The temperature values are normalised with the T40 limit.

there is a decrease in SFC for both the FIXED and the VAFN cases, with a higher drop for the second case, as it will be explained later in this chapter. Remaining in Figure 4.1, it can also be noticed how the optimiser pushes the T30 and T40 values for all the optimum engines to the limits imposed by the constraints. The limits in both the cases are the same, since they are defined by the technological level of the manufacturer, and it has been assumed to be constant through all the cases. These two temperatures are essential due to the fact that they determine crucial cycle parameters. In fact, considering that T30 is the temperature at the exit of the HPC, its value determines the maximum OPR that can be reached by the engine. Meanwhile, T40 determines the BPR of the engine. In fact, if we consider a certain fan diameter with a specified fan pressure ratio, the mass flow at the engine inlet is defined as well as the fan power requirement. Since T40 is

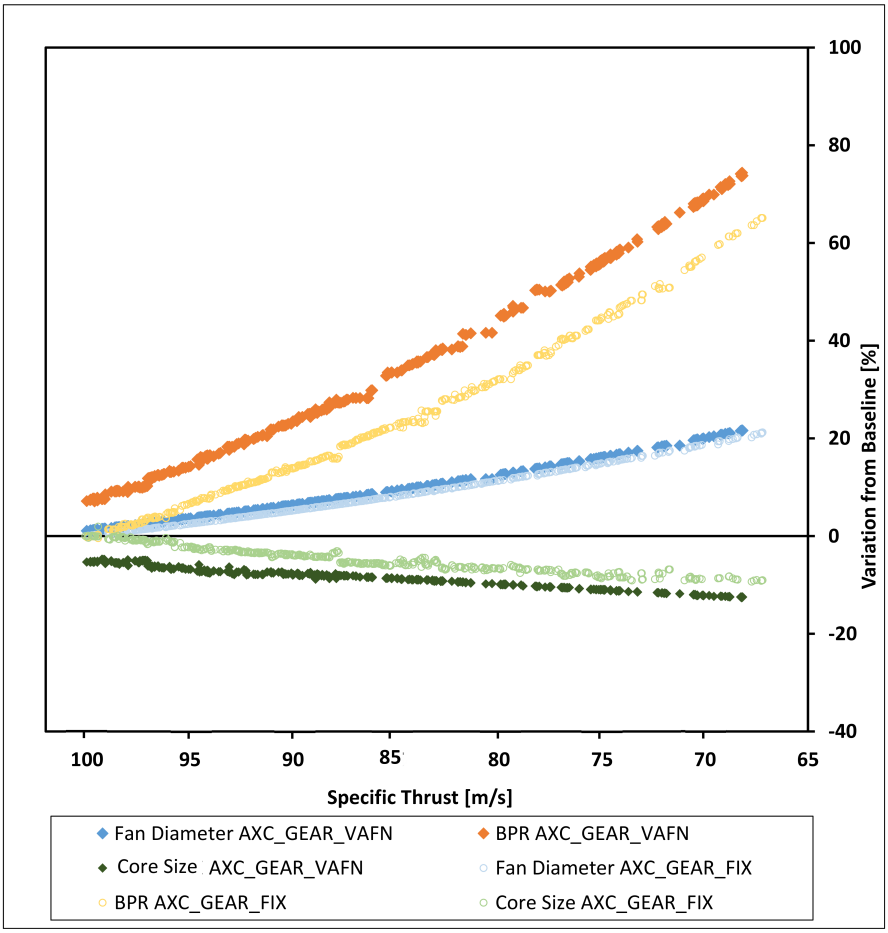

Figure 4.2: Variation of BPR, fan diameter and core size as a function of specific thrust for the axi-centrifugal HPC geared cases. The baseline is represented by the AXC_GEAR_FIX with the smallest fan diameter.

the maximum temperature within the cycle and it determines the specific power of the core, for a specified fan power requirement it determines the core mass flow as well. Eventually, it determines the BPR, since the mass flow at the inlet of the engine is previously fixed. Moreover, it can be seen that the T40 values at ToC and CRZ are increasing going to lower specific thrust. In fact, the core is reducing and the BPR increasing as we move towards lower specific thrusts, as it can be seen in Figure 4.2; therefore the core specific power needs to be higher, thus T40 increases.

It has been mentioned before that the core size decreases as we go to lower specific thrust values. This brings to a consequent increase in BPR, as it can be

seen in Figure 4.2. Moreover, in Figure 4.2 it can be noticed that the reduction in core size of the VAFN case is higher than the fixed counterpart and the increase in bypass ratio is consequently higher. The reason for that is the fact that increasing the fan nozzle area at take-off increases the gross thrust produced by the engine, and the net follows as well. In this case, the net thrust requirement at take-off is fixed and, therefore, for a fixed T40 at EOR and a fixed core specific power, less core mass flow is required; hence the core can be smaller. The decrease in core size is always limited by the turbine cooling requirements at EOR. In fact, sufficient core mass flow has always to be available at EOR to guarantee the required core power and turbine cooling air.

In Figure 4.3 there are represented the OPRs in the three main design points. The absolute values and trends in both the VAFN and the FIXED cases are similar. With the decrease in specific thrust, both the cases present an increasing OPR in ToC and CRZ with the same slope angle, while the OPR at EOR remains nearly constant. It can be noticed a peculiar characteristic in both the cases in the very low specific thrust region. In fact, in this region the OPR values at CRZ are crossing the EOR ones, becoming higher.

In Figure 4.4 are represented the efficiency values. It has been mentioned previously that going to lower specific thrust causes the T40 values and OPRs at CRZ to increase. Since the thermal efficiency is a function of OPR and TET at cruise, as it has been widely demonstrated in literature ([6][10] [13][21]), it improves as well. Moreover, the results confirm the improvement in propulsive efficiency going to lower specific thrusts, since the BPR increases and the jet velocities decrease. It can be noticed a difference between the propulsive efficiency of the VAFN case compared to the FIXED one, with the first being slightly higher. This can be explained thanks to the considerations made before, based on the results shown in Figure 4.2. In fact, as it has been said, the VAFN case goes to slightly smaller core sizes relative to the FIXED, therefore it has bigger BPR

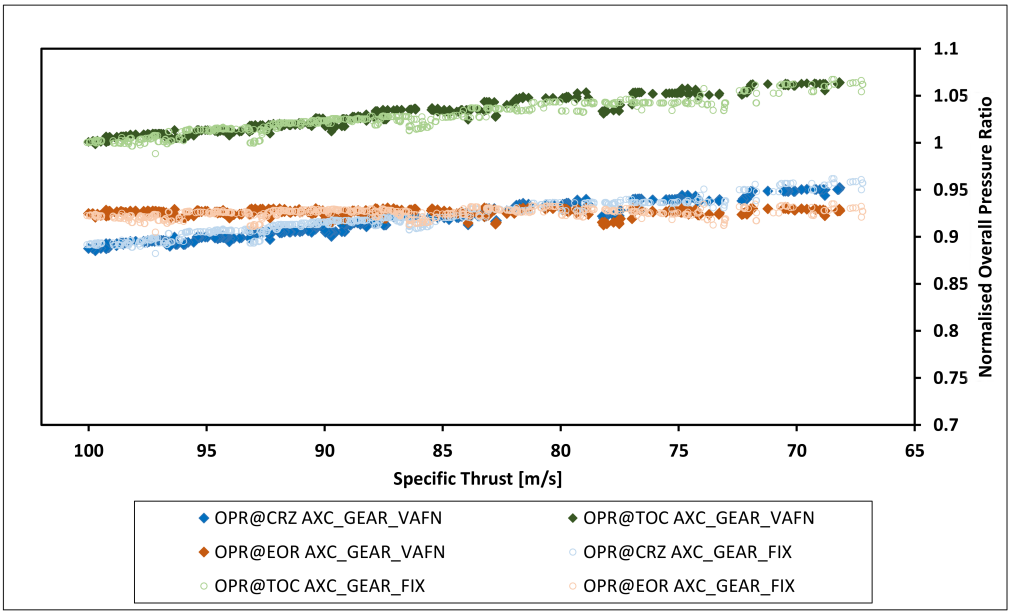

Figure 4.3: Variation of OPR at EOR, ToC and CRZ as a function of the specfic thrust for the axi-centrifugal HPC geared cases. The OPR values are normalised with the OPR at TOC of the AXC_GEAR_FIX with the smallest fan diameter.

values and, consequently, marginally better propulsive efficiency. The same can't be said for the thermal efficiency, where the two models present very similar results. In fact, as it can be seen in Figure 4.1 and Figure 4.3 there are no relevant differences in the values of TET and OPR at cruise in the two cases; therefore the thermal efficiency does not present different values. Transfer efficiency presents a slight increase going to lower specific thrust values. Since it is proportional to the polytropic efficiencies of the fan and LPT, the adoption of a gearbox helps to obtain high absolute values, because it allows the two components to run at their optimal rotational speeds.

Eventually, the VAFN case presents an overall efficiency slightly higher than the FIXED counterpart since, at the same values of thermal and transfer, it has a marginally better propulsive efficiency. Overall, the SFC improvement at cruise allowed by the implementation of the VAFN is substantially limited. This can still represent a small advantage combined with the higher thrust provided at take-off and the safe operability of the fan. On the other hand, the disadvantages

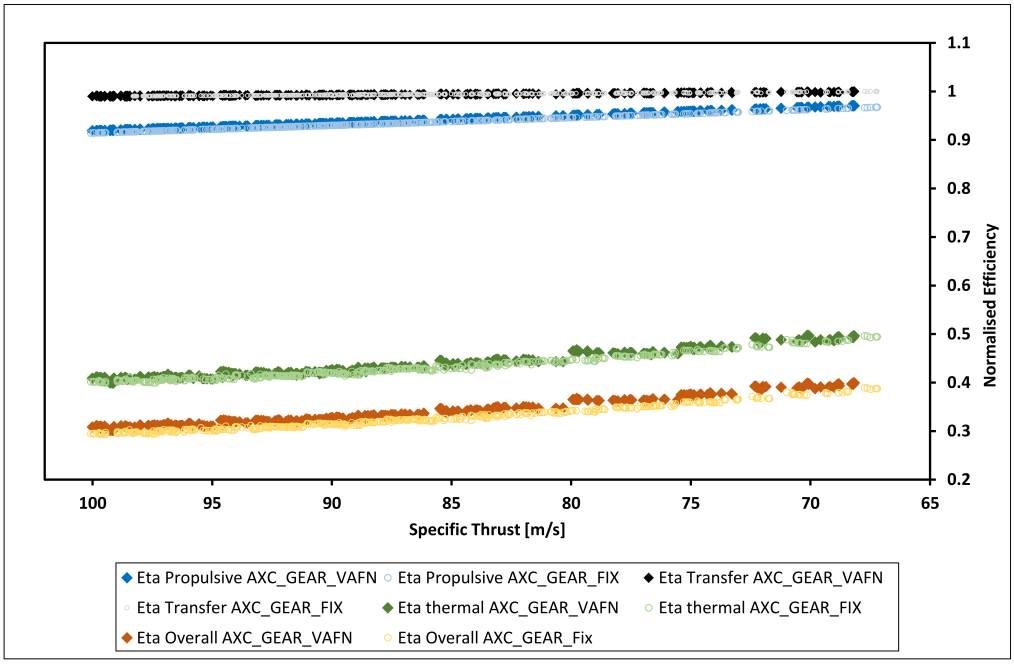

Figure 4.4: Variation of efficiencies as a function of specific thrust for the axi-centrifugal HPC geared cases. The efficiency values are normalised with the transfer efficiency of the AXC_GEAR_FIX with the smallest fan diameter.

are multiple as well: higher weight and drag penalty as well as increased cost and complexity. In conclusion, it is necessary to assess properly this system prior the implementation, because the advantages aren't clearly overcoming the drawbacks.

4.1.2 Axi-centrifugal HPC direct drive turbofan cases

In this case, the main difference with the previous one is the fact that the power gearbox has been removed, nevertheless both the VAFN and the FIXED configurations are represented by different markers and shades. Figure 4.5 presents the Pareto fronts for the two direct drive cases indicating a reduction in SFC going to lower specific thrust values. The temperatures T40 and T30 are pushed to the limits at EOR, while T40 at cruise and ToC increases with the decrease in specific thrust for the same reasons described in the axi-centrifugal geared case.

The decrease of specific thrust leads to an increase in the fan diameter and a

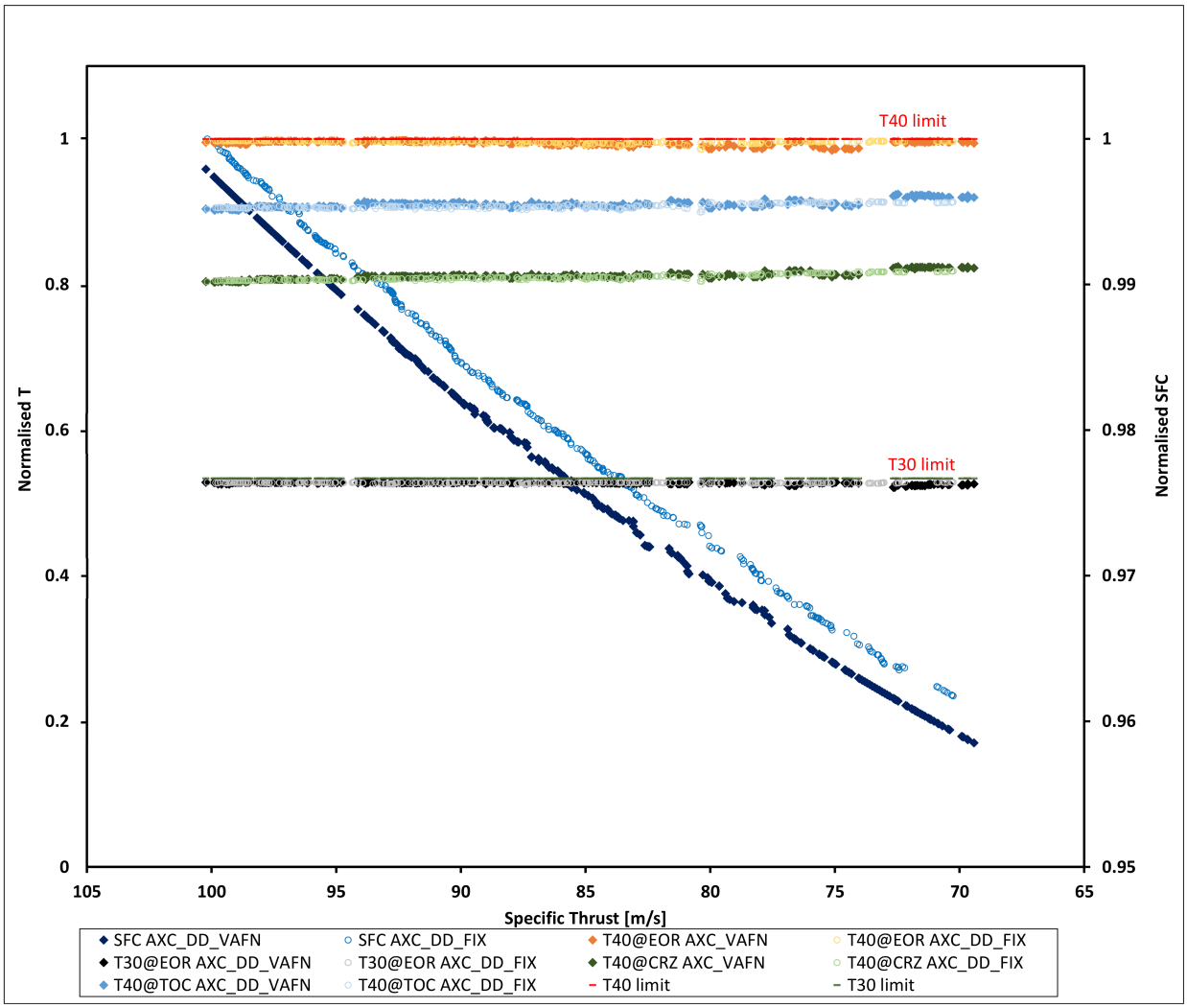

Figure 4.5: Variation of SFC and cycle determining temperatures as a function of specific thrust for the axi-centrifugal HPC direct drive cases. The SFC values are normalised with the SFC of the AXC_DD_FIX with the smallest fan diameter. The temperature values are normalised with the T40 limit.

reduction in the core size, with a consequent increase in BPR, as it is represented in Figure 4.6. In the same way it was described in the axi-centrifugal geared case, the adoption of the VAFN component allows the core to shrink more relative to the FIXED case; therefore Figure 4.6 shows higher core reduction in the VAFN that, at the same fan diameter, leads these engines to higher values of BPR.

Figure 4.7 presents the trends in OPRs with the reduction of specific thrust. The same increasing trends in OPR at ToC and CRZ that were present in the geared case can be seen in the direct drive case, with the OPR at EOR being

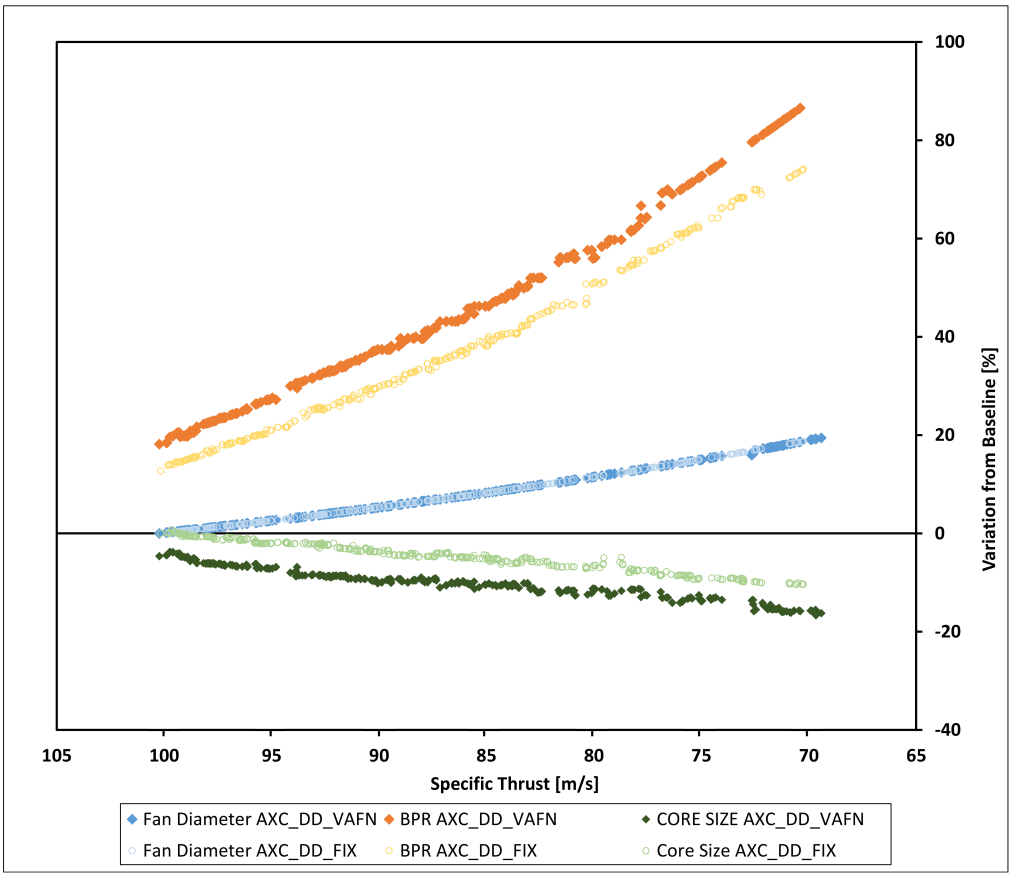

Figure 4.6: Variation of BPR, fan diameter and core size as a function of specific thrust for the axi-centrifugal HPC direct drive cases. The baseline is represented by the AXC_DD_FIX with the smallest fan diameter.

almost constant along the whole range of specific thrust variation. The peculiar intersection of the OPR values at CRZ and EOR is present also in this case as it was for the geared models.

Figure 4.8 represents the variation in efficiencies with the reduction of specific thrust. The increase in fan diameter causes the propulsive efficiency to increase. The increase in TET and OPR causes the increase of the thermal efficiency going to lower specific thrust values. The overall efficiency increases as well since it is a function of the propulsive and thermal efficiencies. Because of the higher BPR values that they can reach, the propulsive efficiency of the VAFN cases appears to be around half a per cent higher than the FIXED counterpart. This, consequently, creates a discrepancy in the overall efficiency values, with the VAFN ones being

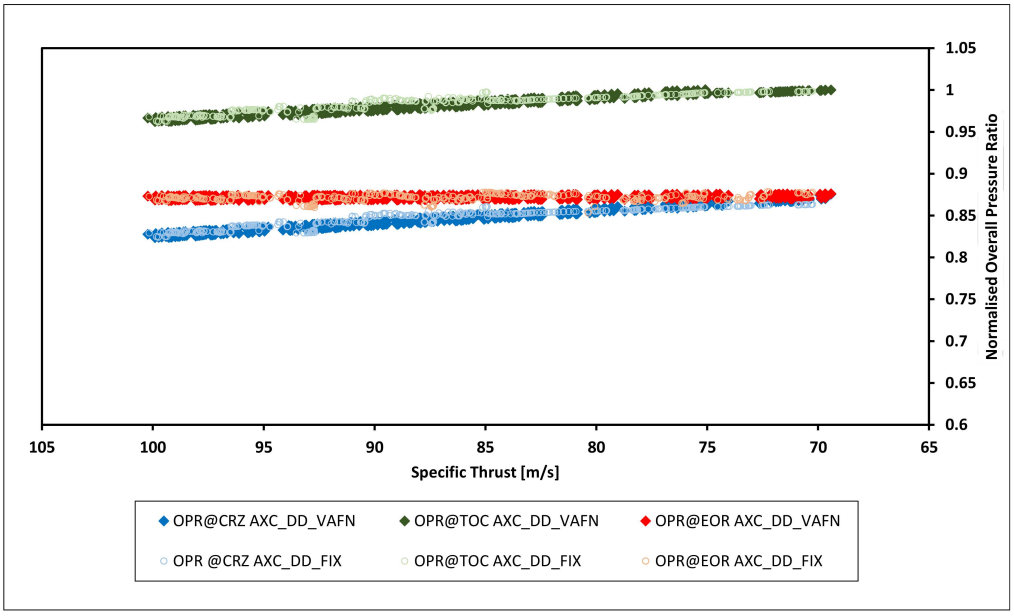

Figure 4.7: Variation of OPR at EOR, ToC and CRZ as a function of the specfic thrust for the axi-centrifugal HPC direct drive cases. The OPR values are normalised with the OPR at TOC of the AXC_DD_FIX with the smallest fan diameter.

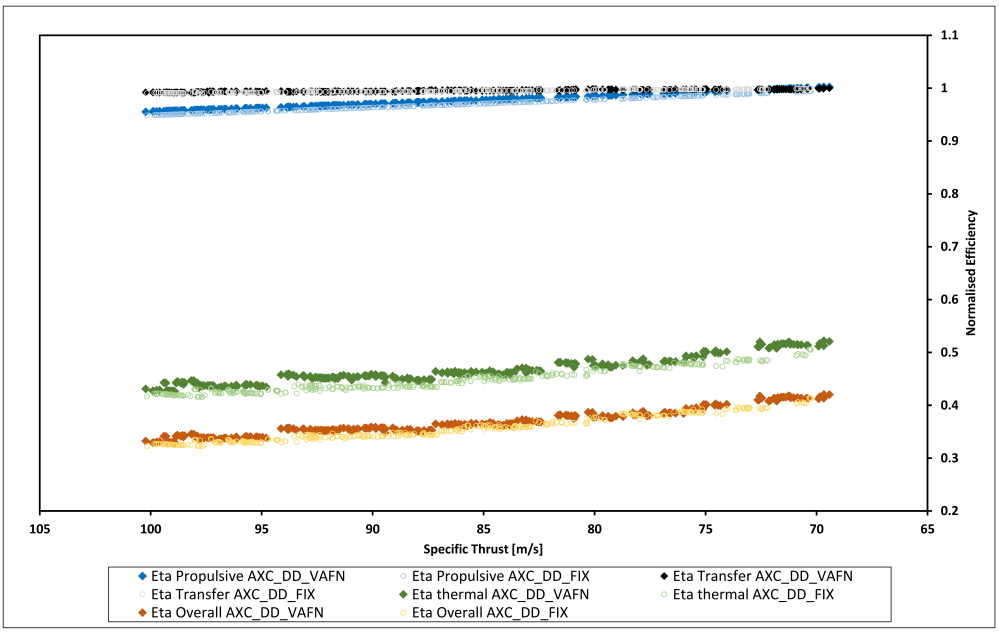

Figure 4.8: Variation of efficiencies as a function of specific thrust for the axi-centrifugal HPC direct drive cases. The efficiency values are normalised with the transfer efficiency of the AXC_DD_FIX with the smallest fan diameter.

slightly higher than the FIXED. The transfer efficiency presents a nearly constant value across all the range of specific thrust. Nevertheless, its absolute values

result lower than the geared cases because of the lower polytropic efficiencies in the LTP and fan in the direct drive models relative to the geared ones, as it will be explained later in this chapter. This brings to an intersection between the propulsive efficiency and the transfer efficiency values at low specific thrust values.

4.1.3 VAFN effect on running lines

It has been mentioned previously, in the ”Literature review” chapter, that, in the very low specific thrust region, fan operability issues could arise during the EOR condition, in particular surge and flutter. The adoption of a variable area fan nozzle could represent a remedy for these issues. Nevertheless, this component adds weight, cost and complexity to the engine architecture; therefore an in-depth analysis should be performed prior to its implementation. In this project, a visual check of the surge margin in the fan maps has been conducted in order to deliberate about the necessity of a VAFN.

In Figure 4.9 it is represented the fan map of the axi-centrifugal direct drive fixed turbofan with the largest fan diameter in the Pareto front. A bypass nozzle area variation is then applied to the model to simulate the effect of a VAFN on the EOR running line.

It emerges that the EOR running line of the fixed nozzle area model moves towards the surge region, nevertheless a sufficient surge margin is still visible. Increasing the fan nozzle area conducts effectively the operating point to the maximum fan efficiency region, causing an improvement in SFC and increasing the surge margin.

The same analysis can be conducted for the geared turbofans. Figure 4.10 represents the fan tip map for the axi-centrifugal geared fixed turbofan with the maximum fan diameter in the Pareto front.

In this case it is again visible a shift of the EOR running line towards the surge

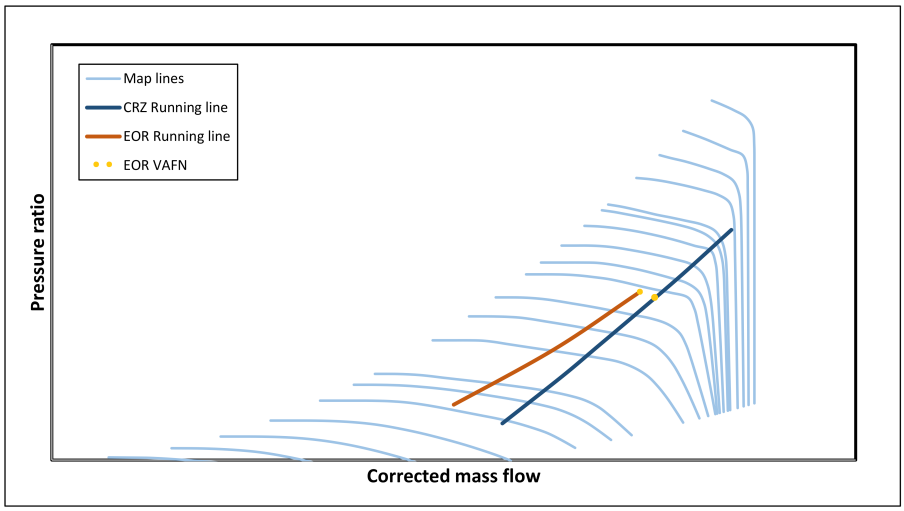

Figure 4.9: Fan tip map of an axi-centrifgual HPC direct drive turbofan.

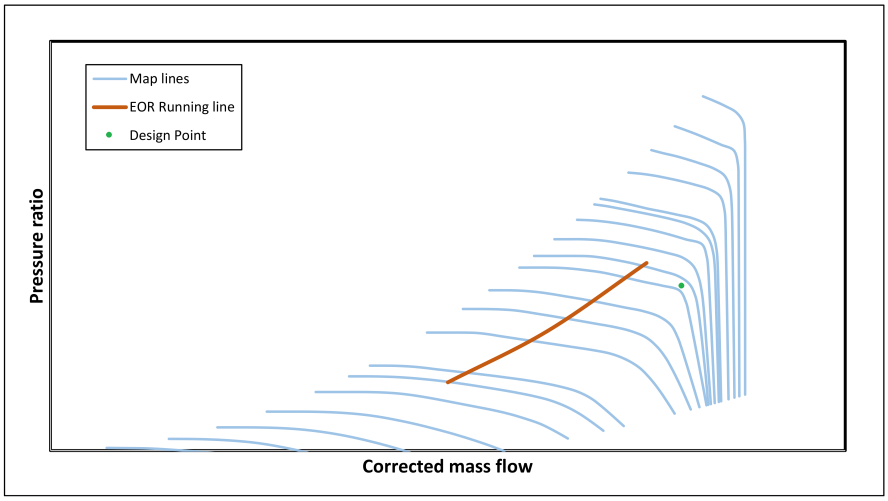

Figure 4.10: Fan tip map of an axi-centrifgual HPC geared turbofan.

region, nevertheless the surge margin remains still acceptable. An increase in the fan nozzle could bring the EOR operating point back to the maximum fan efficiency region, where it is present the design operating point.

Eventually, in both the geared and direct drive cases it has been demonstrated that there is no apparent necessity to adopt a VAFN due to operability issues in terms of fan surge. Nevertheless, flutter issues need still to be analysed, but it goes beyond the interest boundaries of this project.

4.1.4 Axial HPC geared turbofan case

The crucial difference between these cases and the previous ones is represented by the configuration of the HPC, that, in this case, is a full-axial compressor. Having already demonstrated the major differences between the VAFN and the FIXED versions in the axi-centrifugal models, the axial model is considered only in the FIXED configuration with both the geared and the direct drive options. The analysis of the full axial cases follows the same steps as the axi-centrifugal ones.

In Figure 4.11, the Pareto front, resulted from the optimisation process, shows a reduction in SFC with the decrease in specific thrust. The optimiser has pushed the values of T40 and T30 at EOR at their respective limits. Moreover, as it was for the axi-centrifugal cases, also in this case the values of T40 at CRZ and EOR show a positive slope with the reduction of specific thrust.

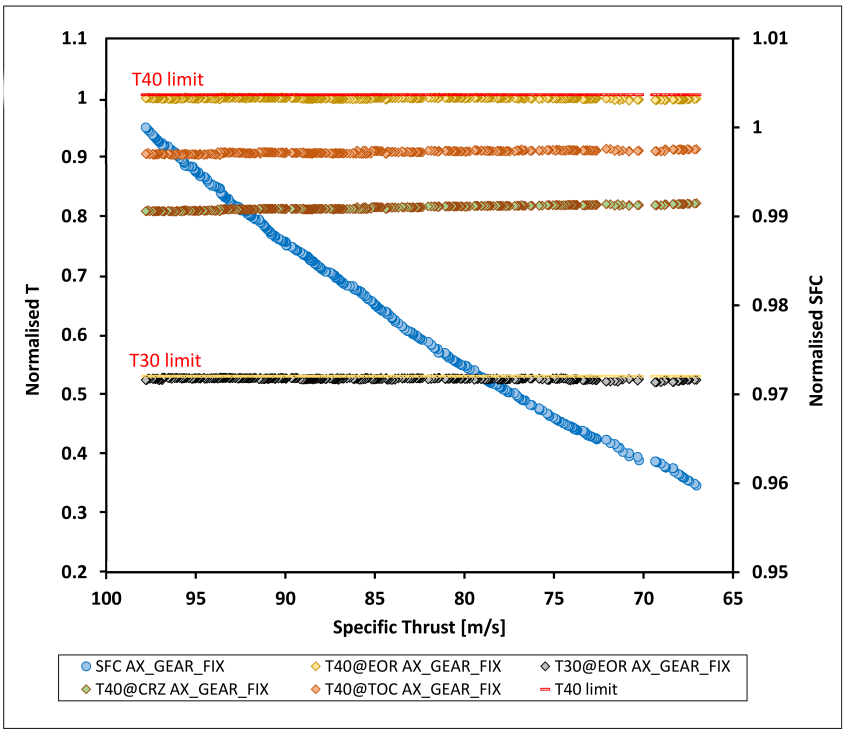

Figure 4.11: Variation of SFC and cycle determining temperatures as a function of specific thrust for the axial HPC geared case. The SFC values are normalised with the SFC of the AX_GEAR_FIX with the smallest fan diameter. The temperature values are normalised with the T40 limit.

Figure 4.12 represents the increase in fan diameters and the reduction of the

core size with the decrease in specific thrust. The consequence of these trends is an increase in the BPR values going to the low specific thrust region.

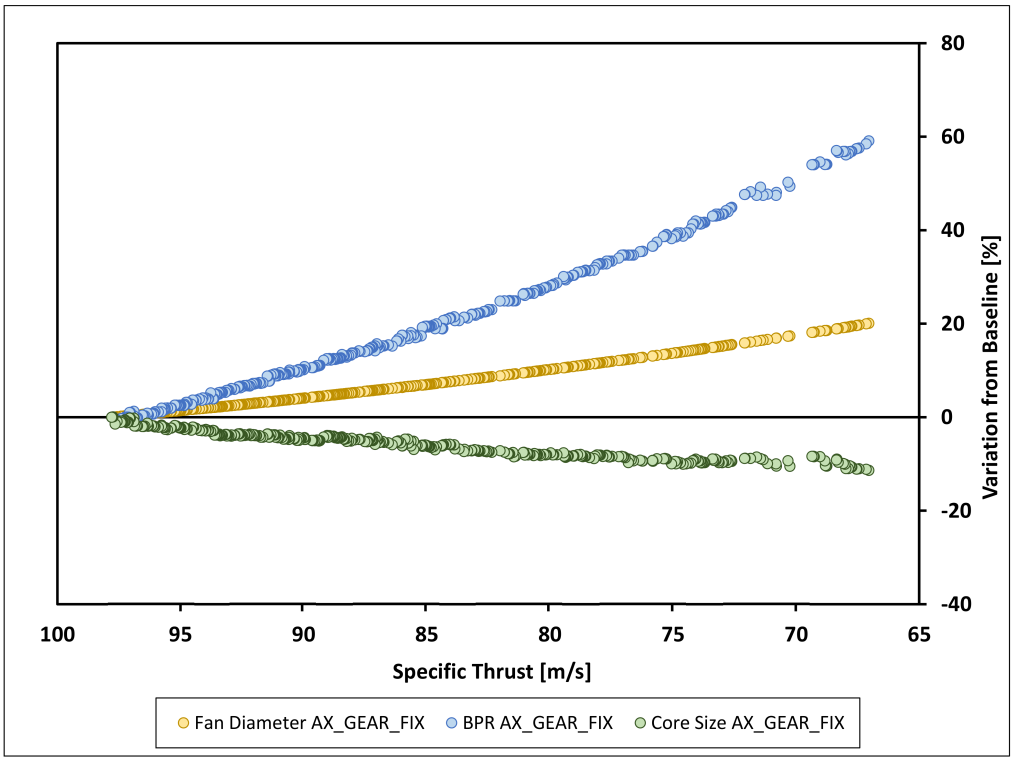

Figure 4.12: Variation of BPR, fan diameter and core size as a function of specific thrust for the axial HPC geared case. The baseline is represented by the AX_GEAR_FIX with the smallest fan diameter.

Figure 4.13 shows the trends in OPRs as the specific thrust decreases. Even in this case, there is an increase in OPR at CRZ and TOC, while the EOR value remains constant, due to the fact that the optimiser pushes the T30 values to the limit. It is again visible the crossing between the OPR values at CRZ and EOR at low values of specific thrust. The trends in OPR at CRZ and ToC present a visible positive slope at the high values region of specific thrusts and they flatten at the low values of specific thrust.

In Figure 4.14 there are represented the variations in the efficiencies with the reduction in specific thrust.

Similarly to the previous cases, the thermal, the propulsive and, consequently, the overall efficiencies increase with the decrease in specific thrust. The thermal

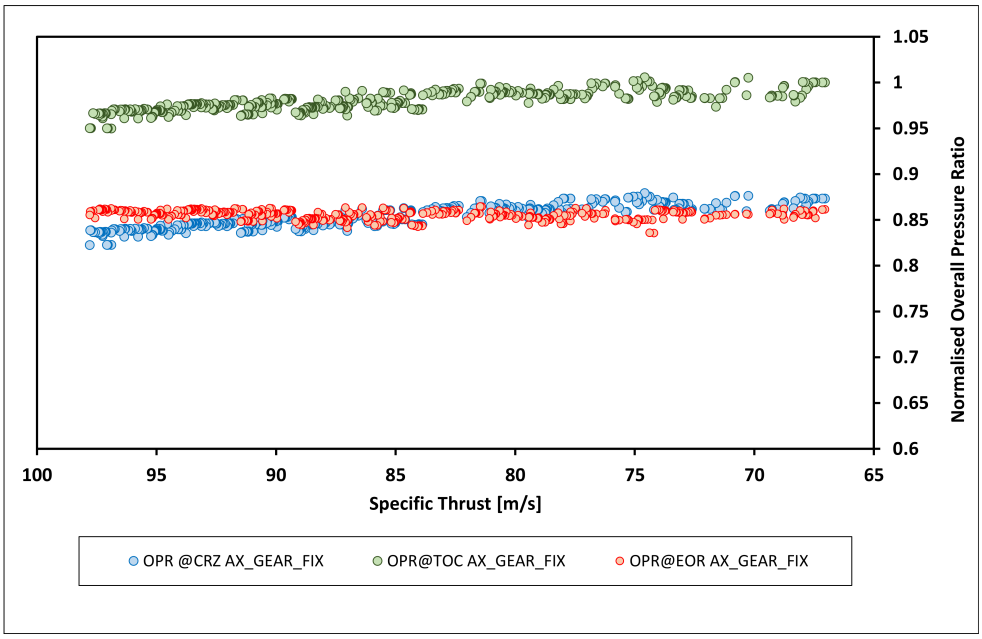

Figure 4.13: Variation of OPR at EOR, ToC and CRZ as a function of the specfic thrust for the axial HPC geared case. The OPR values are normalised with the OPR at TOC of the AX_GEAR_FIX with the smallest fan diameter.

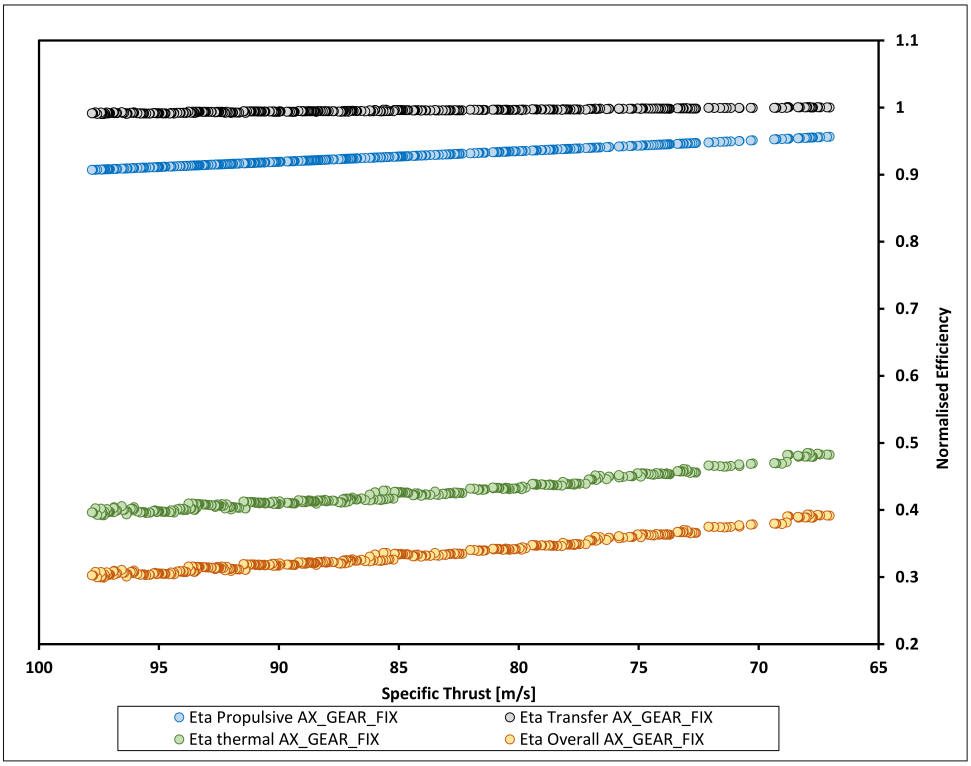

Figure 4.14: Variation of efficiencies as a function of specific thrust for the axial HPC geared case. The efficiency values are normalised with the transfer efficiency of the AX_GEAR_FIX with the smallest fan diameter.

increases because of the increase in TET and OPR at cruise, as it can be noticed in Figure 4.11 and 4.13, while the propulsive because of the increase in fan diameter, observable in Figure 4.12. The transfer efficiency presents a slight growth with the decrease in specific thrust.

4.1.5 Axial HPC direct drive turbofan case

This section presents the charts resulting from the analysis of the axial direct drive models. Figure 4.15 represents the Pareto front with the reduction in SFC

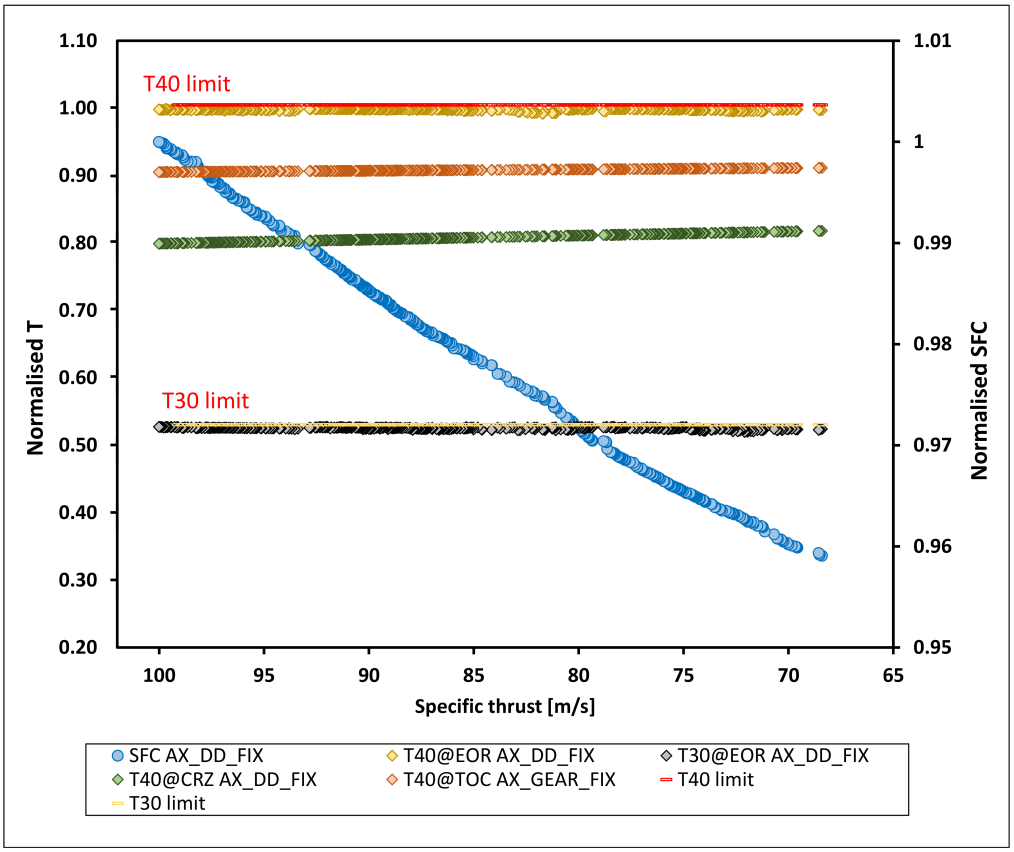

Figure 4.15: Variation of SFC and cycle determining temperatures as a function of specific thrust for the axial HPC direct drive case. The SFC values are normalised with the SFC of the AX_DD_FIX with the smallest fan diameter. The temperature values are normalised with the T40 limit.

as the specific thrust decreases. In the same way and for the same reasons of the previous cases, there is an increase in the T40 at CRZ and ToC with the reduction

of the specific thrust, while the values of T30 and T40 at EOR are pushed to the limits.

The decrease in specific thrust is accompanied by an increase in fan diameter and reduction of core size that leads to an increase in BPR, as it can be seen in Figure 4.16.

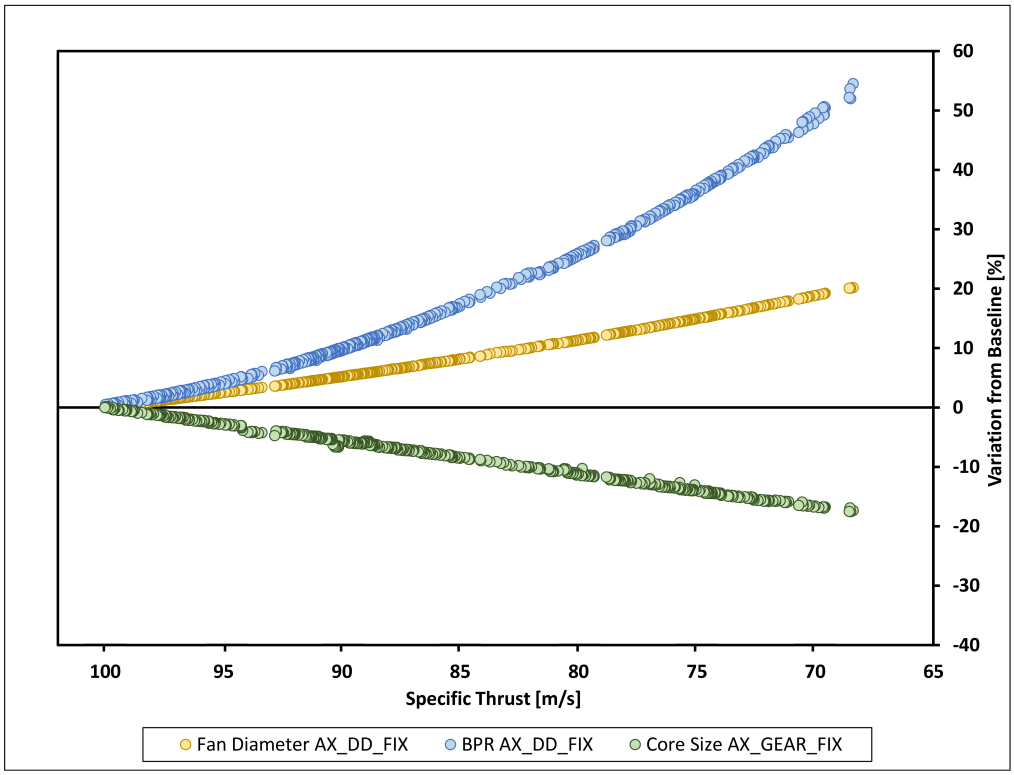

Figure 4.16: Variation of BPR, fan diameter and core size as a function of specific thrust for the axial HPC direct drive case. The baseline is represented by the AX_DD_FIX with the smallest fan diameter.

In the same way it happened in the previous cases, the reduction of the specific thrust leads to an increase in the OPR values at TOC and CRZ, while the EOR remains constant. It is again present a crossover between the OPR at CRZ and EOR at the low region of specific thrust values, as shown in Figure 4.17. In this case, as it was for the axial geared one, there is a reduction in the slope of the OPR curves at CRZ and ToC and they flatten in the low specific thrust region.

Figure 4.18 shows the increase of propulsive efficiency with the decrease of specific thrust. The increases of T40 and OPR at CRZ lead the thermal efficiency

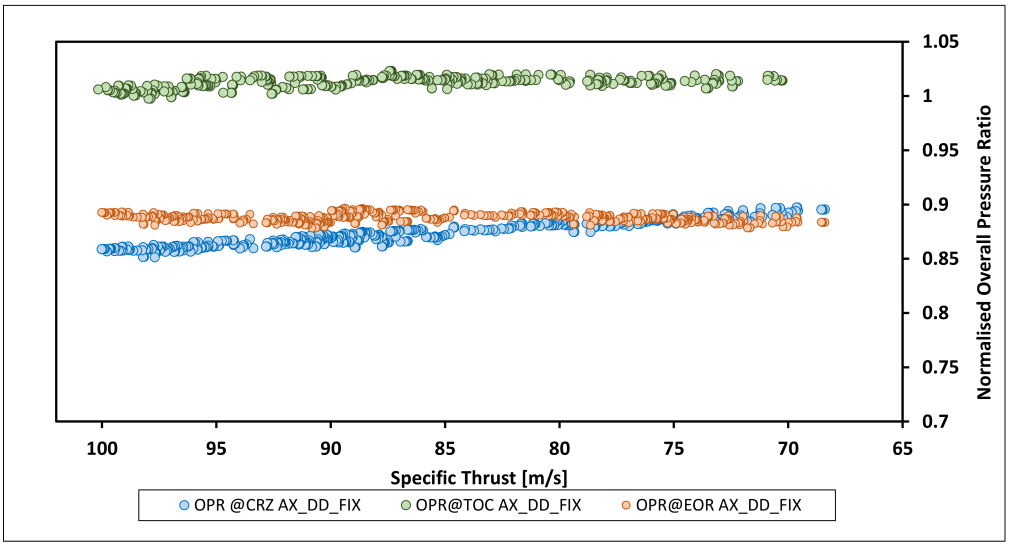

Figure 4.17: Variation of OPR at EOR, ToC and CRZ as a function of the specfic thrust for the axial HPC direct drive case. The OPR values are normalised with the OPR at TOC of the AX_DD_FIX with the smallest fan diameter.

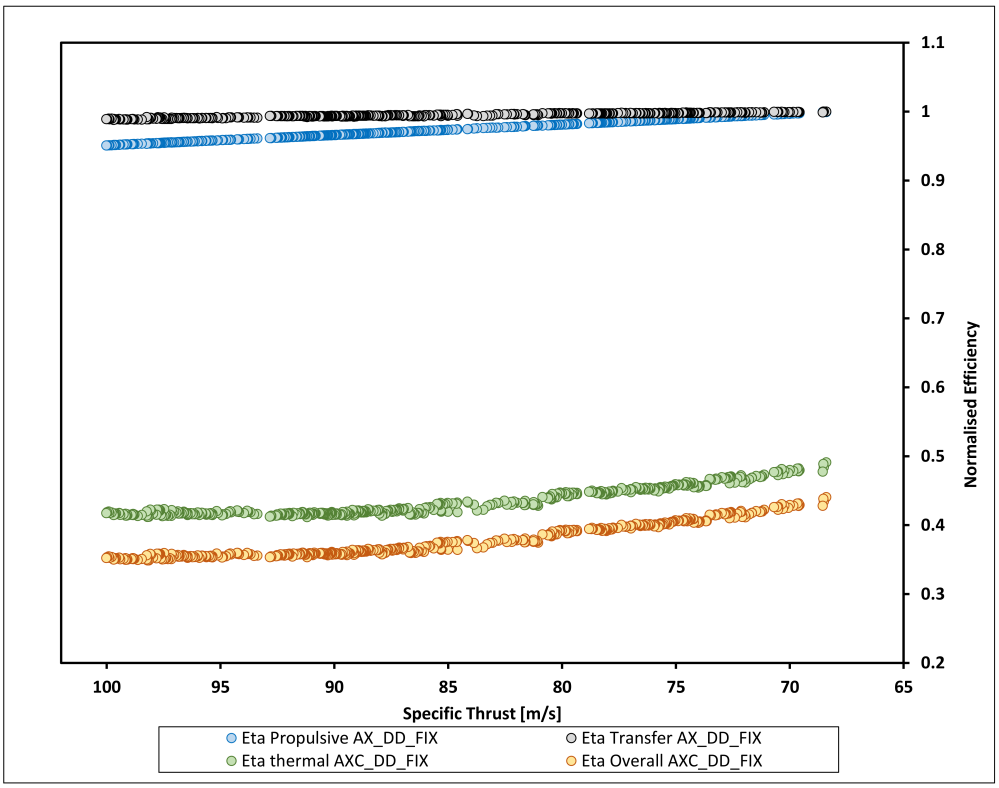

Figure 4.18: Variation of efficiencies as a function of specific thrust for the axial HPC direct drive case. The efficiency values are normalised with the transfer efficiency of the AX_DD_FIX with the smallest fan diameter.

to increase as well going to lower specific thrust values and consequently, the overall efficiency augments as well. Since this is a direct drive case, the transfer efficiency results lower in absolute value relative to the geared counterpart because of the lower polytropic efficiencies of the fan and LPT, as it will be explained later in this section. In the same way it happened for the axi-centrifugal direct drive case, also in the axial direct drive there is an intersection between the propulsive efficiency and transfer efficiency curves in the low specific thrust region.

4.1.6 Cycle designs comparison

A primary comparison that can be made at this point is between the SFC values of the different architectures analysed in this study. In Figure 4.19 the cruise SFC curves are normalised with the value of the highest SFC among all the models that belongs to the AX_DD_FIX model with the smallest fan diameter. The values indicated on the right side represent the reductions in the minimum SFC allowed by the modification of the axial HPC direct drive FIXED architecture. The introduction of the power gearbox gives a reduction in the minimum SFC value of 2.31%, moreover the modification of the HPC architecture to an axi-centrifugal one in the geared turbofans allows an additional reduction of 1.2%. Eventually, the installation of the VAFN component can provide an additional advantage in the minimum SFC of 0.2%.

In order to make comparisons between different SFC values, it is significant to have in mind how this value is determined. In multiple literature sources ([6], [10], [13], [21]) it is possible to find a simple expression of SFC:

$$SFC = \frac{V_0/Q_R}{\eta_p \eta_{th}} \tag{4.1}$$

Considering that the engines are designed to fly at the same velocity at cruise

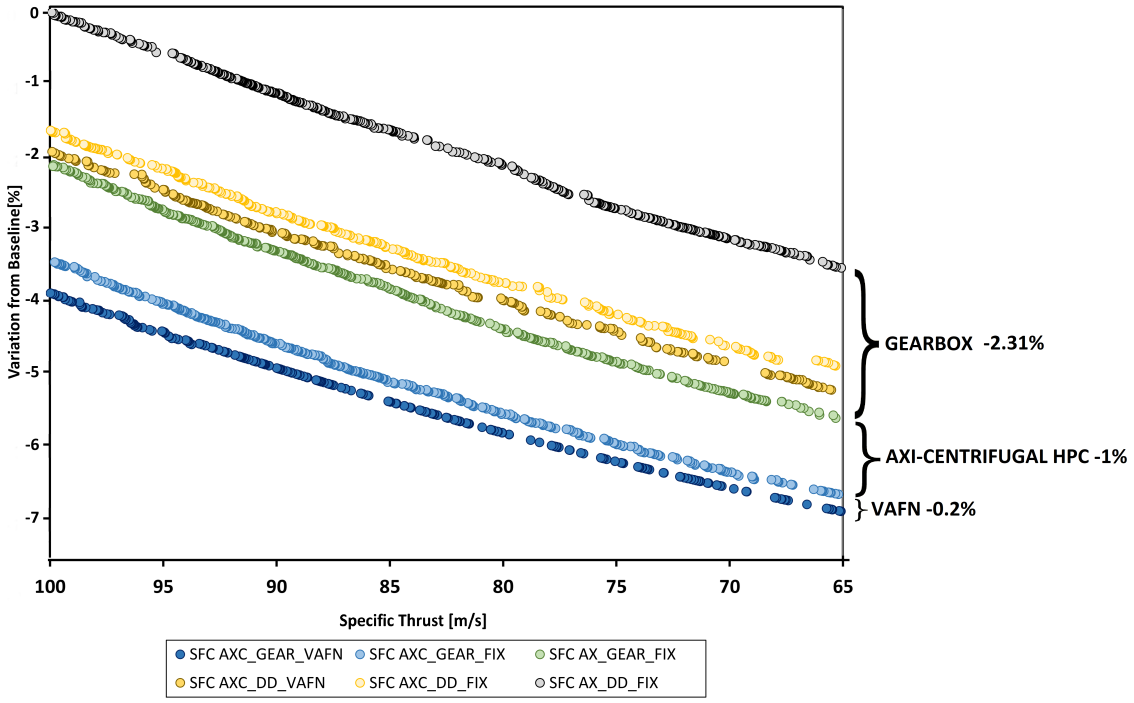

Figure 4.19: Comparison of the variation of SFC as a function of the specific thrust for all the models studied.

(V_0) and that the fuel heating value (Q_R) is the same in all the cases, equation 4.1 leads to the conclusion that different SFC values are caused by variations in thermal and propulsive efficiency. Based on this last statement it is possible to make comparisons between the different engine architectures in terms of SFC at design point.

4.1.6.1 Comparison between VAFN and FIXED configurations

Starting with the differences between the VAFN and the FIXED models, it emerges that in both the geared and the direct drive axi-centrifugal cases the VAFN component provides a decrease in SFC. Observing Figures 4.4 and 4.8, there are no significant changes in the thermal efficiency, since the OPR and TET values are similar between the two architectures. What causes the SFC values of the VAFN configurations to be lower is the propulsive efficiency. In fact, it has been explained previously that the VAFN configuration allows reducing the core dimen-

sions more than the FIXED one, therefore, at the same fan diameter, it allows a higher BPR. Since a higher bypass ratio determines an improvement in propulsive efficiency, the VAFN architectures give a small advantage in SFC relative to the FIXED ones.

4.1.6.2 Comparison between axi-centrifugal and axial HPC configurations

Another significant difference that can be noticed in Figure 4.19 is between the axial and the axi-centrifugal architectures in both geared and direct drive configurations. The difference in this occasion cannot be imputed to the propulsive efficiency, since the difference between the two architectures is present in the engine core and not in the values of fan diameter, BPR or transfer efficiency. In fact, in both the geared and direct drive declinations the axi-centrifugal and the axial architectures reach similar propulsive efficiency values.

Since there is a difference in the core architecture of the engines, the discrepancy in the SFC values can be justified by looking at the thermal efficiencies. It has been proven in several literature resources ([6][10][21]) that the thermal efficiency depends on the TET and OPR values in the cycle. Since there are no significant changes in the TET values between the two considered architectures, the differences in the thermal efficiency are given by different OPR values. In Figure 4.20 there are represented the values of OPR at cruise for the axi-centrifugal and axial geared and direct drive models. In this case the variations are relative to the minimum of the OPR values belonging to the AX_DD_FIX model with the smallest fan diameter. In order to make more readable the chart and more understandable the trends, a quadratic interpolation has been used to eliminate the scatter in the data.

Overall, the OPR values of the axi-centrifugal models result higher than the respective axial models. The highest OPR at CRZ is reached by the geared axi-centrifugal engine followed by the direct drive configuration. In the axial models

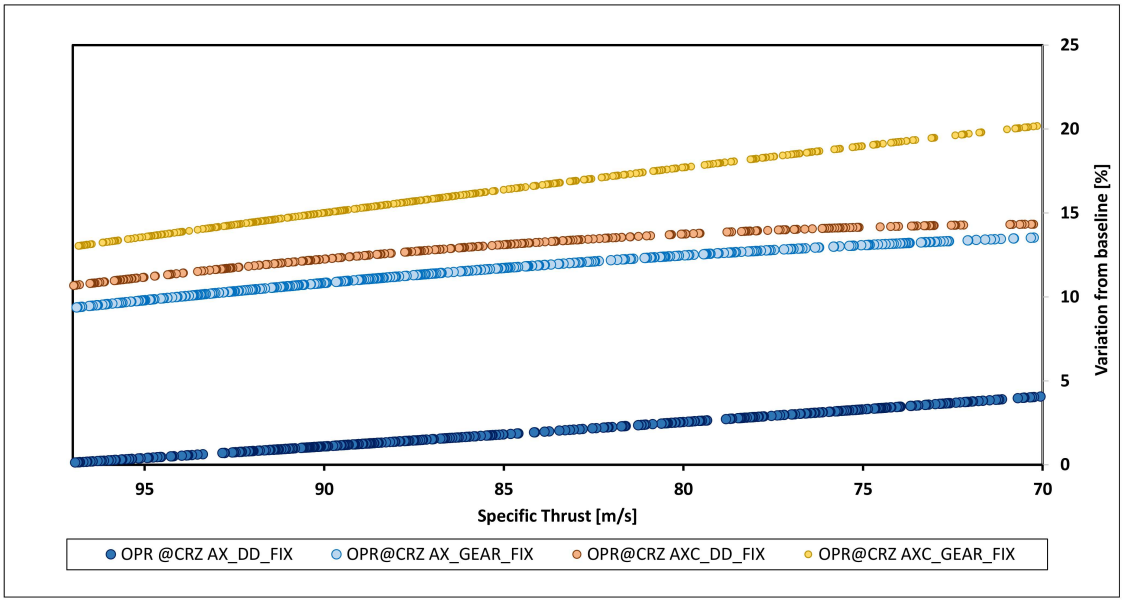

Figure 4.20: Variation of OPR at CRZ as a function of the specific thrust for the axi-centrfugal and axial HPC geared and direct drive models.

a similar behaviour can be observed, with the geared configuration having higher OPR values than the direct drive. This can be justified by looking at the values of polytropic efficiencies of the HPC for the different architectures in Figure 4.21. In this case, a nominal polytropic efficiency has been taken as a reference to normalise all the other values.

The axi-centrifugal HPC architecture reaches higher values of polytropic efficiency compared to the full axial counterpart in both the geared and the direct drive cases. In fact, the axial section of the axi-centrifugal HPC presents relatively low hub to tip ratios, therefore is less affected by the aerodynamic losses and presents higher values of polytropic efficiency, eventually mitigated by the lower values in the centrifugal section. The last stages of the full-axial HPC have hub to tip ratio values near the maximum limit, therefore they suffer more from aerodynamic losses, penalising the performance of the whole HPC and causing lower values of polytropic efficiencies.

In the direct drive models, the polytropic efficiency values are lower than the geared ones. This is due to the fact that the HPC is loaded more, since the IPC

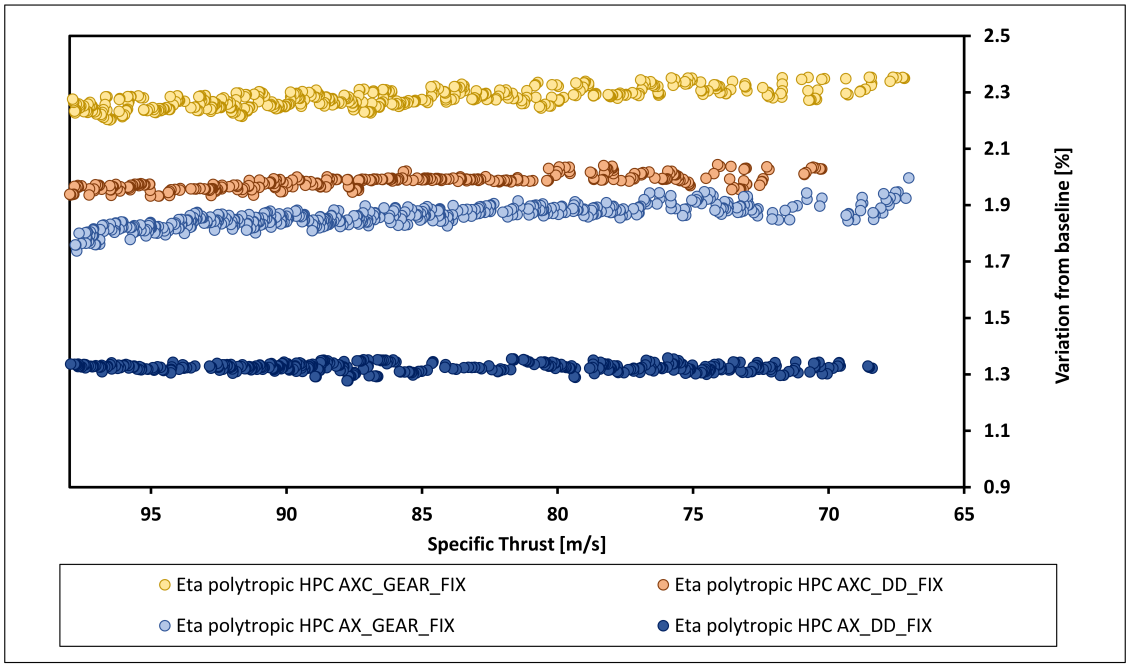

Figure 4.21: Variation of HPC polytropic efficiency as a function of specific thrust for axi-centrifugal and axial architectures.

has to rotate at the fan rotational speed; therefore it can provide lower pressure ratios. More loading on the stages of the compressor causes lower polytropic efficiencies.

A simple expression of polytropic efficiency is given by Saravanammuttoo in Reference [10]:

$$\eta_p = \frac{ln(P_2/P_1)^{\frac{\gamma-1}{\gamma}}}{ln(T_2/T_1)} \tag{4.2}$$

Considering firstly the geared models, it has been said that the axi-centrifugal architecture allows higher OPR values at cruise than the full-axial configuration. Two causes can explain this phenomenon.

The first cause is the lower polytropic efficiency value in the HPC. In fact, equation 4.2 demonstrates that the polytropic efficiency relates the pressure ratio to the temperature ratio across the compressor. If we now think about the EOR condition, the optimiser pushes T30 at the limit value for both the architectures, as it demonstrated in Figures 4.1 and 4.11. The components before the HPC compressor are the same in both the architectures; therefore it may be assumed

that the total temperature and pressure at the inlet of the HPC are equal. Equation 4.2 demonstrates that at the same temperature ratio, a lower value of polytropic efficiency leads to a lower pressure ratio. The polytropic efficiency of the axial models is lower than the one of the axi-centrifugal; therefore the pressure ratio across the HPC is lower as well and the OPR results in lower values. Eventually, a lower OPR in EOR implies lower values also in CRZ and ToC.

The second cause that limits the OPR in the axial architectures is represented by the hub-to-tip ratio of the blades in the last stage of the HPC. In fact, in order to reach higher pressure ratio across the HPC in the axial case, an additional stage may be required, but its hub-to-tip ratio may be over the maximum limit, resulting detrimental to the polytropic efficiency due to the high impact of the aerodynamic losses.

Considering the direct drive models, the above consideration limits even more the pressure ratios reachable by the engines, since the polytropic efficiencies are even lower. Moreover, since the pressure ratios in the HPC are generally higher in a direct drive configuration, the consideration about additional HPC stages may be even more limiting. In fact, in order to reach OPR values similar to the geared cases, the pressure ratio in the HPC have to compensate for the reduction in the pressure ratio of the IPC. This requires higher loading on each stage but even more stages. In a situation in which the core size is decreasing with the specific thrust the hub-to-tip ratio of the last blade becomes critical, therefore it is detrimental for the efficiency to add more stages in the HPC.

4.1.6.3 Comparison between geared and direct drive configurations

The SFC difference between geared and direct drive models can be justified with considerations in both thermal and transfer efficiencies. From the thermal point of view, the fact that the direct drive models can reach lower OPR levels at cruise affects negatively the thermal efficiency.

On the other side, the considerations about the transfer efficiency lead to the analysis of the polytropic efficiencies of the fan and LPT. To simplify and clarify the explanation of the differences between the geared and the direct drive configurations, only the axi-centrifugal architectures are considered in this subsection. Since there is no significant difference in the fan and LPT components between the axial and the axi-centrifugal architectures, the same observations are valid in both the cases. In Figure 4.22 are represented the polytropic efficiencies of the fan and LPT of the axi-centrifugal geared and direct drive configurations. The values are normalised with the fan and LPT polytropic efficiencies of the AXC_GEAR_FIX model with the minimum fan diameter.

The fan polytropic efficiency increases in both the direct drive and geared cases with the increase in fan diameter, but the absolute values of the direct drive models are lower. This is caused by the absence of the gearbox that allows the fan to rotate at its optimum rotational speed; therefore obtain higher polytropic efficiency values.

On the LPT side, the geared models present repeatedly higher values of polytropic efficiencies relative to the direct drive cases. Observing the Smith diagram in Figure 2.6, it can be noticed that, for a determined value of stage loading factor ($\Delta H/U^2$) there is only one value of flow coefficient (V_a/U) that allows the turbine to stay in the line of the optimum polytropic efficiencies. In the case of the geared turbofans, the optimum flow factor can be maintained by changing the gear ratio, while in the direct drive case it increases with the fan diameter since a slower rotational speed is required and, if the stage loading factor is fixed, the polytropic efficiency drops rapidly. In this analysis, the stage loading varies with the fan diameter in order to optimise the LPT performance in accordance with the number of LPT stages.

Since the transfer efficiency is a function of the fan and LPT polytropic efficiencies, it is lower in the direct drive cases relative to the geared and this explains

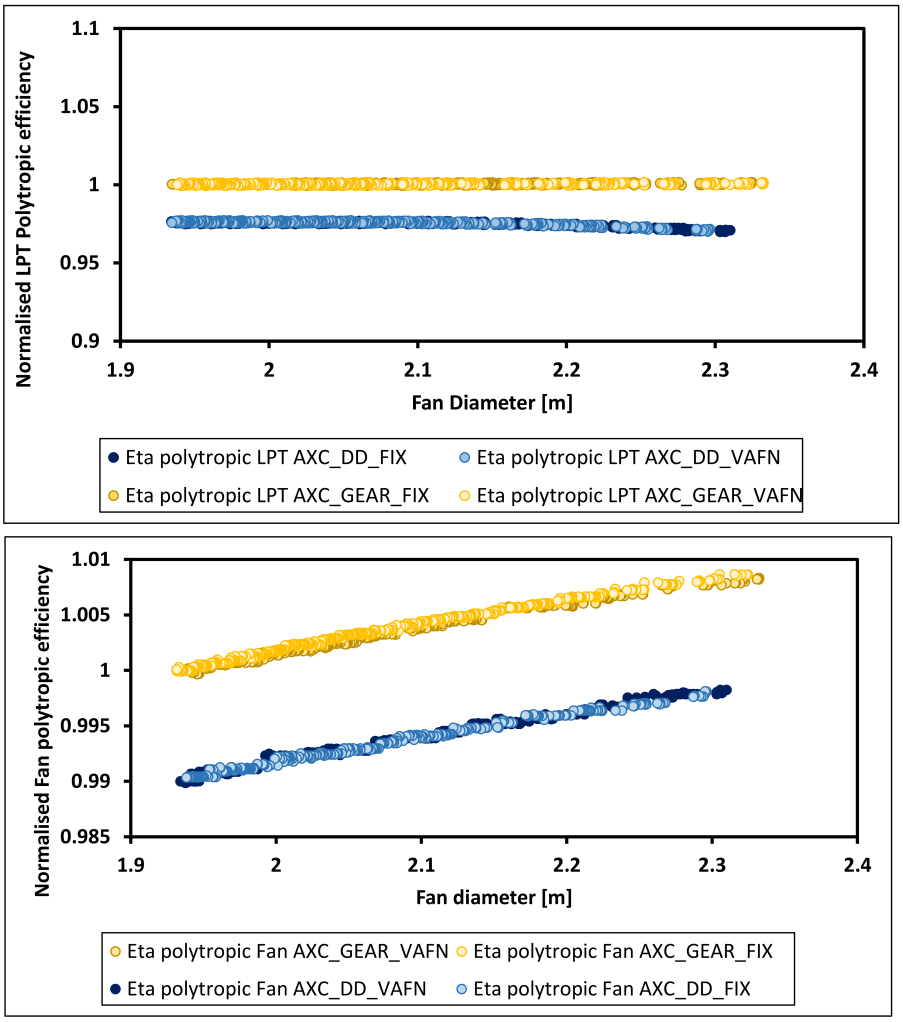

Figure 4.22: LPT (above) and fan (below) polytropic efficiency variations as a function of the fan diameter for the axi-centrifugal HPC geared and direct drive engines.

the trends previous presented in Figure 4.8. A lower transfer efficiency leads to a lower overall efficiency of the cycle; therefore to a higher SFC value.

4.1.6.4 Overview of comparisons

Once the differences in the SFC values have been explained, it is significant to quantify in terms of percentages the advantage that one architecture can give relative to another. In order to do so, Table 4.2 presents all the average SFC percentual differences among all the models analysed in this study. The negative sign in the values represents an advantage, while the positive a disadvantage in

terms of SFC.

	AXC GEAR VAFN	AXC GEAR FIX	AXC DD VAFN	AXC DD FIX	AX GEAR FIX	AX DD FIX
AXC GEAR VAFN		-0.2	-1.85	-2.27	-1.22	-3.51
AXC GEAR FIX	0.2		-1.65	-2.07	-1.02	-3.31
AXC DD VAFN	1.85	1.65		-0.4	0.61	-1.71
AXC DD FIX	2.27	2.07	0.4		1.06	-1.27
AX GEAR FIX	1.22	1.02	-0.61	-1.06		-2.31
AX DD FIX	3.51	3.31	1.71	1.27	2.31	

Table 4.2: Percentual differences between the optimum SFC values among all the architectures studied.

The best architecture in terms of SFC is the axi-centrifugal geared equipped with a variable area fan nozzle. The axial direct drive FIXED architecture presents the highest values of SFC among all the models. In general, the difference between the VAFN and FIXED models is less than 0.5%, between the axi-centrifugal and the axial models is lower than 1.5% and between the geared and direct drive models is lower than 2% in the axi-centrifugal models and 2.31% in the axial ones.

The SFC indicates the uninstalled performance of a turbofan. Therefore, the sequent step is to assess the installed performance of all the architectures, which means to analyse the mission fuel burn. In this analysis, the weight and size of the engine becomes an important parameter and influences the performance. After the mission fuel burn analysis, a similar matrix will be built to understand the variations between the unistalled and the installed performance that are caused by the engine size and weight.

4.2 Engine weight and size estimation results

The process that follows the cycle design optimisation is the engine weight and size estimation, as it has been explained in the project workflow in Methodology. In particular, a Matlab code has been created in order to compile the correct input files and successively launch ATLAS for all the individuals in the Pareto front. In order to reduce the computational time, one engine each 5 in the Pareto front has been assessed; nevertheless it resulted sufficient to develop trends in weight and size and make comparisons between different configurations. Since the process is automatic, a manual check has been conducted for different engines covering all the range of fan diameter variation in order to control that the outcome was realistic and consistent.

The result of ATLAS is the bare weight of the engine without the nacelle; therefore in this project the nacelle weight is estimated by the NASA FLOPS software during the mission fuel burn. This leads to the fact that all the sequent weight comparisons are made on the bare engine. Since NASA FLOPS does not estimate the weight of the VAFN component, a weight penalty has been introduced on the engine models that are equipped with it.

In the following charts, the results have been normalised with the weight and length values of the engine with the smallest fan diameter in the considered range taken as a baseline.

4.2.1 Axi-centrifugal HPC geared engines

Starting from the axi-centrifugal geared FIXED models, it is possible to observe in Figure 4.23 that the weight increases almost linearly with the fan diameter. The same trend can be seen for the engine's length as well, but with a lower slope. In this case, in all the range of fan diameter variation there has been no change in the engine configuration that has remained as follows: 3 stages of IPC, 3 stages

of axial HPC plus 1 of centrifugal HPC, 2 stages of HPT and 3 stages of LPT.

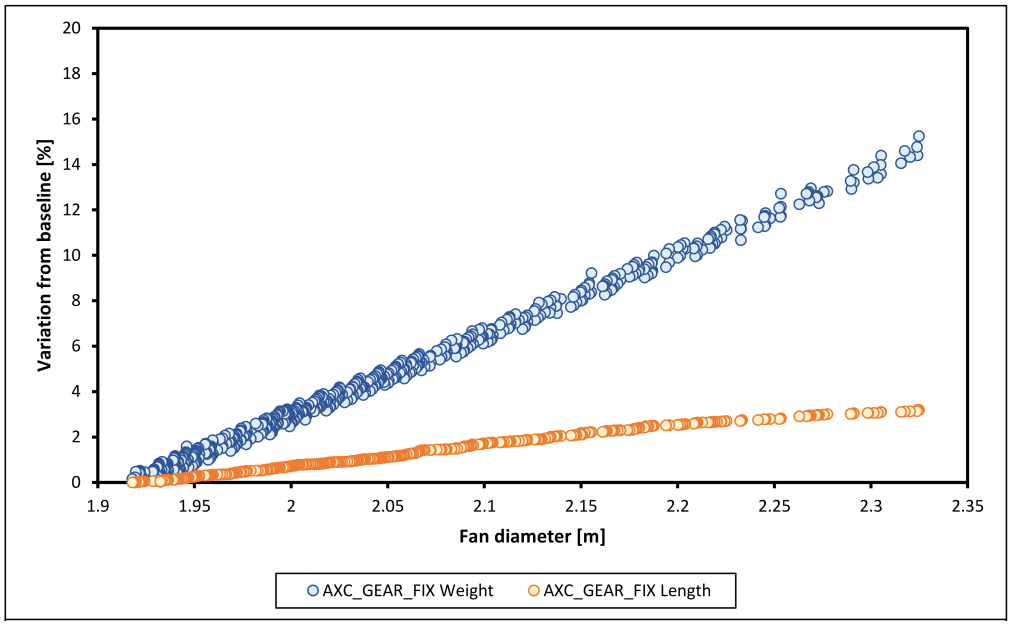

Figure 4.23: Weight and length variation as a function of the fan diameter for the axi-centrifugal geared FIXED models. The model with the smallest fan diameter is taken as a baseline.

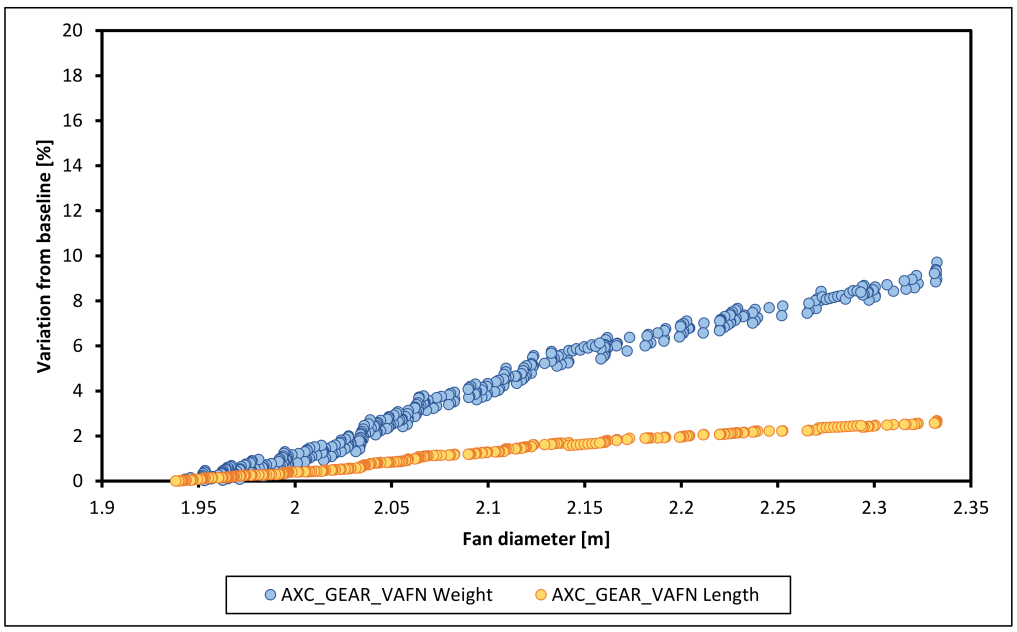

Figure 4.24: Weight and length variation as a function of the fan diameter for the axi-centrifugal geared VAFN models. The model with the smallest fan diameter is taken as a baseline.

What has been observed for the FIXED models applies for the VAFN as well.

In fact, in Figure 4.24 it can be seen that the weight and length increase almost linearly with the fan diameter. The configurations of the engines across the whole fan diameter range has not changed and it has been equal to the FIXED models.

4.2.2 Axi-centrifugal HPC direct drive engines

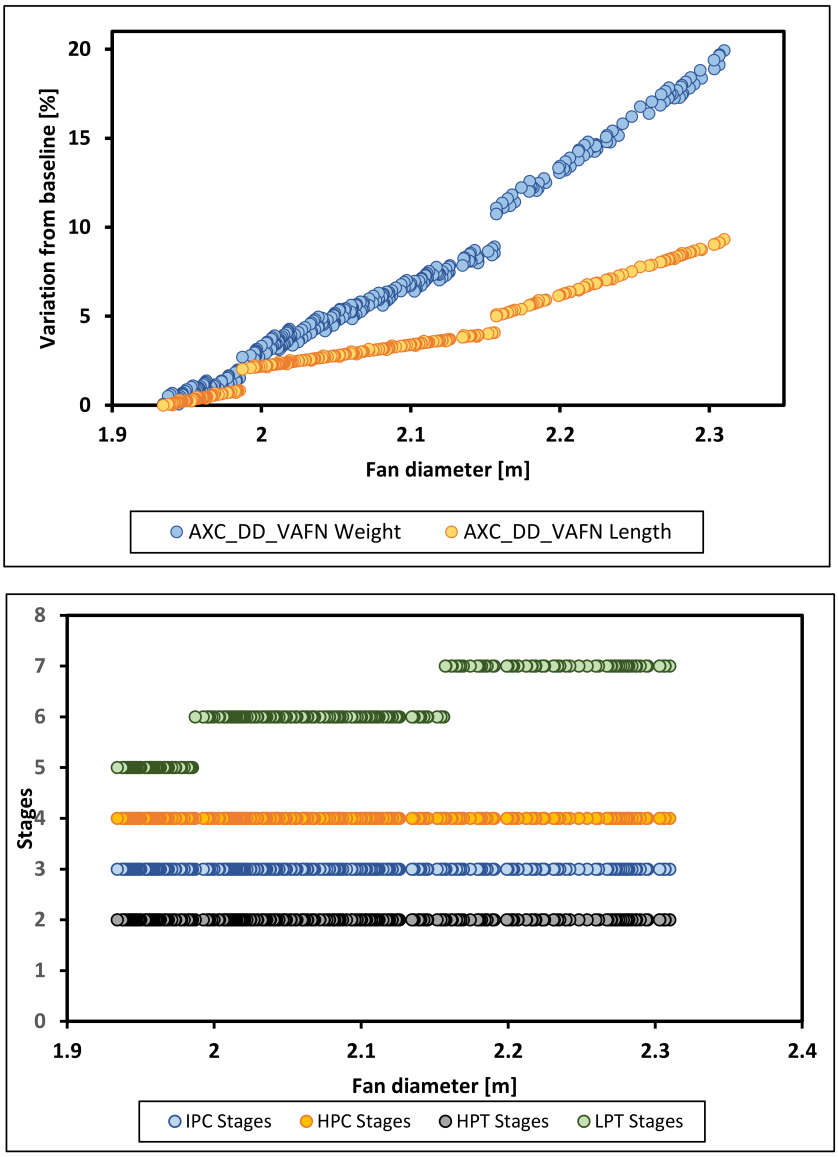

Figure 4.25: Variation of weight and length (above) and configuration (below) as a function of the fan diameter for the axi-centrifugal direct drive VAFN case. The model with the smallest fan diameter is taken as a baseline.

In the direct drive axi-centrifugal models, similarly to the geared ones, there

is an almost linear trend in the increase of the engine weight and length with the incrementation of the fan diameter, as it can be seen in Figure 4.25 for the VAFN cases and in Figure 4.26 for the FIXED ones.

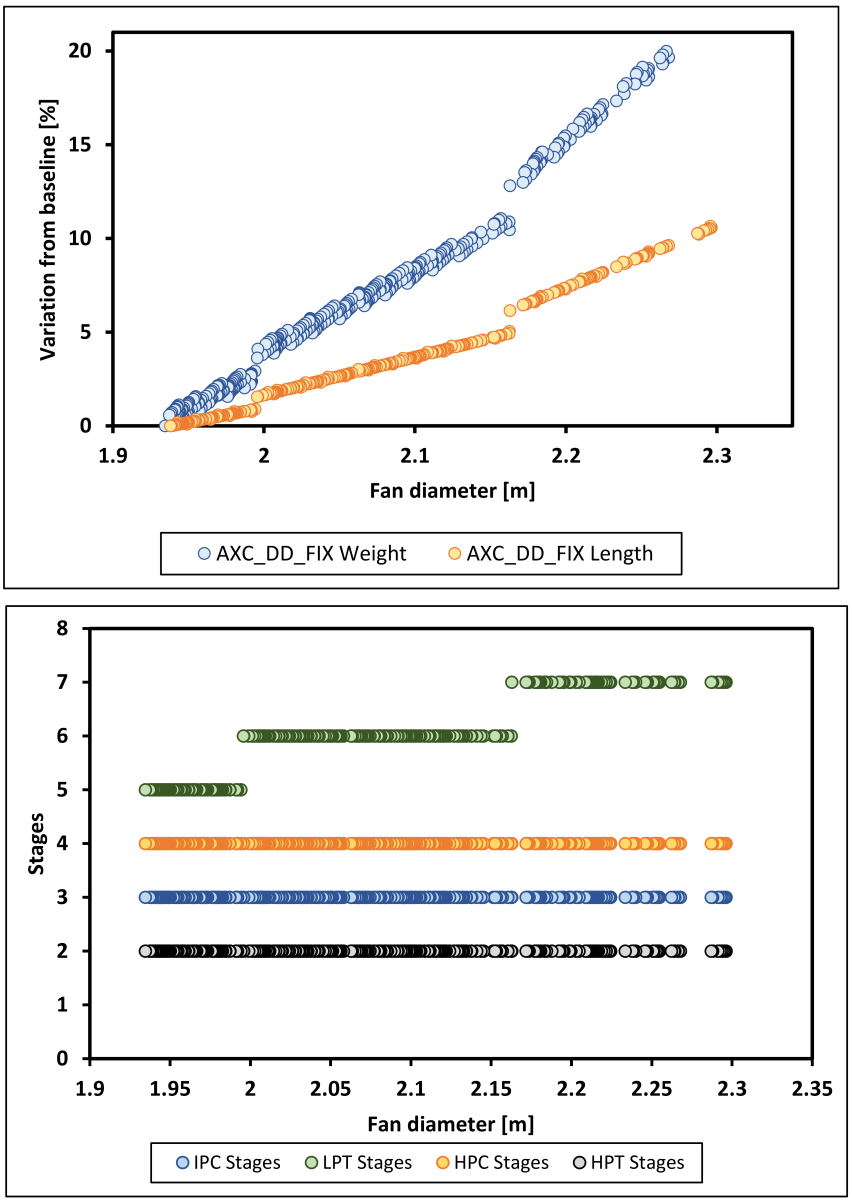

Figure 4.26: Variation of weight and length (above) and configuration (below) as a function of the fan diameter for the axi-centrifugal direct drive FIXED case. The model with the smallest fan diameter is taken as a baseline.

However, in the direct drive models the trends show step climbs at the fan diameters at which there is an addition of an LPT stage. In fact, in the direct drive cases the configuration does not remain constant across the whole range of fan

diameter variation, but it presents an increase in the number of LPT stages from 5 to 7 as the fan diameter augments. Moreover, also a variation in the weight and length slopes can be observed with the addition of the 7th LPT stage.

4.2.3 Axial HPC geared engines

The fully axial geared architecture shows the same behaviour as its axi-centrifugal counterpart. In fact, as it can be noticed in Figure 4.27, the weight and the length of the engines increase linearly with the fan diameter.

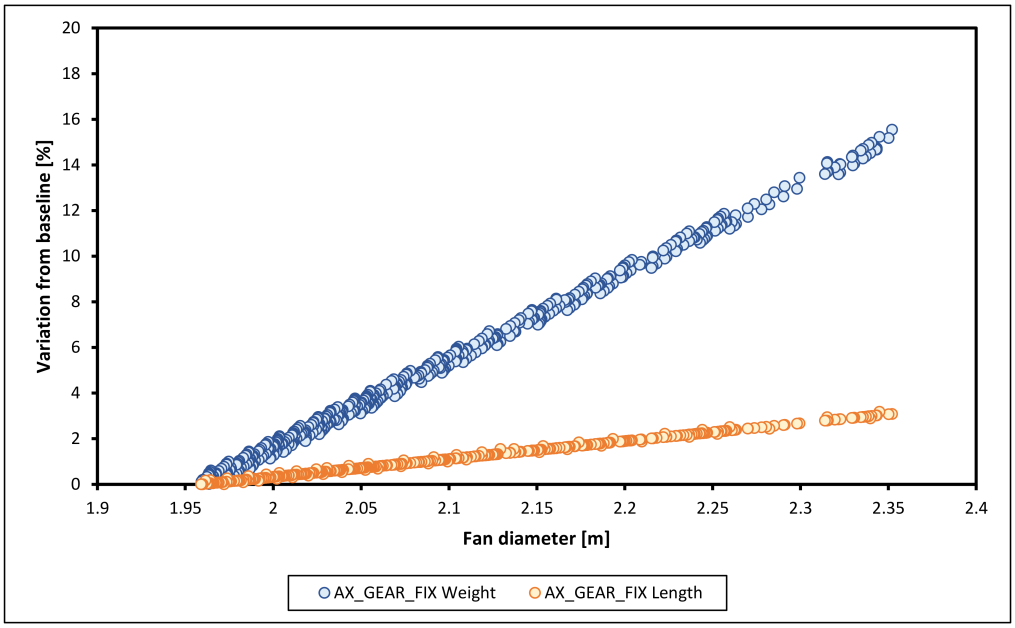

Figure 4.27: Weight and length variation as a function of the fan diameter for the axial geared FIXED models. The model with the smallest fan diameter is taken as a baseline.

No step climbs can be observed in this case, since in the fan diameter variation range considered there has not been any configuration change in the engines. The configuration has been constant as follows: 3 stages IPC, 10 stages HPC, 2 stages HPT and 3 stages LPT.

4.2.4 Axial HPC direct drive engines

These engines follow the same behaviour of the previous architectures analysed.

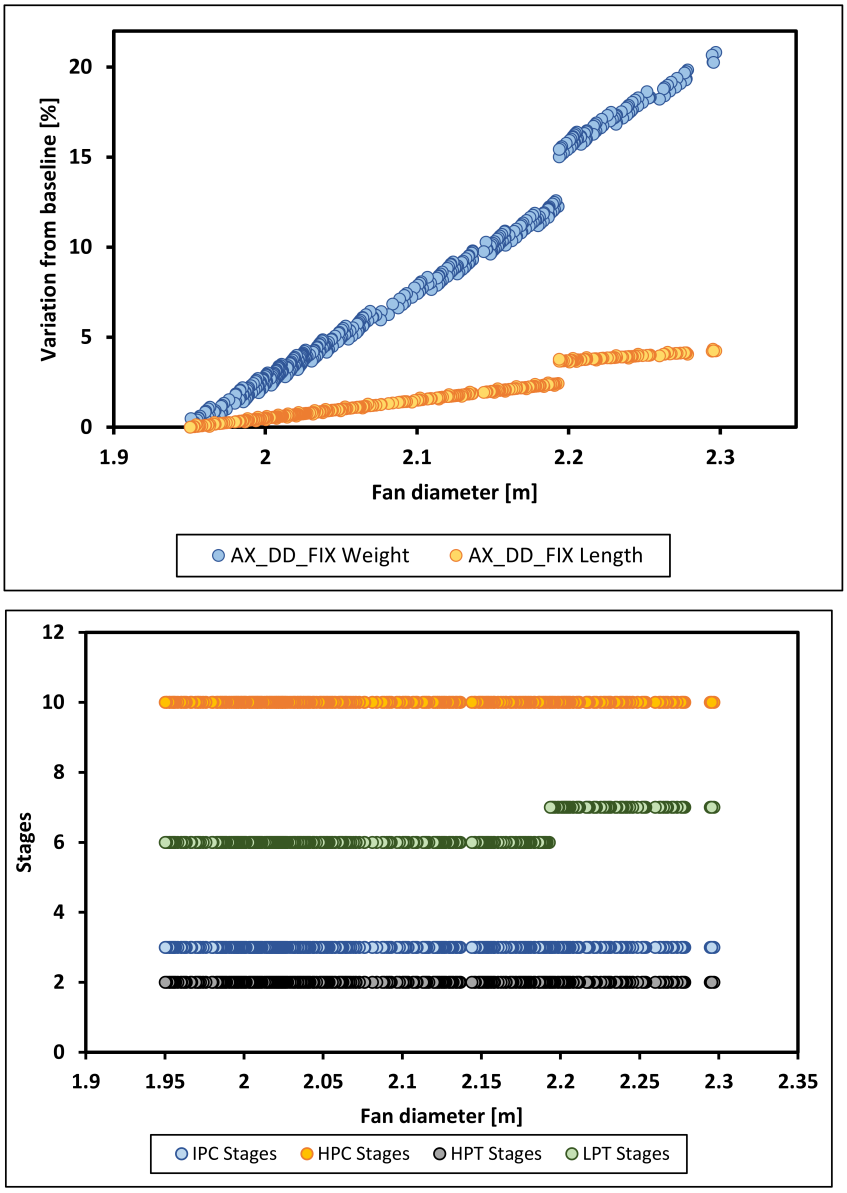

Figure 4.28: Variation of weight and length (above) and configuration (below) as a function of the fan diameter for the axial direct drive FIXED engines. The model with the smallest fan diameter is taken as the baseline.

In Figure 4.28 it can be seen that the weights and lengths of the engines increase with the increase in fan diameter. Similarly to the axi-centrifugal direct drive models, there is a step climb in the trend at the fan diameter in which there

is an addition in the LPT stages. However, in this case the configuration with 6 LPT stages covers a higher range of fan diameters relative to the axi-centrifugal. Moreover, the transition to a 5 stages LPT architecture occurs at a fan diameter otuside the interest range of this analysis.

4.2.5 Weight and size comparisons

Since the aim of this project is to assess different engine architectures from a mission fuel burn prospective , it is significant to compare weights and sizes, due to the fact that they are part of the parameters that influence the mission fuel burn. This section is divided into two subsections in which two main comparisons are made: geared versus direct drive and axi-centrifugal versus axial models. In order to have a common base for the axial and axi-centrifugal cases and to keep the comparison clear and concise, only the FIXED models will be considered in these comparisons, since the difference relative to the VAFN models is represented only by the weight penalty introduced by the VAFN component.

4.2.5.1 Geared and direct drive models

It is a common belief that one of the main advantages in a geared turbofan is the weight and length reduction due to the reduced number of LPT stages. The anlysis conducted in this project confirms the second assertion, while the first depends on the fan diameter considered. This can be seen in Figures 4.29 and 4.30, which charts have been normalised with the weight and length of the lowest fan diameter direct drive turbofan.

In both the axial and axi-centrifugal architectures, at low values of fan diameters the direct drive configuration presents a lighter weight compared to the geared. This is caused primarily by the weight of the power gearbox that is not completely mitigated by the reduced number of LPT stages, since the difference

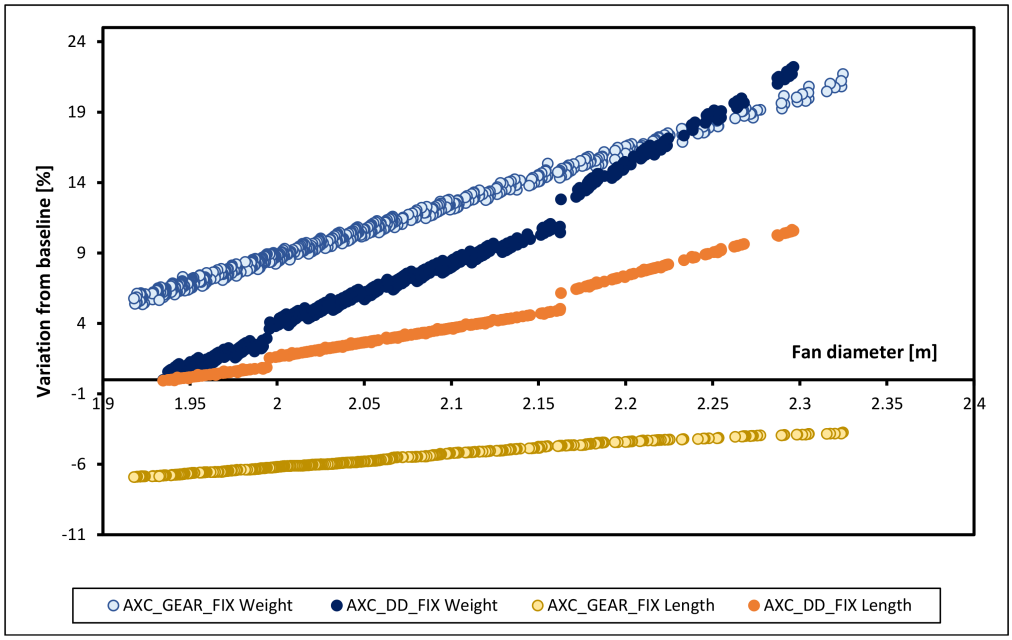

Figure 4.29: Variation of weight and length as a function of fan diameter for the axi-centrifugal geared and direct drive models FIXED. The baseline is represented by the AXC_DD_FIX model with the smallest fan diameter.

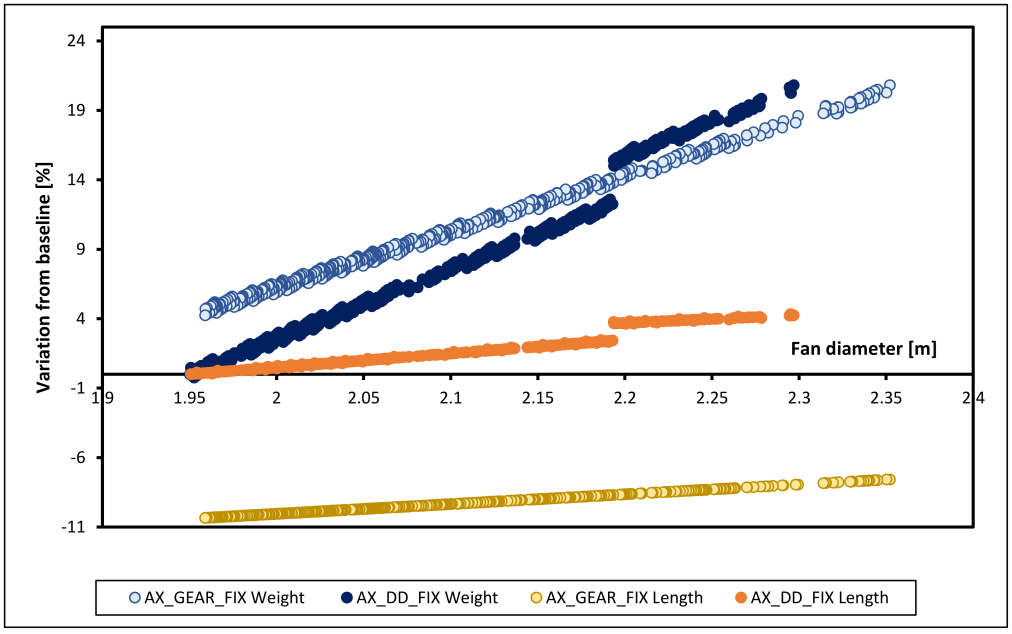

Figure 4.30: Variation of weight and length as a function of fan diameter for the axial geared and direct drive models FIXED. The baseline is represented by the AX_DD_FIX model with the smallest fan diameter.

in the number of stages between the geared and ungared cases is still limited.

Despite having fewer stages than the direct drive architecture, the LPT discs in

the geared case weight more than the direct drive ones, since the rotational speed in the LPT is higher.

At high values of fan diameter the geared configuration starts to show an advantage in terms of weight relative to the direct drive one. In fact, in both the axi-centrifugal and axial architectures there is an intersection of the weight curves, with the geared one passing below the direct drive. In fact the increase in fan diameter requires additional LPT stages in the direct drive configurations, while the geared once can almost maintain the same LPT configuration by changing the gear ratio; therefore the weight penalty introduced by the power gearbox and the LPT discs remains similar to the low fan diameter cases, while in the direct drive architectures the LPT weight keeps increasing. In both the axi-centrifugal and the axial cases the intersection happens in a region in which the direct drive configuration presents 4 LPT stages more than the geared one.

In terms of length, both the axi-centrifugal and the axial architecture show a clear advantage of the geared configuration relative to the direct drive. The difference increases at higher fan diameters because of the addition of LPT stages in the direct drive configurations.

4.2.5.2 Axi-centrifugal and axial models

From the weight and size estimation process conducted in this project the axi-centrifugal architecture results in a lighter engine in all the range of fan diameter variation considered, for both the geared and direct drive configurations. This can be seen in Figure 4.31 and 4.32, which have been normalised with the weight and length of the axial model with the smallest fan diameter.

In the range from 2.16 m to 2.19 m of fan diameter in the direct drive configurations, the axial models result being lighter than the respective axi-centrifugals. This is due to the fact that the axi-centrifugal direct drive models requires a transition to 7 stages of LPT at a lower fan diameter value. In fact, at the same number

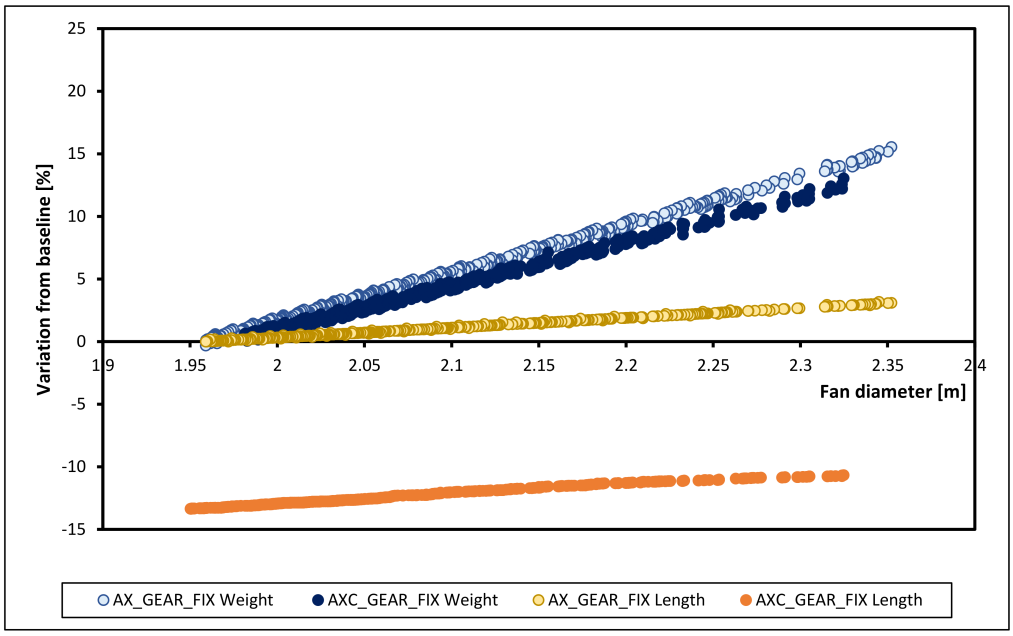

Figure 4.31: Variation of weight and length as a function of fan diameter for the axial and axi-centrifugal geared FIXED models. The baseline is represented by the AXC_GEAR_FIX model with the smallest fan diameter.

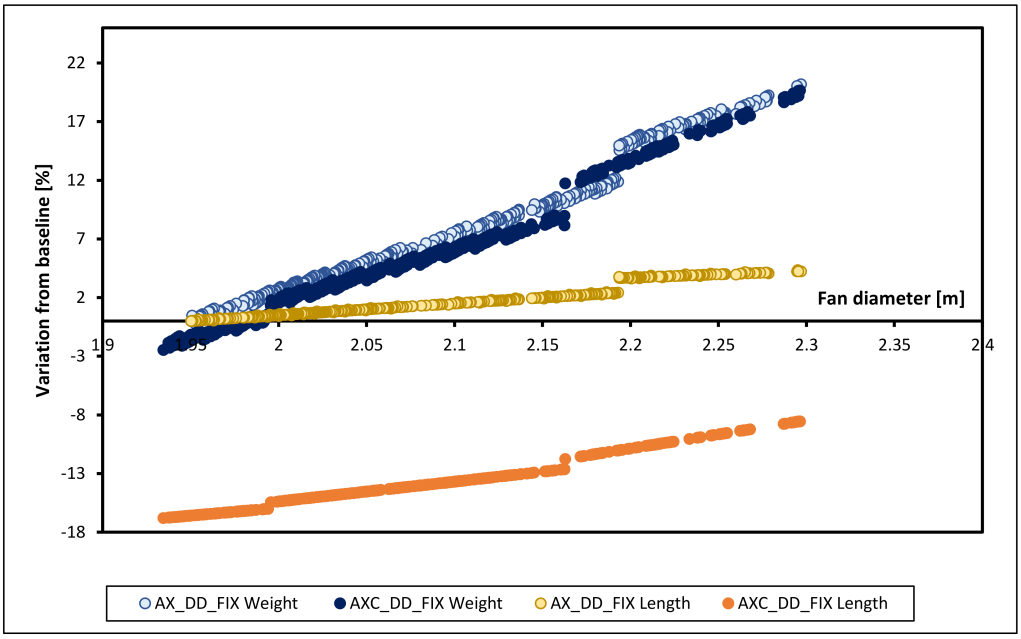

Figure 4.32: Variation of weight and length as a function of fan diameter for the axi-centrifugal and axial direct drive FIXED models. The baseline is represented by the AX_DD_FIX model with the smallest fan diameter.

of LPT stages the axi-centrifgual configuration results always lighter than the axial counterpart. In the geared models, across the range of fan diameters of interest,

the axi-centrifugal architecture results averagly 1.5% lighter, with the difference increasing going to higher fan diameters, and 15% shorter. In the direct drive axi-centrifugal models the advantage in terms of weight is similar to the geared ones. In terms of length the axi-centrifugal models result 17% shorter at low fan diameters and 13% in the high values region.

The differences in weight and length given by the axi-centrifugal architecture are primarily imputable to the HPC component. The advantage in terms of length, compared to the axial architecture, is significant, while the same cannot be said in terms of weight. In fact it is true that the centrifugal is more compact than the axial compressor, but only in the longitudinal direction. Considering the radial direction, the centrifugal compressor stages goes to much higher diameters, therefore the centrifugal loads on the disc increase, leading to a weight much more elevated than a single axial stage.

4.2.5.3 Overall comparison

Figure 4.33 presents an overall comparison between the weights of all the architectures investigated in this project. The engine with the smalles fan diameter among all the axi-centrifugal HPC geared FIXED models has been taken as a reference for this comparison.

In the lower fan diameters region the direct drive models resulted lighter than the geared counterparts. The lowest weight values in this region belong to the axi-centrifugal HPC direct drive FIXED model. Moving towards higher fan diameter values, there's the crossing between the curves and the geared models start being lighter than the direct drive ones. At the highest fan diameter value considered in this study, the architecture that presents the lowest weight is the axi-centrifugal HPC geared with a FIXED area fan nozzle.

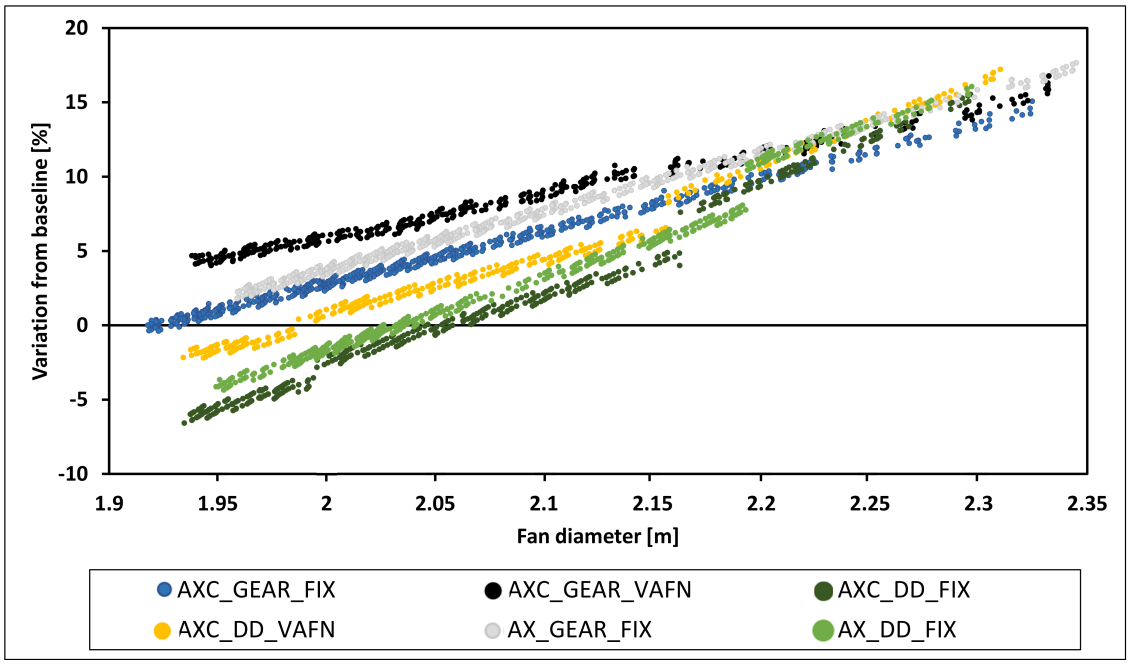

Figure 4.33: Engine weight variation as a function of the fan diameter for all the models considered in this study.

4.2.6 Engine annulus designs comparison

Among the capabilities of ATLAS there is also the possibility to represent schematically the annulus design of the engines. In figure 4.34 there are exposed 4 different annulus designs representative of all the turbofan architectures studied in this project. The models chosen are the ones with the highest fan diameter. It can be noticed that the turbofans with axi-centrifugal HPC architecture appear to be shorter in both the gerared and direct drive declinations. The principal difference comes out in the HPC section, in fact in the axi-centrifugal models it appears more compact in length but it has a higher frontal area in the centrifugal compressor part. The direct drive engines differ from the geared mainly in the LPT component. In fact, the absence of the power gearbox brings a higher number of LPT stages as well as thinner and lighter discs. The geared models present fewer stages in the LPT, but since they rotate faster, the discs are thicker and heavier than the direct drive counterpart. Moreover the mean diameter of the last stages of the LPT is higher in the direct drive cases relative to the geared ones.

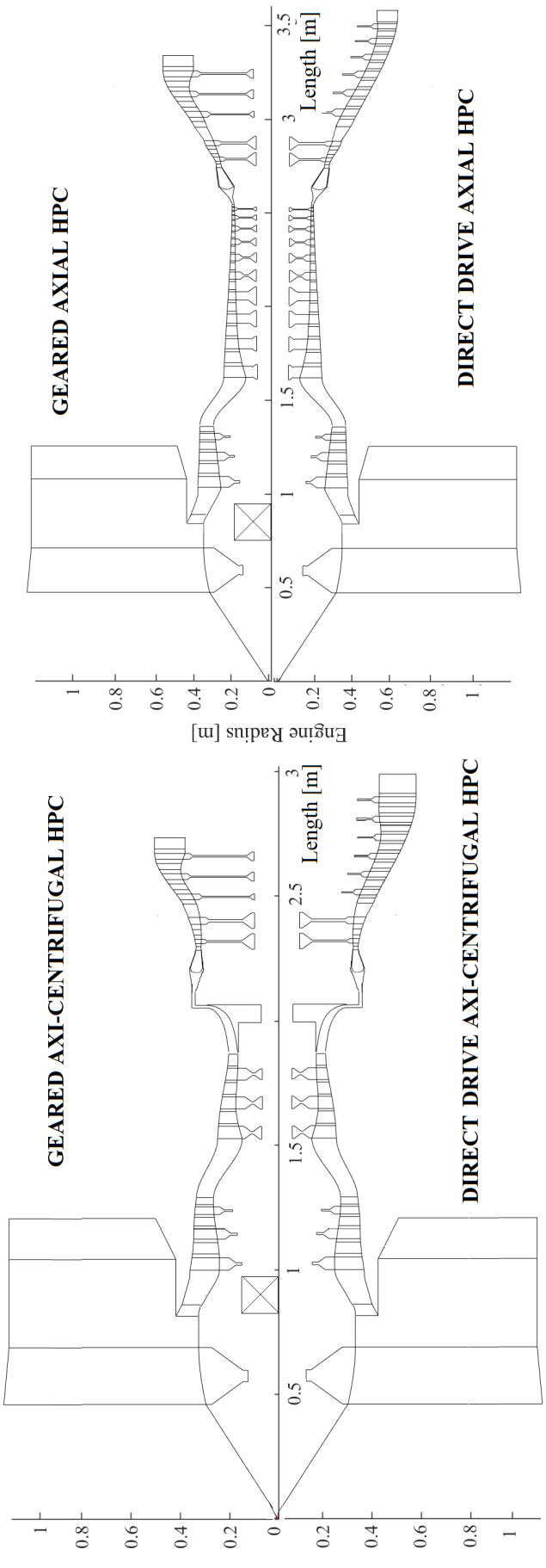

Figure 4.34: Annulus design of the architectures under investigation.

4.3 Mission fuel burn results

It has been described in the Methodology chapter that the step that follows the weight and size estimation is the mission fuel burn analysis. An automatic system has been utilised in order to create the engine deck for each individual, compile the input file and run NASA FLOPS, eventually collecting the outcomes. The mission profile has a range of 3000 nm and the aircraft utilised is the Airbus A-321 for each one of the engines investigated.

In Figure 4.35 there are plotted the mission fuel burn curves as a function of the fan diameter for all the architectures investigated in this study. The mission fuel burn values have been normalised with the highest value belonging to the engine with the smallest fan diameter among the axial direct drive engines. For each curve the minimum point is indicated with a star.

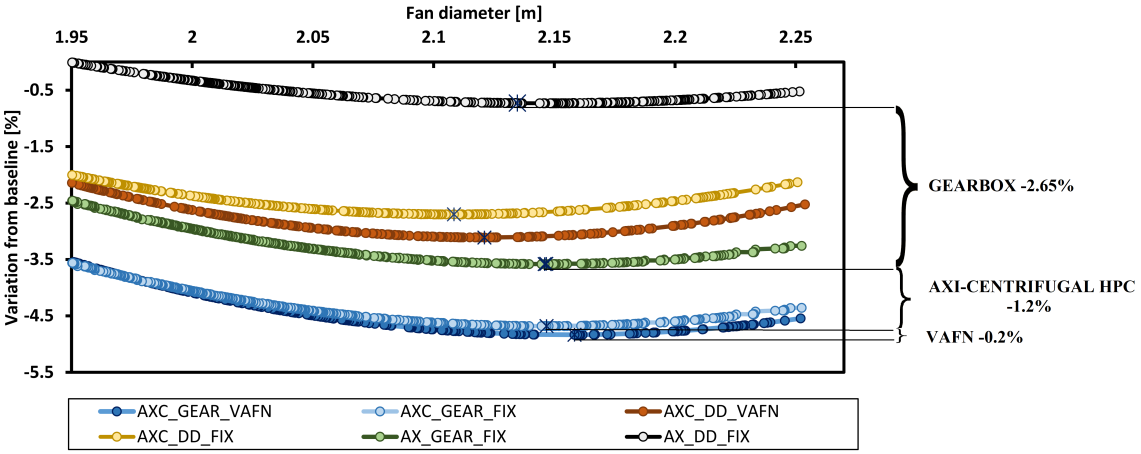

Figure 4.35: Mission fuel burn variation as a function of fan diameter for all the models investigated.

With the increase in fan diameter, the Pareto fronts of all the engines were showing a continuous reduction of the SFC values. In fact, the SFC curve indicates the uninstalled performance of the engine, without taking into consideration the weight and size penalties that come out once it is installed on the aircraft. From the analysis of the MFB curves, it appears clearly that the gain obtained by reducing the specific thrust is not illimited, but there is a fan diameter that al-

lows the engine to obtain the minimum fuel burn. Above this diameter value, the penalties in terms of weight and drag dominate the gain in SFC; therefore the MFB values start increasing again. This behaviour can be seen among all the architectures analysed in this study. It can be noticed that the transition from a direct drive to a geared architecture, for the same core configuration, shifts the minimum MFB fan diameter towards higher values. The same observation can be made for the transition from a FIXED to a VAFN configuration. In fact, in both the direct drive and geared axi-centrifugal HPC architectures the introduction of the VAFN brings the optimum fan diameter to a higher value.

On the right side of the chart in Figure 4.35 there are indicated the advantages in minimum MFB introduced by the modification of the engine architecture. Considering the conventional direct drive axial HPC with a FIXED fan area nozzle as the starting point, it can be seen that the introduction of a gearbox to this architecture leads to a reduction of 2.65% in MFB. Moreover, if the HPC configuration, in the geared architecture, is modified from a fully axial to an axi-centrifugal one, an additional 1.2% reduction can be obtained in the minimum MFB. Eventually, if a VAFN is installed on the axi-centrifugal HPC geared architecture, the minimum MFB is reduced by another 0.2%. This brings to an overall reduction of 4.05% in the minimum MFB if all the alternative component investigated in this project are included in the turbofan architecture.

The percentual differences between the minimum MFB values of all the architectures investigated are represented in Table 4.3. A negative sign indicates an advantage in MFB of an architecture over the other, while a positive indicates a disadvantage.

There are variations in the differences compared to the uninstalled performance matrix. A first difference that can be seen in the MFB curves relative to the SFC ones is that the VAFN and FIXED model curves are not parallel anymore but they become incident at low values of fan diameter. In fact, in this region of

	AXC GEAR VAFN	AXC GEAR FIX	AXC DD VAFN	AXC DD FIX	AX GEAR FIX	AX DD FIX
AXC GEAR VAFN		-0.19	-2.02	-2.42	-1.39	-4.05
AXC GEAR FIX	0.19		-1.83	-2.23	-1.2	-3.85
AXC DD VAFN	2.02	1.83		-0.39	0.733	-1.92
AXC DD FIX	2.42	2.23	0.39		1.13	-1.53
AX GEAR FIX	1.39	1.2	-0.733	-1.13		-2.65
AX DD FIX	3.95	3.75	1.92	1.53	2.65	

Table 4.3: Percentual differences at the minimum MFB value among all the architectures investigated.

fan diameter the weight of the engine is lower, as it has been demonstrated in the weight and size estimation section, therefore the penalty introduced by the VAFN component takes a significant percentage of the engine weight, therefore the small efficiency advantage given by the VAFN component is almost cancelled because of the higher engine weight. On the high fan diameter region the weight of the engines becomes higher as well, therefore the penalty introduced by the VAFN component becomes less important; therefore the VAFN engines present a MFB advantage of around 0.2% in the geared cases and 0.4% in the direct drive configurations.

The advantage of the axi-centrifugal architectures relative to the axial ones has increased to 1.2% in the MFB values. This means that the thermodynamic advantage of the axi-centrifugal models has been slightly improved also by the mechanical advantage of lighter and shorter engines.

In general, the advantage of the geared cases relative to the direct ones re-

sults improved in the installed performance. In the weight and size estimation section it has been demonstrated that up to a certain fan diameter the direct drive models were lighter than the geared counterpart, but this matrix takes into consideration the difference between the minimum fuel burn values that occurs at fan diameters in which the geared configurations are lighter. Moreover the weight of the entire aircraft increases in the direct drive models, because of the additional fuel that is needed to complete the mission.

Overall, the study of the mission fuel burn reveals that the optimum engine in mission fuel burn for the Middle-of-Market type of aircraft is represented by the axi-centrifugal HPC geared architecture. In this architecture the adoption of the VAFN component can lead to a slight gain in MFB at the high values of fan diameter, but doesn't result necessary for the fan operability in terms of surge at take-off.

The architecture with the highest mission fuel burn is the axial HPC direct drive. Actually it represents the turbofan architecture most utilised in the Middle-of-Market sector nowadays; therefore, depending on the type of architectural modifications that are made on this engine, this study shows that different levels of advantages in MFB can be obtained.

Chapter 5

Conclusions and future work

This project focused on the optimisation and comparison of near future turbofan architectures for the Middle-of-Market sector. The analysis was conducted on a preliminary design level utilising the EPYDOSIS platform developed by the Cranfield University UTC. Overall, the outcomes demonstrate the potential advantage of the geared architectures over the direct drive ones. Moreover, among the geared turbofan, variations in the HPC from a full axial architecture to an axi-centrifugal demonstrate an ulterior improvement in mission fuel burn.

5.1 Significant outcomes

The major outcomes of this project are listed below:.

- For a specific set of thrust requirements and technological level assumptions, the exploration of the design space demonstrated that the reduction of the specific thrust leads to a continuous reduction in SFC, while the mission fuel burn reaches a minimum point. The reduction in specific thrust goes with the increase in fan diameter; therefore the main parameter that affects the performance of the turbofans in this project appeared to be the fan diameter. Moreover, the weight and size estimation process demon-

strated that these two parameters are dependant on the fan diameter as well.

- The cycle design optimisation process showed that, apart from the fan diameter, other three parameters affect significantly the performance of the engines:

  1. T30 determines the maximum OPR that the cycle can reach;
  2. T40 determines the BPR value of the turbofans;
  3. the technological level, intended as maximum allowed metal temperature on the turbine blades, determines the turbine cooling requirements.

- The geared architectures demonstrated superiority in terms of SFC and mission fuel burn relative to the direct drive ones. In the axial HPC architecture the difference, between the geared and the direct drive configurations, in optimum SFC values resulted 2.31%, while in minimum MFB 2.65%. In the axi-centrifugal HPC architecture the differences resulted about 2% in optimum SFC and 2.2% in minimum MFB.

  This superiority is primarily caused by the higher transfer efficiency due to the better fan and LPT polytropic efficiencies in the geared architectures. Moreover, an advantage to the geared architectures appeared to be also given by the higher OPR values achievable.

  From a weight point of view, the direct drive architectures resulted in lighter engines in the low fan diameters region, but the increase in the number of LPT stages with the increase in fan diameter caused a crossover in the weight curves that resulted in lighter geared architectures in the region of high fan diameters. In length, the geared architectures demonstrated an advantage relative to the direct drive ones in the whole range of fan diameters.

- Among the geared turbofans, the adoption of an axi-centrifugal HPC allows the engines to achieve higher OPR values, resulting in an advantage on the thermal efficiency that leads to a improvement in SFC of 1% and in minimum MFB of 1.2% . Moreover, the geared turbofans with axi-centrifugal HPC architectures resulted around 1.5% lighter and 14% shorter compared to the axial counterparts.

- The adoption of a VAFN component demonstrated the possibility to reduce more the core size compared to the FIXED configuration. This allowed higher BPR values that lead to slightly improved propulsive efficiencies relative to the FIXED configurations. The advantage in the optimum SFC and minimum MFB resulted small, around 0.2% in the geared and 0.4% in the direct drive models. Overall, the safe fan operability in terms of surge at the EOR condition, for the geared and the direct drive models, eliminated the necessity of a VAFN in this range of specific thrust.

5.2 Future work possibilities

This project has started a preliminary design analysis on a class of turbofans that will gain significant importance in the following years because of the growing interest that the aircraft manufacturers are showing in the Middle-of-Market sector. This thesis presents several starting points for future researches that can expand and improve its results. The future work possibilities that are worthy to be carried on according to the author are listed below:

- **Expand the current analysis**. In fact, following its aim, this project is focused only on SFC, weight and mission fuel burn analysis. In order to have a more complete view of the different architectures and their comparison, further aspect should be analysed:

  - Emissions: it represents one of the most important parameters in turbofan performance nowadays and comparing different architectures can lead to the identification of the ”greenest” one;
  - Operating costs: in the Middle-of-Market sector the cost is what leads the choice of an engine relative to another. The geared architectures demonstrated an advantage in MFB but, in economic terms, it can be reduced by a higher maintenance cost of the PGB. Among the geared turbofans the axi-centrifugal HPC architecture presents a lower number of components; therefore it may lead to a reduced initial and maintenance cost of the engine. The cost analysis can overturn completely the comparison made on the MFB basis and explain the reasons the airliners may opt for one architecture rather than another.

- **Include core work split in the optimisation process**. In fact, this analysis found out that the full-axial HPC architecture was limited in the pressure ratios it could reach because of the size of the blade in the last stage. If a variable core work split could have been used, the outcomes could have been different since the pressure ratio distribution could have retarded the pressure ratio limitation on the HPC to higher OPR values.

- **Include an estimation method for the centrifugal compressor polytropic efficiency**. In this project, the polytropic efficiency of the centrifugal compressor has been estimated in a basic way by matching the values given by ATLAS. A future research may benefit from a more complete estimation method that varies the polytropic efficiency of the centrifugal compressor during the design space exploration.

- **Examine the aerodynamics of the axi-centrifugal HPC**. It was not in the intentions of this project to define the aerodynamic interactions between the axial and the centrifugal sections in the axi-centrifugal HPC. It would be

of primary importance to examine in depth, through 3D CFD methods, the interactions between these two parts in order to assess the real feasibility of such a design.

- **Examine in depth the VAFN architecture**. This project demonstrated that the VAFN component, despite adding weight, cost and complexity to the architecture, isn't strictly necessary for the specific thrust range analysed and it does not provide a significant MFB advantage. A more in-depth analysis can demonstrate higher improvements that overcome the disadvantages. A significant research could be the optimisation of the fan nozzle areas along the whole cruise to improve fan performance.

References

[1] Darecki, M., Edelstenne, C., Enders, T. et al. (2011) 'Flightpath 2050', *Flightpath 2050 Europes Vision for Aviation*. Available at: https://ec.europa.eu/transport/sites/transport/files/modes/air/doc/flightpath2050.pdf (Accessed: 5 May 2018)

[2] Arguelles, P., Bischoff, M., Busquin P. et al. (2001), European Aeronautics: a Vision for 2020, *Report of the group of personalities*. Available at: http://www.acare4europe.org/sites/acare4europe.org/files/document/Vision2020.pdf (Accessed: 5 May 2018).

[3] Whurr, J. (2013), 'Future Civil Aeroengine Architectures & Technologies' [Presentation], *10th European Turbomachinery Conference*. Lappeenranda, Finland, April 2013. Available at: http://www.etc10.eu/mat/Whurr.pdf (Accessed: 8 May 2018).

[4] BOEING (2017), *Current Market Outlook 2017-2036.* Seattle: Boeing Commercial Airplanes. Available at: http://www.boeing.com/resources/boeingdotcom/commercial/market/current-market-outlook-2017/assets/downloads/2017-cmo-6-19.pdf (Accessed: 29 July 2018).

[5] Ausick, P. (2016), *Is This Boeings Middle-of-the-Market Airplane?* Available at: https://247wallst.com/aerospace-defense/2016/07/01/is-this-boeings-middle-of-the-market-airplane/ (Accessed: 29 July 2018).

[6] Pilidis, P. (2016), 'Gas turbine perfromance' [Lecture Notes], *Gas turbine performance, simulation and diagnostics*. Cranfield University. Available at: https://bb.cranfield.ac.uk/bbcswebdav/pid-601413-dt-content-rid-913934_2/courses/N-THP-GPSD-17-A17/Performance%20Notes%20PILIDIS%20March%20AYR16%20-%20Printing%20and%20Blackboard.pdf (Accessed 02/08/2018).

[7] Kurzke, J. (2008), 'Preliminary design', in Denos, R. and Paniagua G. (ed.) *Lecture series 2008-03: Aero-engine design: from state of the art turbofans towards innovative architectures.* Belgium: Von Karman Institute for Fluid Dynamics, pp. 4-12.

[8] Giannakakis, P. (2013), *Design space exploration and performance modelling of advanced turbofan and open-rotor engines*, EngD Thesis. Cranfield University.

[9] Guha, A. (2001), 'Optimisation of Aero Gas Turbine Engines, *The Aeronautical Journal of the Aeronautical Society*, vol. July, p. 345. Available at: https://www.researchgate.net/publication/281964543_Optimisation_of_aero_gas_turbine_engines (Accessed: 08 May 2018)

[10] Cohen, H., Rogers, GFC. and Saravanamuttoo, HIH. (1996) *Gas Turbine Theory.* 4th edn. Harlow: Longman Group Ltd.

[11] Mourouzidis, C. (2016), *Cycle optimisation & preliminary design of very low specific thrust turbofan engines*, PhD Thesis. Cranfield University.

[12] Rolls-Royce plc (2006), *Aero Data*, VCOM11141 Issue 3, Derby: Rolls-Royce plc.

[13] Cumpsty, N. (2007), *Jet Propulsion*. 2nd edn. Cambridge: Cambridge University Press.

[14] Halliwell, I. (1998). 'Preliminary engine design-A practical overview.', 34th AIAA/ASME/SAE/ASEE Joint Propulsion Conference and Exhibit, p. 3891. Cleveland, Ohio, 13-15 July 1998. Available at: https://arc.aiaa.org/doi/pdf/10.2514/6.1998-3891 (Accessed: 22 June 2018).

[15] Walsh, P. and Fletcher, P. (2004), *Gas Turbine Performance*, 2nd edn. Oxford: Blackwell Science Ltd.

[16] Pilidis, P. and Palmer, J.R. (2012), *Gas Turbine Theory and Performance*, 3rd edn. Department of Power & Propulsion, Cranfield University.

[17] Smith, S. (1965). 'A Simple Correlation of Turbine Efficiency'.*The Journal of the Royal Aeronautical Society*, 69(655), pp. 467-470. Available at: doi 10.1017/S0001924000059108 (Accessed: 23 June 2018).

[18] Wilfert, G. (2008), 'Geared Fan', in Denos, R. and Paniagua G. (ed.) *Lecture series 2008-03: Aero-engine design: from state of the art turbofans towards innvative architectures.* Belgium: Von Karman Institute for Fluid Dynamics, pp. 14-21.

[19] Arvai, S.E. (2011), 'Comparing the new technology Narrow-body engines: GTF vs LEAP maintenance costs', *AirInsight*. Available at: https://airinsight.com/comparing-the-new-technology-narrow-body-engines-gtf-vs-leap-\maintenance-costs/ (Accessed: 05 July 2018).

[20] Misel, O.W. (1977), *NASA CR- 134669: Quiet Clean Short-Haul Experimental Engine (QCSEE) Main Reduction Gears Test Program*. Cleveland: NASA Lewis Research Center. Available at: https://ntrs.nasa.gov/search.jsp?R=19800006844 (Accessed: 21 July 2018).

[21] Farokhi, S. (2015), *Aircraft Propulsion*, 2nd edn. Chichester: John Wiley & Sons Ltd.

[22] Chang, K. and Sitt, D. (2017), *The Implementation of Powered Gearboxes into Turbofans to Improve Engine Efficiency*. University of Pittsburgh. Available at: https://www.semanticscholar.org/paper/The-Implementation-of-Powered-Gearboxes-into-to-Sitt/4bcdcba062ffc04b7afe3e16600ad6668a9a28cb?tab=abstract (Accessed: 5 July 2018).

[23] Mohd Tobi, A. L. and Ismail, A. E. (2016), 'Development in Geared Turbofan Aeroengine', *IOP Conference Series: Materials Science and Engineering*. Bali, 19 Mar-20 Mar 2016. Available at: http://iopscience.iop.org/article/10.1088/1757-899X/131/1/012019 (Accessed: 5 July 2018).

[24] Dudley, D.W (1962), *The design, manufacture, and application of gears .* New York: McGraw Hill.

[25] McGuinn, J. (2008), 'Gearbox speed reducer: helps fan technology for "greener" jet fuel efficiency', *Gear Technology.* Available at: https://www.geartechnology.com/issues/0808x/turbofan.pdf. (Accessed: 21 July 2018).

[26] Dixon, S.L. (2005), *Fluid Mechanics Thermodynamics of Turbomachinery*, 5th edn. Burlington: Elsevier Butterworth-Heinemann.

[27] Wilson, D.G. and Korakianitis, T. (2014), *The design of high-efficiency turbomachines and gas turbines*, 2nd edn. Massachusetts: The MIT Press.

[28] Massachusetts Institue of Technology (2006), *A typical multistage axial flow compressor*. Available at: http://web.mit.edu/16.unified/www/FALL/thermodynamics/notes/node92.html (Accessed: 19 July 2019)

[29] Meherwan, P. and Boyce, P.E. (2003), *Centrifugal compressors: a basic guide*. Tulsa: PennWell Corporation.

[30] Nisenfeld, A.E. (1982), *Centrifugal Compressors*, North Carolina: The Instrument Society of America.

[31] Baxter, A.D.(1952) 'A Comparison of Axial and Centrifugal Compressor Gas Turbines: An Objective Examination of the Pros and Cons of a Much Debated Subject', Aircraft Engineering and Aerospace Technology, Vol. 24 Issue: 7, pp.186-197. Available at: https://doi.org/10.1108/eb032175 (Accessed: 21 July 2018)

[32] Nolcheff, N., Repp, J., Reynolds, B.D. and Hanson, D.R. (2017), *US 2017/0276070 A1: Axi-centrifugal compressor.* United States Patent and Trademark Office. Available at: https://patents.google.com/patent/EP3222854A1/en (Accessed: 21 July 2018).

[33] Jackson, A. B. (1976), 'Some Future Trends in Aero Engine Design for Subsonic Transport Aircraft.' *ASME. J. Eng. Power*, 98(2), pp. 281-289. Available at: doi:10.1115/1.3446164 (Accessed: 23 July 2018)

[34] Borradaile, J.A. (1988), 'Towards the optimum ducted UHBR engine', *Proceedings of 24th AIAA/ASME/SAE/ASEE Joint Propulsion Conference and Exhibit*, AIAA-88-2954. Boston, Massachusetts, July 1988. Available at: https://doi.org/10.2514/6.1988-2954 (Accessed: 23 July 2018).

[35] Peacock, N.J. and Sadler, J.H.R. (1992), 'Advanced propulsion systems for large subsonic transports', *Journal of Propulsion and Power*, 8(3), pp. 703-708. Available at: https://arc.aiaa.org/doi/abs/10.2514/3.23535 (Accessed: 23 July 2018).

[36] Daggett, D.L., Brown, S.T. and Kawai, R.T. (2003), NASA CR-2003-212309: *Ultra-efficient engine diameter study.* Cleveland: NASA Glenn Research Center. Available at: https://ntrs.nasa.gov/search.jsp?R=20030061085(Accessed. 21 July 2018).

[37] Zimbrick, R.A. and Colehour, J.L. (1988), 'An investigation of very high bypass ratio engines for subsonic transports', *Proceedings of 24th AIAA/ASME/SAE/ASEE Joint Propulsion Conference and Exhibit*. Boston, Massachusetts, July 1988. Available at: https://doi.org/10.2514/3.25461 (Accessed: 21 July 2018).

[38] Kyritsis, V. E. (2006), *Thermodynamic preliminary design of civil turbofans and variable geometry implementation*, PhD Thesis. Cranfield University.

[39] Chetan, K., Hoeschler, K. and Mischke, M. (2015), 'Concept Study of Variable Area Fan Nozzle for Ultra-High By-Pass Ratio Turbofan Engine', *22nd International Symposium on Air Breathing Engines - ISABE*. Phoenix, Arizona, 25-30 October 2015. Available at: http://hdl.handle.net/2374.UC/745788 (Accessed: 21 July 2018).

[40] Van Leeuwen, M. (2016), *PurePower Engines by Pratt&Whitney Transform Aviation with VivaAerobus*. Available at: http://aviationnews.eu/news/2016/11/purepower-engines-pratt-whitney-transform-aviation-vivaaerobus/ (Accessed: 21 July 2018).

[41] Pratt&Whitney Canada (2015), *PurePower Family of Engines*. Available at: http://www.purepowerengine.com/pdf/brochures/PurePowerBrochure_160601.pdf (Accessed: 18 July 2018).

[42] Pratt&Whitney Canada (2012), *Pure Power Engine Family*. Available at: https:==www.pw.utc.com=Content=PurePowerPW1000GEngine=pdf=B-1-1PurePowerEngineFamilySpecsChart.pdf (Accessed: 18 July 2019).

[43] Gunston, B. (2001) *Jane's aero-engines.* London: Jane's Information Group.

[44] Duncan, R., Kilmartin, P. and Heinonen, L. (2001), *An Historical Look at the TFE731 Engine*. Nebraska: Duncan Aviation.

[45] Honeywell Aerospace (2005), *TFE731-2 to -2C: Engine Upgrade Program.* Phoenix: Honeywell International Inc. Avialable at: https://aerocontent.honeywell.com/aero/common/documents/myaerospacecatalog-documents/BA_brochures-documents/Engines-documents/TFE731-2_upgrade_for_learjet_31-35-36.pdf (Accessed: 22 July 2018).

[46] Honeywell Aerospace (2006), *TFE731-60: Proven Turbofan Propulsion Technology.* Phoenix: Honeywell International Inc. Avialable at: https://aerocontent.honeywell.com/aero/common/documents/myaerospacecatalog-documents/BA_brochures-documents/tfe731-60.pdf (Accessed: 22 July 2018).

[47] Airbus (2018), *A321: Aircraft Characteristics Airport and Maintenance Planning*. Available at: https://www.airbus.com/content/dam/corporate-topics/publications/backgrounders/techdata/aircraft_characteristics/Airbus-Commercial-Aircraft-AC-A321-Feb18.pdf (Accessed: 24 July 2018).

[48] Lolis, P. (2014), *Development of a Novel Preliminary Aero Engine Weight Estimation Method*, PhD Thesis. Cranfield University.

[49] McCullers, L.A. (2011), *FLOPS: Flight Optimization System. Release 8.23, User's Guide*. Hampton: Langley Research Center.

[50] Deb, K., Pratap, A., Agarwal, S. and Meyarivan, T. A. M. T. (2002). 'A fast and elitist multiobjective genetic algorithm: NSGA-II'. *IEEE transactions on evolutionary computation*, 6(2), pp. 182-197. Available at doi: doi: 10.1109/4235.996017 (Accessed: 29 July 2018).

[51] Cranfield University (2017), *The Turbomatch Scheme*[Manual]. Department of Power & Propulsion, Cranfield University.

[52] Horlock, J.H. (2003), *Advanced Gas Turbine Cycles*. Oxford: Elsevier Science Ltd.

[53] Onat, E. and Tolle, F. (1979), NADC-78103-60: *An extension of engine weight estimation techniques to compute engine production cost.* Warminster: Naval Air Development Center. Available at: http://www.dtic.mil/dtic/tr/fulltext/u2/a074454.pdf (Accessed: 27 July 2018).

[54] Sagerser, D.A., Lieblein, S. and Krebs, R.P. (1971), NASA TM X-2406: *Empirical Expressions for Estimating Length and Weight of Axial-Flow Components of VTOL Powerplants.* Cleveland: Lewis Research Center. Available at: https://ntrs.nasa.gov/archive/nasa/casi.ntrs.nasa.gov/19720005136.pdf (Accessed: 27 July 2018).

[55] Tong, M. and Naylor, B. (2009), NASA/TM-2009-215656: *An Object-Oriented Computer Code for Aircraft Engine Weight Estimation*. Cleveland: Glenn Research Center. Available at: https://ntrs.nasa.gov/archive/nasa/casi.ntrs.nasa.gov/20100000016.pdf (Accessed: 28 July 2018)

[56] Rockyimage (2018), *A320 Electrical System Diagram Unique Potential Of Future thermoelectric Energy Recuperation for Aviation*. Available at: http://hollywoodnepotism.net/a320-electrical-system-diagram/a320-electrical-system-diagram-unique-potential-of-future-\thermoelectric-energy-recuperation-for-aviation/ (Accessed: 28 July 2018)

[57] Wells, D.P., Horvath, B.L. and McCullers, L.A. (2017), NASA/TM2017219627/Volume I: *The Flight Optimization System Weights*

and Estimation Method. Hampton: Langley Research Center. Available at: https://ntrs.nasa.gov/archive/nasa/casi.ntrs.nasa.gov/20170005851.pdf (Accessed: 28 July 2018).

Appendix A

NASA FLOPS input data

Parameter	Value
Wing mounted engines	2
First class PAX	16
Second class PAX	169
Wing span [ft]	111.549
Fuselage Length [ft]	146
Fuselage width [ft]	13
Fuselage depth [ft]	13.4
Horizontal tail area [sq ft]	333.681
Horizontal tail sweep angle [deg]	29
Horizontal tail aspect ratio	5
Horizontal tail taper ratio	0.256
Horizontal tail thickness-chord ratio	0.11
Vertical tail area [sq ft]	512.9
Vertical tail sweep angle [deg]	34
Vertical tail aspect ratio	1.82
Vertical tail taper ratio	0.303
Vertical tail thickness-chord ratio	0.176
Wing area [sq ft]	1317.41
Wing thickness-chord ratio	0.11
Wing taper ratio	0.24
Wing sweep angle [deg]	25
Range [nm]	3000
Cruise Mach number	0.82

Table A.1: NASA FLOPS input data regarding the aircraft geometry. [47]